

3
4 **GW190814: Gravitational Waves from the Coalescence of a $23 M_{\odot}$ Black Hole
with a $2.6 M_{\odot}$ Compact Object**

5 LIGO SCIENTIFIC COLLABORATION AND VIRGO COLLABORATION
6

7 (Dated: May 21, 2020)

8 **ABSTRACT**

9 We report the observation of a compact binary coalescence involving a $22.2 - 24.3 M_{\odot}$ black hole and
10 a compact object with a mass of $2.50 - 2.67 M_{\odot}$ (all measurements quoted at the 90% credible level).
11 The gravitational-wave signal, GW190814, was observed during LIGO's and Virgo's third observing
12 run on August 14, 2019 at 21:10:39 UTC and has a signal-to-noise ratio of 25 in the three-detector
13 network. The source was localized to 18.5 deg^2 at a distance of $241^{+41}_{-45} \text{ Mpc}$; no electromagnetic
14 counterpart has been confirmed to date. The source has the most unequal mass ratio yet measured
15 with gravitational waves, $0.112^{+0.008}_{-0.009}$, and its secondary component is either the lightest black hole
16 or the heaviest neutron star ever discovered in a double compact-object system. The dimensionless
17 spin of the primary black hole is tightly constrained to ≤ 0.07 . Tests of general relativity reveal no
18 measurable deviations from the theory, and its prediction of higher-multipole emission is confirmed at
19 high confidence. We estimate a merger rate density of $1\text{--}23 \text{ Gpc}^{-3} \text{ yr}^{-1}$ for the new class of binary
20 coalescence sources that GW190814 represents. Astrophysical models predict that binaries with mass
21 ratios similar to this event can form through several channels, but are unlikely to have formed in
22 globular clusters. However, the combination of mass ratio, component masses, and the inferred merger
23 rate for this event challenges all current models for the formation and mass distribution of compact-
24 object binaries.

25 **1. INTRODUCTION**

26 The first two observing runs (O1 and O2) with
27 Advanced LIGO (Aasi et al. 2015) and Advanced
28 Virgo (Acernese et al. 2015) opened up the field of
29 gravitational-wave astrophysics with the detection of
30 the first binary black hole (BBH) coalescence signal,
31 GW150914 (Abbott et al. 2016a). Another nine such
32 events (Abbott et al. 2016b, 2019a) were discovered by
33 the LIGO Scientific and Virgo Collaborations (LVC)
34 during this period, and additional events were reported
35 by independent groups (Zackay et al. 2019a,b; Venumad-
36 hav et al. 2019; Nitz et al. 2020). The first binary neu-
37 tron star (BNS) coalescence signal, GW170817, was dis-
38 covered during the second of these observing campaigns
39 (Abbott et al. 2017a, 2019b). It proved to be a multi-
40 messenger source with emission across the electromag-
41 netic spectrum (Abbott et al. 2017b), with implications
42 for the origin of short gamma-ray bursts (Abbott et al.
43 2017c), the formation of heavy elements (Chornock et al.
44 2017; Tanvir et al. 2017; Abbott et al. 2017d; Rosswog
45 et al. 2018; Kasliwal et al. 2019; Watson et al. 2019),
46 cosmology (Abbott et al. 2017e, 2019c) and fundamen-
47 tal physics (Abbott et al. 2017c, 2019d).

48 The first six months of the third observing run (O3)
49 were completed between April 1 and September 30,
50 2019. The LVC recently reported on the discovery of
51 GW190425, the coalescence signal of what is most likely
52 a BNS with unusually large chirp mass and total mass
53 compared to the Galactic BNSs known from radio pul-
54 sar observations (Abbott et al. 2020a). Another dis-
55 covery from O3 is that of GW190412, the first BBH
56 coalescence with an unequivocally unequal mass ratio
57 $q = m_2/m_1$ of $0.28^{+0.12}_{-0.06}$ (all measurements are reported
58 as symmetric 90% credible intervals around the median
59 of the marginalized posterior distribution, unless other-
60 wise specified). It is also the first event for which higher-
61 multipole gravitational radiation was detected with high
62 significance (Abbott et al. 2020d).

63 Here we report on another O3 detection, GW190814,
64 the signal of a compact binary coalescence with the
65 most unequal mass ratio yet measured with gravitational
66 waves: $q = 0.112^{+0.008}_{-0.009}$. The signal was first identified
67 in data from two detectors, LIGO Livingston and Virgo,
68 on 2019 August 14, 21:11:00 UTC. Subsequent analysis
69 of data from the full three-detector network revealed a
70 merger signal with signal-to-noise ratio (SNR) of $\simeq 25$.

The primary component of GW190814 is conclusively a black hole (BH) with mass $m_1 = 23.2^{+1.1}_{-1.0} M_\odot$. Its dimensionless spin magnitude is constrained to $\chi_1 \leq 0.07$. The nature of the $2.59^{+0.08}_{-0.09} M_\odot$ secondary component is unclear. The lack of measurable tidal deformations and the absence of an electromagnetic counterpart are consistent with either a neutron star (NS) or a BH given the event's asymmetric masses and distance of 241^{+41}_{-45} Mpc. However, we show here that comparisons with the maximum NS mass predicted by studies of GW170817's remnant, by current knowledge of the NS equation of state, and by electromagnetic observations of NSs in binary systems indicate that the secondary is likely too heavy to be a NS. Either way, this is an unprecedented source because the secondary's well-constrained mass of $2.50-2.67 M_\odot$ makes it either the lightest BH or the heaviest NS ever observed in a double compact-object system.

As in the case of GW190412, we are able to measure the presence of higher multipoles in the gravitational radiation, and a set of tests of general relativity with the signal reveal no deviations from the theory. Treating this event as a new class of compact binary coalescences, we estimate a merger rate density of $1-23 \text{ Gpc}^{-3} \text{ yr}^{-1}$ for GW190814-like events. Forming coalescing compact binaries with this unusual combination of masses at such a rate challenges our current understanding of astrophysical models.

We report on the status of the detector network and the specifics of the detection in Sections 2 and 3. In Section 4, we estimate physical source properties with a set of waveform models, and we assess statistical and systematic uncertainties. Tests of general relativity are described in Section 5. In Section 6, we calculate the merger rate density and discuss implications for the nature of the secondary component, compact binary formation and cosmology. Section 7 summarizes our findings.

2. DETECTOR NETWORK

At the time of GW190814, LIGO Hanford, LIGO Livingston and Virgo were operating with typical O3 sensitivities (Abbott et al. 2020a). Although LIGO Hanford was in a stable operating configuration at the time of GW190814, the detector was not in observing mode due to a routine procedure to minimize angular noise coupling to the strain measurement (Kasprzack & Yu 2017). This same procedure took place at LIGO Hanford around the time of GW170608; we refer the reader to Abbott et al. (2017f) for details of this procedure. Within a 5 min window around GW190814, this procedure was not taking place, therefore LIGO Hanford data for GW190814 are usable in the nominal range

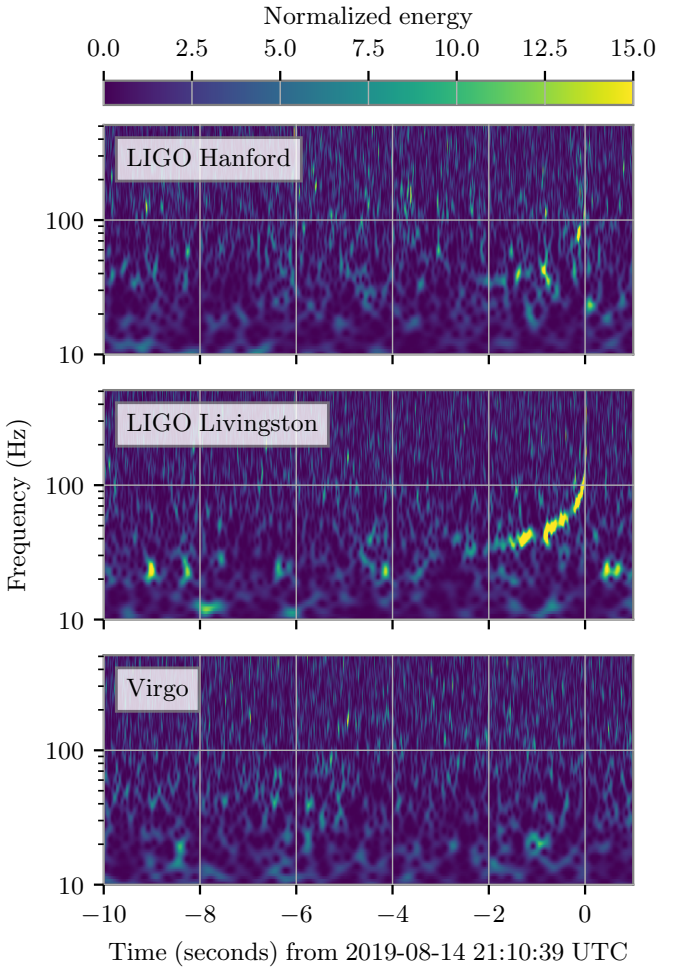


Figure 1. Time–frequency representations (Chatterji et al. 2004) of data containing GW190814, observed by LIGO Hanford (top), LIGO Livingston (middle), and Virgo (bottom). Times are shown relative to 2019 August 14, 21:10:39 UTC. Each detector’s data are whitened by their respective noise amplitude spectral density and a Q-transform is calculated. The colorbar displays the normalized energy reported by the Q-transform at each frequency. These plots are not used in our detection procedure and are for visualization purposes only.

of analyzed frequencies. A time–frequency representation (Chatterji et al. 2004) of the data from all three detectors around the time of the signal is shown in Figure 1.

We used validation procedures similar to those used to vet previous gravitational-wave events (Abbott et al. 2016c, 2019a). Overall we found no evidence that instrumental or environmental disturbances (Effler et al. 2015) could account for GW190814. However, we did identify low-frequency transient noise due to scattered light at LIGO Livingston, a common source of noise in all three

interferometers (Nuttall 2018). Scattered light features in the strain data are produced when a small fraction of the main laser beam reflects off a moving surface and is phase modulated before recombining with the main beam. This recombination can result in excess noise with the morphology of arches in the time–frequency plane; the frequency of this noise is determined by the velocity of the moving surface (Accadia et al. 2010). Thunderstorms near LIGO Livingston around the time of GW190814 resulted in acoustic noise coupling to the detector and caused features in the strain data associated with scattered light (Abbott et al. 2019a). In this instance, this form of noise affects frequencies up to 30 Hz from roughly 22 s to 8 s before and 0.2 s to 1.5 s after the detected time of GW190814, as seen in the middle panel of Figure 1. Since this noise could bias the estimation of GW190814’s source parameters, we used a starting frequency of 30 Hz to analyse LIGO Livingston data. Virgo was operating nominally and there are no quality issues in the Virgo data.

The LIGO and Virgo detectors are calibrated by photon pressure from modulated auxiliary lasers inducing test-mass motion (Karki et al. 2016; Viets et al. 2018; Acernese et al. 2018). Over the frequency range 20–2048 Hz, the maximum 1σ calibration uncertainties for strain data used in the analysis of GW190814 were 6% in amplitude and 4 deg in phase for LIGO data, and 5% in amplitude and 7 deg in phase for Virgo data. These calibration uncertainties are propagated into the parameter estimation reported in Section 4 via marginalization.

3. DETECTION

3.1. Low-latency Identification of a Candidate Event

GW190814 was first identified on 2019 August 14, 21:11:00 UTC as a loud two-detector event in LIGO Livingston and Virgo data (SNR 21.4 and 4.3) by the low-latency GstLAL matched-filtering search pipeline for coalescing binaries (Cannon et al. 2012; Privitera et al. 2014; Messick et al. 2017; Hanna et al. 2020; Sachdev et al. 2019). Matched-filtering searches use banks (Sathyaprakash & Dhurandhar 1991; Blanchet et al. 1995; Owen 1996; Owen & Sathyaprakash 1999; Damour et al. 2001; Blanchet et al. 2005; Cokelaer 2007; Harry et al. 2009; Brown et al. 2013; Ajith et al. 2014; Harry et al. 2014; Capano et al. 2016b; Indik et al. 2018; Roy et al. 2017, 2019) of modeled gravitational waveforms (Arun et al. 2009; Blanchet 2014; Buonanno & Damour 1999; Bohé et al. 2017; Pürer 2016) as filter templates. A Notice was issued through NASA’s Gamma-ray Coordinates Network (GCN) 20 min later (LIGO Scientific Collaboration, Virgo Collaboration 2019a) with a two-detector source local-

ization computed using the rapid Bayesian algorithm BAYESTAR (Singer & Price 2016) that is shown in Figure 2. The event was initially classified as “Mass-Gap” (Kapadia et al. 2020; LIGO Scientific Collaboration, Virgo Collaboration 2019b), implying that at least one of the binary merger components was found to have a mass between $3\text{--}5 M_{\odot}$ in the low-latency analyses.

Other low-latency searches, including the matched-filtering based MBTA (Adams et al. 2016) and PYCBC (Usman et al. 2016; Nitz et al. 2017, 2018, 2019) pipelines, could not detect the event at the time as its SNR in Virgo data was below their single-detector detection thresholds, although a test version of MBTA with a lower SNR threshold did identify the event.

Shortly thereafter, reanalyses including LIGO Hanford data were performed using GstLAL and PYCBC. A coincident gravitational-wave signal was identified in all three detectors by both searches, with SNR 21.6 in LIGO Livingston, 10.6 in LIGO Hanford, and 4.5 in Virgo data (as measured by GstLAL, consistent with SNRs reported by PYCBC). Results of these 3-detector analyses were reported in a GCN Circular within 2.3 hours of the time of the event (LIGO Scientific Collaboration, Virgo Collaboration 2019c,d), providing a 3-detector localization (Singer & Price 2016) constraining the distance to 220–330 Mpc and the sky area to 38 deg^2 at the 90% credible level. Another GCN Circular (LIGO Scientific Collaboration, Virgo Collaboration 2019e) sent 13.5 hours after the event updated the source localization to a distance of 215–320 Mpc, the sky area to 23 deg^2 , and the source classification to “NSBH” (Kapadia et al. 2020; LIGO Scientific Collaboration, Virgo Collaboration 2019b), indicating that the secondary had a mass below $3 M_{\odot}$. These updated sky localizations are also shown in Figure 2. The two disjoint sky localizations arise because the low SNR in the Virgo detector (4.5) means that the data are consistent with two different signal arrival times in that detector.

3.2. Multi-messenger Follow-up

Several external groups performed multi-messenger follow-up of the source with observations across the electromagnetic spectrum (e.g., Lipunov et al. 2019; Gomez et al. 2019; Antier et al. 2020; Andreoni et al. 2020; Dobie et al. 2019; Watson et al. 2020; Ackley et al. 2020; Vieira et al. 2020) and with neutrino observations (e.g., Ageron et al. 2019; The IceCube Collaboration 2019). No counterpart candidates were reported. The non-detection is consistent with the source’s highly unequal mass ratio and low primary spin (LIGO Scientific Collaboration, Virgo Collaboration 2019d,e). Tentative constraints placed by multi-messenger studies on

the properties of the system, such as the ejecta mass and maximum primary spin (Andreoni et al. 2020; Ackley et al. 2020; Kawaguchi et al. 2020; Coughlin et al. 2020) or the circum-merger density (Dobie et al. 2019) assuming a neutron-star–black-hole (NSBH) source, may need to be revisited in light of the updated source parameters we present in Sec. 4.1.

3.3. Significance

The significance of GW190814 was estimated by follow-up searches using improved calibration and refined data-quality information that are not available in low latency. They also used longer stretches of data for better precision (Abbott et al. 2016b,c). With LIGO Hanford data being usable but not in nominal observing mode at the time of GW190814, we used only data from the LIGO Livingston and Virgo detectors for significance estimation. GW190814 was identified as a confident detection in analyses of detector data collected over the period from August 7 to August 15, 2019 by the two independent matched-filtering searches GstLAL and PyCBC, with SNR values consistent with the low-latency analyses. The production version of PyCBC for O3 estimates significance only for events that are coincident in the LIGO Hanford and LIGO Livingston detectors, and therefore an extended version (Davies et al. 2020) was used for GW190814 in order to enable the use of Virgo data in significance estimation.

GstLAL and PyCBC use different techniques for estimating the noise background and methods of ranking gravitational-wave candidates. Both use results from searches over non time-coincident data to improve their noise background estimation (Privitera et al. 2014; Messick et al. 2017; Usman et al. 2016). Using data from the first six months of O3 and including all events during this period in the estimation of noise background, GstLAL estimated a false-alarm rate (FAR) of 1 in 1.3×10^3 yr for GW190814. Using data from the 8-day period surrounding GW190814 and including this and all quieter events during this period in noise background estimation, the extended PyCBC pipeline (Davies et al. 2020) estimated a FAR for the event of 1 in 8.1 yr. The higher FAR estimate from PyCBC can be attributed to the event being identified by the pipeline as being quieter than multiple noise events in Virgo data. As PyCBC estimates background statistics using non-coincident data from both detectors, these louder noise events in Virgo data can form chance coincidences with the signal in LIGO Livingston data and elevate the noise background estimate for coincident events, especially when considering shorter data periods. All estimated background events that were ranked higher than

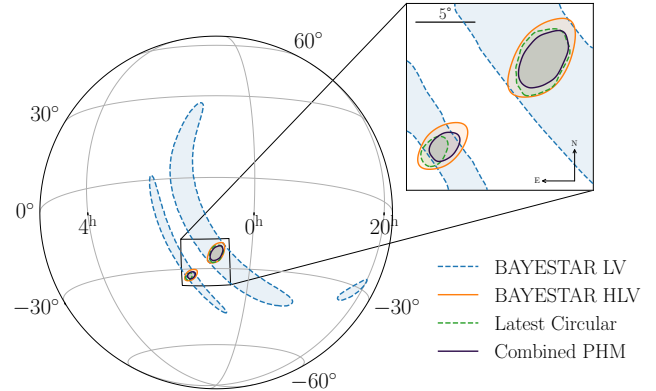


Figure 2. Posterior distributions for the sky location of GW190814. The contours show the 90% credible interval for a LIGO Livingston–Virgo (blue) and LIGO Hanford–LIGO Livingston–Virgo (orange) detector network based on the rapid localization algorithm BAYESTAR (Singer & Price 2016). The sky localization circulated 13.5 hours after the event, based on a LIGO Hanford–LIGO Livingston–Virgo analysis with the LALINFERERENCE stochastic sampling software (Veitch et al. 2015), is shown in green. The purple contour indicates the final sky localization as presented in this paper, which constrains the source to within 18.5 deg^2 at 90% probability.

GW190814 by PyCBC were indeed confirmed to be coincidences of the candidate event itself in LIGO Livingston with random noise events in Virgo. The stated background estimates are therefore conservative (Capano et al. 2016a). We also estimate the background excluding the candidate from the calculation, a procedure that yields a mean-unbiased estimation of the distribution of noise events (Capano et al. 2016a; Abbott et al. 2016d). In this case, with GstLAL we found a FAR of < 1 in 10^5 yr while with PyCBC we found a FAR of < 1 in 4.2×10^4 yr. With both pipelines identifying GW190814 as more significant than any event in the background, the FARs assigned are upper bounds.

When data from LIGO Hanford were included, GW190814 was also identified by the unmodelled coherent Wave Burst (cWB) search that targets generic gravitational-wave transients with increasing frequency over time without relying on waveform models (Klimenko et al. 2008, 2016; Abbott et al. 2016e). We found a FAR of < 1 in 10^3 yr of observing time against the noise background from LIGO Hanford and LIGO Livingston data, consistent with the other searches.

4. PROPERTIES OF GW190814

We infer the physical properties of GW190814 using a coherent Bayesian analysis of the data from LIGO Livingston, LIGO Hanford and Virgo following the methodology described in Appendix B of Abbott et al. (2019a).

	EOBNR PHM	Phenom PHM	Combined
Primary mass m_1/M_\odot	$23.2^{+1.0}_{-0.9}$	$23.2^{+1.3}_{-1.1}$	$23.2^{+1.1}_{-1.0}$
Secondary mass m_2/M_\odot	$2.59^{+0.08}_{-0.08}$	$2.58^{+0.09}_{-0.10}$	$2.59^{+0.08}_{-0.09}$
Mass ratio q	$0.112^{+0.008}_{-0.008}$	$0.111^{+0.009}_{-0.010}$	$0.112^{+0.008}_{-0.009}$
Chirp mass \mathcal{M}/M_\odot	$6.10^{+0.06}_{-0.05}$	$6.08^{+0.06}_{-0.05}$	$6.09^{+0.06}_{-0.06}$
Total mass M/M_\odot	$25.8^{+0.9}_{-0.8}$	$25.8^{+1.2}_{-1.0}$	$25.8^{+1.0}_{-0.9}$
Final mass M_f/M_\odot	$25.6^{+1.0}_{-0.8}$	$25.5^{+1.2}_{-1.0}$	$25.6^{+1.1}_{-0.9}$
Upper bound on primary spin magnitude χ_1	0.06	0.08	0.07
Effective inspiral spin parameter χ_{eff}	$0.001^{+0.059}_{-0.056}$	$-0.005^{+0.061}_{-0.065}$	$-0.002^{+0.060}_{-0.061}$
Upper bound on effective precession parameter χ_p	0.07	0.07	0.07
Final spin χ_f	$0.28^{+0.02}_{-0.02}$	$0.28^{+0.02}_{-0.03}$	$0.28^{+0.02}_{-0.02}$
Luminosity distance D_L/Mpc	235^{+40}_{-45}	249^{+39}_{-43}	241^{+41}_{-45}
Source redshift z	$0.051^{+0.008}_{-0.009}$	$0.054^{+0.008}_{-0.009}$	$0.053^{+0.009}_{-0.010}$
Inclination angle Θ/rad	$0.9^{+0.3}_{-0.2}$	$0.8^{+0.2}_{-0.2}$	$0.8^{+0.3}_{-0.2}$
Signal to noise ratio in LIGO Hanford ρ_H	$10.6^{+0.1}_{-0.1}$	$10.7^{+0.1}_{-0.2}$	$10.7^{+0.1}_{-0.2}$
Signal to noise ratio in LIGO Livingston ρ_L	$22.21^{+0.09}_{-0.15}$	$22.16^{+0.09}_{-0.17}$	$22.18^{+0.10}_{-0.17}$
Signal to noise ratio in Virgo ρ_V	$4.3^{+0.2}_{-0.5}$	$4.1^{+0.2}_{-0.6}$	$4.2^{+0.2}_{-0.6}$
Network Signal to noise ratio ρ_{HLV}	$25.0^{+0.1}_{-0.2}$	$24.9^{+0.1}_{-0.2}$	$25.0^{+0.1}_{-0.2}$

Table 1. Source properties of GW190814: We report the median values along with the symmetric 90% credible intervals for the SEOBNRv4PHM (EOBNR PHM) and IMRPhenomPv3HM (Phenom PHM) waveform models. The primary spin magnitude and the effective precession is given as the 90% upper limit. The inclination angle is folded to $[0, \pi/2]$. The last column is the result of combining the posteriors of each model with equal weight. The sky location of GW190814 is shown in Figure 2.

Results presented here are obtained using 16 s of data around the time of detection. We use a low-frequency cutoff of 20 Hz for LIGO Hanford and Virgo and 30 Hz for LIGO Livingston for the likelihood evaluations, and we choose uninformative and wide priors, as defined in Appendix B.1 of Abbott et al. (2019a). The LALINFER-ENCE stochastic sampling software (Veitch et al. 2015) is the primary tool used to sample the posterior distribution. A parallelized version of the parameter estimation software BILBY (PBILBY; Smith & Ashton 2019; Ashton et al. 2019) is used for computationally expensive signal models. The power spectral density used in the likelihood calculations is a fair draw estimate calculated with BAYESWAVE (Cornish & Littenberg 2015; Littenberg & Cornish 2015a).

This signal is analyzed under two different assumptions: that it represents a BBH, or that it represents a NSBH. For the BBH analyses, two different waveform families are used, one based on the effective-one-body approach (EOBNR; Bohé et al. 2017; Babak et al. 2017; Cotesta et al. 2018; Ossokine et al. 2020) and the other on a phenomenological approach (Phenom; Khan et al. 2016; Husa et al. 2016; London et al. 2018; Khan et al. 2019; Khan et al. 2020).

For the NSBH analyses, we use BBH waveform models augmented with tidal effects (Matas et al. 2020; Thompson et al. 2020). When sampling the parameter space with the SEOBNRv4_ROM_NRTIDALV2_NSBH (Matas et al. 2020) and IMRPhenomNSBH (Thompson et al. 2020) waveform models, we obtained posterior distributions for the secondary component’s tidal deformability Λ_2 that are uninformative relative to a uniform prior in $\Lambda_2 \in [0, 3000]$. The absence of a measurable tidal signature is consistent with the highly unequal mass ratio (Foucart et al. 2013; Kumar et al. 2017) and with the relatively large secondary mass (Flanagan & Hinderer 2008). The large asymmetry in the masses implies that the binary will merge before the neutron star is tidally disrupted for any expected NS equation of state (Foucart et al. 2013). Given that the signal carries no discernible information about matter effects, here we present quantitative results only from BBH waveform models.

Our primary analyses include the effect of subdominant multipole moments in precessing waveform template models (PHM): IMRPhenomPv3HM (Phenom PHM; Khan et al. 2019; Khan et al. 2020) from the phenomenological family and SEOBNRv4PHM (EOBNR

361 PHM; Babak et al. 2017; Ossokine et al. 2020) from the
 362 EOBNR family.¹ Analyses that assume the spins are
 363 aligned with the orbital angular momentum were also
 364 performed, either including (Phenom/EOBNR HM) or
 365 excluding (Phenom/EOBNR) the effect of subdominant
 366 multipole moments.

367 4.1. Properties

368 From the ~ 300 observed cycles above 20 Hz, we
 369 are able to tightly constrain the source properties of
 370 GW190814. Our analysis shows that GW190814's
 371 source is a binary with an unequal mass ratio $q =$
 372 $0.112^{+0.008}_{-0.009}$, with individual source masses $m_1 =$
 373 $23.2^{+1.1}_{-1.0} M_\odot$ and $m_2 = 2.59^{+0.08}_{-0.09} M_\odot$, as shown in
 374 Figure 3. A summary of the inferred source prop-
 375 erties is given in Table 1. We assume a standard
 376 flat Λ CDM cosmology with Hubble constant $H_0 =$
 377 $67.9 \text{ km s}^{-1} \text{ Mpc}^{-1}$ (Ade et al. 2016).

378 We report detailed results obtained from the two pre-
 379 cessing BBH signal models including subdominant mul-
 380 tipole moments: Phenom PHM and EOBNR PHM. In
 381 order to compare the template models, we compute their
 382 Bayes factor ($\log_{10} \mathcal{B}$). We find no significant evidence
 383 that one waveform family is preferred over the other as
 384 the Bayes factor between Phenom PHM and EOBNR
 385 PHM is $\log_{10} \mathcal{B} \simeq 1.0$. As a result, we combine the
 386 posterior samples with equal weight, in effect marginal-
 387 izing over a discrete set of signal models with a uniform
 388 probability. This is shown in the last column of Table 1,
 389 and we refer to these values throughout the paper unless
 390 stated otherwise.

391 We find that the secondary mass lies in the
 392 range $2.50\text{--}2.67 M_\odot$. This inferred secondary mass
 393 exceeds the bounds of the primary component in
 394 GW190425 ($1.61\text{--}2.52 M_\odot$; Abbott et al. 2020a) and the
 395 most massive known pulsar in the Galaxy: $2.14^{+0.10}_{-0.09} M_\odot$
 396 at 68.3% credible interval (Cromartie et al. 2019). Fur-
 397 thermore, the secondary is more massive than bounds on the
 398 maximum NS mass from studies of the remnant of
 399 GW170817, and from theoretical (Abbott et al.
 400 2018) and observational estimates (Farr & Chatzioan-
 401 nou 2020). The inferred secondary mass is comparable
 402 to the putative BH remnant mass of GW170817 (Abbott
 403 et al. 2019b).

404 The primary object is identified as a BH based on its
 405 measured mass of $23.2^{+1.1}_{-1.0} M_\odot$. Due to accurately ob-
 406 serving the frequency evolution over a long inspiral, the

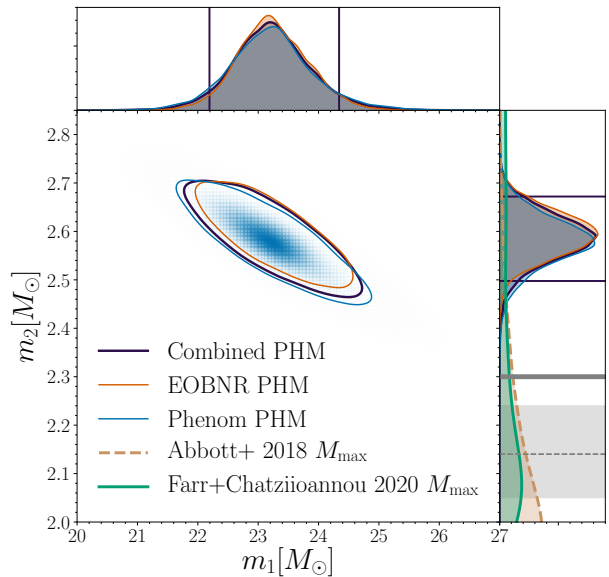


Figure 3. The posterior distribution of the primary and secondary source masses for two waveform models that include precession and subdominant multipole moments. The posterior distribution resulting from combining their samples is also shown. Each contour, as well as the colored horizontal and vertical lines, shows the 90% credible intervals. The right panel compares m_2 to predictions for the maximum NS mass, M_{\max} (see Section 6). The posterior distribution for M_{\max} from the spectral equation of state analysis of GW170817 (Abbott et al. 2018) is shown in orange, and the empirical M_{\max} distribution from the population model of Farr & Chatzioannou (2020) is shown in green. The grey dashed line and shading represent the measured mass of the heaviest pulsar in the Galaxy (median and 68% confidence interval; Cromartie et al. 2019). The solid grey band at $2.3 M_\odot$ is the upper bound on M_{\max} from studies of GW170817's merger remnant.

407 chirp mass is well constrained to $6.09^{+0.06}_{-0.06} M_\odot$. The in-
 408 ferred mass ratio $q = 0.112^{+0.008}_{-0.009}$ makes GW190814 only
 409 the second gravitational-wave observation with a signif-
 410 icantly unequal mass ratio (Abbott et al. 2019a, 2020d).

411 Given that this system is in a region of the parameter
 412 space that has not been explored via gravitational-
 413 wave emission previously, we test possible waveform sys-
 414 tematics by comparing the Phenom and EOB waveform
 415 families. Differences in the inferred secondary mass are
 416 shown in Figure 4. The results indicate that the inferred
 417 secondary mass is robust to possible waveform sys-
 418 tematics, with good agreement between the Phenom PHM
 419 and EOBNR PHM signal models. Signal models that
 420 exclude higher multipoles or precession do not constrain
 421 the secondary mass as well.

¹ In the co-precessing frame the EOBNR model includes the $(l, m) = (2, \pm 2), (2, \pm 1), (3, \pm 3), (4, \pm 4)$ and $(5, \pm 5)$ multipoles, and the Phenom model includes the $(2, \pm 2), (2, \pm 1), (3, \pm 3), (3, \pm 2), (4, \pm 4)$ and $(4, \pm 3)$ multipoles.

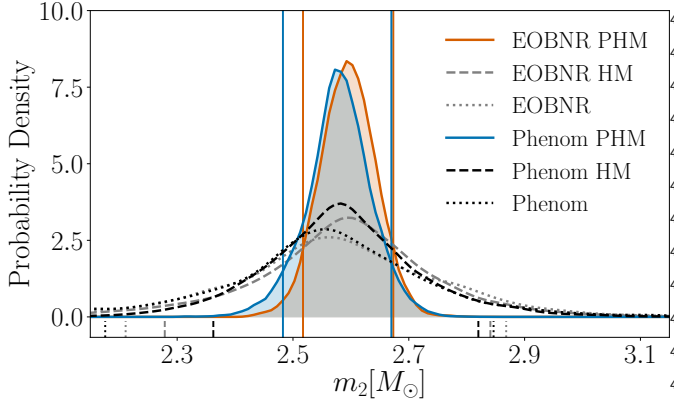


Figure 4. The marginalized posterior distribution for the secondary mass obtained using a suite of waveform models. The vertical lines indicate the 90% credible bounds for each waveform model. The labels Phenom/EOBNR PHM (generic spin directions + higher multipoles), Phenom/EOBNR HM (aligned-spin + higher multipoles) and Phenom/EOBNR (aligned-spin, quadrupole only) indicate the different physical content in each of the waveform models.

The time delay of a signal across a network of gravitational wave detectors, together with the relative amplitude and phase at each detector, allows us to measure the location of the GW source on the sky (Abbott et al. 2020b). We localize GW190814’s source to within 18.5 deg^2 at 90% probability, as shown in Figure 2. This is comparable to the localization of GW170817 (Abbott et al. 2017a, 2019a).

Spins are a fundamental property of BHs. Their magnitude and orientation carry information regarding the evolution history of the binary. The effective inspiral spin parameter χ_{eff} (Damour 2001; Racine 2008; Ajith et al. 2011; Santamaría et al. 2010) contains information about the spin components that are perpendicular to the orbital plane. We infer that $\chi_{\text{eff}} = -0.002^{+0.060}_{-0.061}$. The tight constraints are consistent with being able to measure the phase evolution from the long inspiral.

Orbital precession occurs when there is a significant spin component in the orbital plane of the binary (Apostolatos et al. 1994). We parameterize precession by the effective precession spin parameter $0 \leq \chi_p \leq 1$ (Schmidt et al. 2015). This effect is difficult to measure for face-on and face-off systems (Apostolatos et al. 1994; Buonanno et al. 2003; Vitale et al. 2014, 2017; Fairhurst et al. 2019a,b). GW190814 constrains the inclination of the binary to be $\Theta = 0.8^{+0.3}_{-0.2} \text{ rad}$. Since the system is neither face-on nor face-off, we are able to put strong constraints on the precession of the system: $\chi_p = 0.04^{+0.04}_{-0.03}$. This is both the strongest constraint on the amount of precession for any gravitational-wave detection to date,

and the first gravitational-wave measurement which conclusively measures near-zero precession (Abbott et al. 2019a, 2020a,d).

By computing the Bayes factor between a precessing and non-precessing signal model ($\log_{10}\mathcal{B} \sim 0.5$ in favor of precession), we find inconclusive evidence for in-plane spin. This is consistent with the inferred power from precession SNR ρ_p (Fairhurst et al. 2019a,b), whose recovered distribution resembles that expected in the absence of any precession in the signal; see Figure 5. The ρ_p calculation assumes a signal dominated by the $\ell = 2$ mode; however, we have verified that the contribution of higher harmonics to the measurement of spin precession is subdominant by a factor of 5. The data are therefore consistent with the signal from a non-precessing system.

Figure 4 shows that signal models including spin-precession effects give tighter constraints on the secondary mass compared to their non-precessing equivalents. Signal models that include spin-precession effects can constrain χ_p , whereas non-precessing signal models cannot provide information on in-plane spin components. In all analyses, we assume a prior equivalent to spin orientations being isotropically distributed. We find that the data are inconsistent with large χ_p and consistent with any secondary spin. Therefore, for precessing signal models the allowed $q-\chi_{\text{eff}}$ parameter space is restricted, which helps to break the degeneracy (Poisson & Will 1995; Baird et al. 2013; Farr et al. 2016; Baird et al. 2013; Ng et al. 2018). Consequently, the extra information from constraining χ_p to small values enables a more precise measurement of the secondary mass.

The asymmetry in the masses of GW190814 means that the spin of the more massive object dominates contributions to χ_{eff} and χ_p . As both χ_{eff} and χ_p are tightly constrained, we are able to bound the primary spin of GW190814 to be $\chi_1 \leq 0.07$, as shown in Figure 6. This is the strongest constraint on the primary spin for any gravitational-wave event to date (Abbott et al. 2019a, 2020a,d).

The joint posterior probability of the magnitude and orientation of χ_1 and χ_2 are shown in Figure 6. Deviations from uniform shading indicate a spin property measurement. The primary spin is tightly constrained to small magnitudes, but its orientation is indistinguishable from the prior distribution. The spin of the less massive object, χ_2 , remains unconstrained; the posterior distribution is broadly consistent with the prior.

The final mass M_f and final dimensionless spin χ_f of the merger remnant are estimated under the assumption that the secondary is a BH. By averaging several fits calibrated to numerical relativity (Hofmann et al.

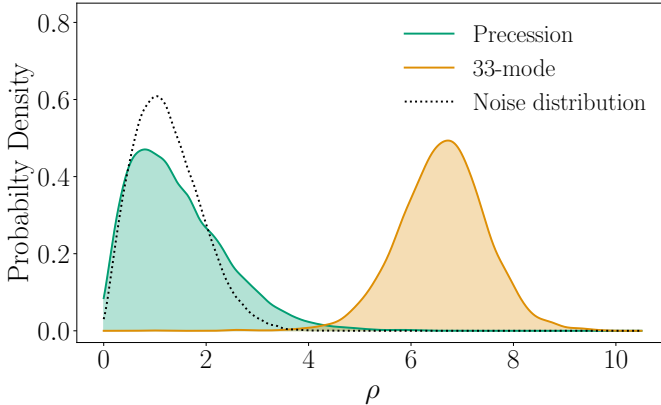


Figure 5. Posterior distributions for the precessing SNR, ρ_p (green) and the optimal SNR in the (3,3) sub-dominant multipole moment, ρ (orange). The grey dotted line shows the expected distribution for Gaussian noise.

2016; Johnson-McDaniel et al. 2016; Healy & Lousto 2017; Jiménez-Forteza et al. 2017), we infer the final mass and spin of the remnant BH to be $25.6^{+1.1}_{-0.9} M_\odot$ and $0.28^{+0.02}_{-0.02}$, respectively. The final spin is lower than for previous mergers (Abbott et al. 2019a, 2020d), as expected from the low primary spin and smaller orbital contribution due to the asymmetric masses.

4.2. Evidence for Higher-order Multipoles

The relative importance of a subdominant multipole moment increases with mass ratio. Each subdominant multipole moment has a different angular dependence on the emission direction. With significant evidence for multipoles other than the dominant $(\ell, m) = (2, 2)$ quadrupole, we gain an independent measurement of the inclination of the source. This allows for the distance-inclination degeneracy to be broken (Cutler & Flanagan 1994; Abbott et al. 2016f; Usman et al. 2019; Kalaghatgi et al. 2019). Measuring higher-order multipoles therefore gives more precise measurements of source parameters (Van Den Broeck & Sengupta 2007a,b; Kidder 2008; Blanchet et al. 2008; Mishra et al. 2016; Kumar et al. 2019).

GW190412 was the first event where there was significant evidence for higher-order multipoles (Payne et al. 2019; Kumar et al. 2019; Abbott et al. 2020d). GW190814 exhibits stronger evidence for higher-order multipoles, with $\log_{10} \mathcal{B} \simeq 9.6$ in favor of a higher-multipole vs. a pure quadrupole model. The $(\ell, m) = (3, 3)$ is the strongest subdominant multipole, with $\log_{10} \mathcal{B} \simeq 9.1$ in favor of a signal model including both the $(\ell, m) = (2, 2)$ and $(3, 3)$ multipole moments. GW190814's stronger evidence for higher multipoles is expected given its more asymmetric masses and the larger network SNR.

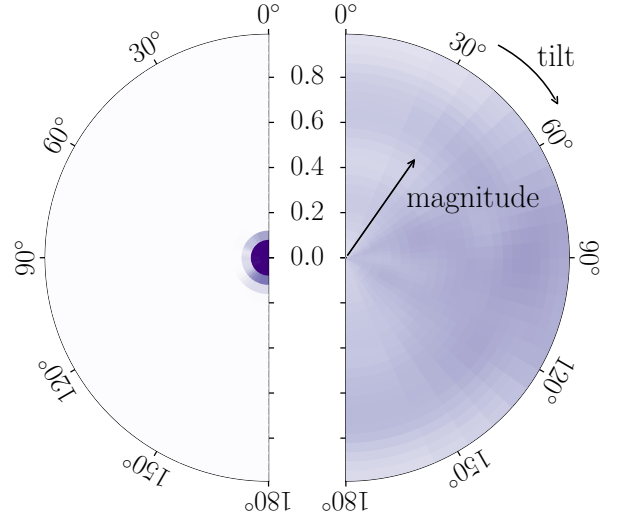


Figure 6. Two-dimensional posterior probability for the tilt-angle and spin-magnitude for the primary object (left) and secondary object (right) based on the Combined samples. The tilt angles are 0° for spins aligned and 180° for spins anti-aligned with the orbital angular momentum. The tiles are constructed linearly in spin magnitude and the cosine of the tilt angles such that each tile contains identical prior probability. The color indicates the posterior probability per pixel. The probabilities are marginalized over the azimuthal angles.

The orthogonal optimal SNR of a subdominant multipole is calculated by decomposing each multipole into components parallel and perpendicular to the dominant harmonic (Mills & Fairhurst 2020; Abbott et al. 2020d). We infer that the orthogonal optimal SNR of the $(\ell, m) = (3, 3)$ multipole is $6.6^{+1.3}_{-1.4}$, as shown in Figure 5. This is the strongest evidence for measuring a subdominant multipole to date (Payne et al. 2019; Kumar et al. 2019; Abbott et al. 2020d).

Finally, we perform two complementary analyses involving time-frequency tracks in the data to provide further evidence for the presence of higher multipoles in the signal. In the first approach (also outlined in Abbott et al. 2020d, Section 4) we predict the time-frequency track of the dominant $(2, 2)$ multipole in the LIGO Livingston detector (as seen in Figure 1, middle panel) from an EOBNR HM parameter estimation analysis. This analysis collects energies along a time-frequency track which is $\alpha \times f_{22}(t)$, the $(2, 2)$ multipole's instantaneous frequency, where α is a dimensionless parameter (Roy et al. 2019; Abbott et al. 2020d). We find prominent

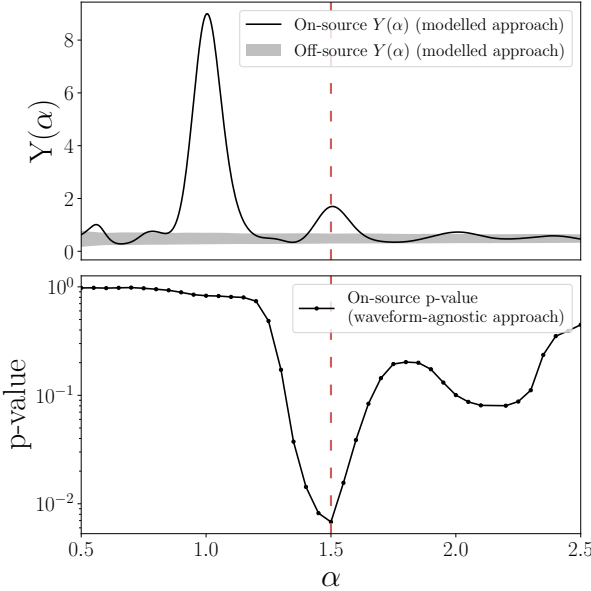


Figure 7. Top panel: Variation of $Y(\alpha)$, i.e., the energy in the pixels along the α -th track defined by $f_\alpha(t) = \alpha f_{22}(t)$, using the modelled approach. The peaks at $\alpha = 1$ and 1.5 indicate the energies in the $m = 2$ and $m = 3$ multipoles, respectively. The grey band indicates the 68% confidence interval on the off-source measurements of $Y(\alpha)$. Bottom panel: The variation of p-value of the on-source results, as a function of α , using the waveform-agnostic approach. The dip at $\alpha = 1.5$ is strong evidence of the presence of the $m = 3$ mode in the underlying signal. The red dashed line in both panels corresponds to general relativity's prediction of $\alpha = 1.5$ for the $m = 3$ mode.

peaks in $Y(\alpha)$, the energy in the pixels along the α -th track defined in Abbott et al. (2020d), at $\alpha = 1$ and 1.5 , as can be seen from the on-source curve in the top panel of Figure 7. These peaks correspond to the $m = 2$ and $m = 3$ multipole predictions in the data containing the signal (on-source data). We also compute a detection statistic β (Roy et al. 2019) of 11.18 for the presence of the $m = 3$ multipole with a p-value of $< 2.5 \times 10^{-4}$, compared to a background distribution estimated over 18 hours of data adjacent to the event (off-source data), where the largest background β is 6.88. The significant difference between on- and off-source values provides much stronger evidence for the presence of higher multipoles than what is reported for GW190412 (Abbott et al. 2020d).

The second analysis uses waveform-agnostic methods to reconstruct the signal. It then compares the observed coherent signal energy in the LIGO Hanford–LIGO Livingston–Virgo network of detectors, as identified by the cWB detection pipeline (Klimenko et al. 2016), with the predictions of a waveform model *without* higher multipoles (EOBNR; Prodi et al. 2020) to

investigate if the description of the underlying signal is incomplete if we do not include contributions from the $m = 3$ multipole in our waveform model. We compute a test statistic, the squared sum of the coherent residuals estimated over selected time–frequency tracks parameterized in terms of the same α parameter defined in the previous analysis (Roy et al. 2019; Abbott et al. 2020d). Each time–frequency track centered on α includes frequencies within $[\alpha - 0.1, \alpha + 0.1] \times f_{22}(t)$, and times within $[t_{\text{merger}} - 0.5 \text{ s}, t_{\text{merger}} - 0.03 \text{ s}]$, where $f_{22}(t)$ and t_{merger} correspond to the maximum likelihood template from the EOBNR parameter estimation analysis. We further compute a background distribution using simulated signals in off-source data (Prodi et al. 2020), and compute p-values for the on-source results as a function of α (Figure 7, bottom panel). We find a minimum p-value of 6.8×10^{-3} at $\alpha = 1.5$, providing strong evidence that the disagreement between the actual event and the EOBNR prediction is because of the absence of the $m = 3$ multipoles in the waveform model. The local minimum near $\alpha = 2$ is not an indication of the $m = 4$ multipoles, but rather a statistical fluctuation which is consistent with similar behaviour seen for studies with simulated signals described in detail in Prodi et al. (2020).

Although the two time–frequency analyses are similar in motivation, the latter differs from the former in that it is not restricted to data from just one detector, but rather uses the coherent signal energy across the three-detector network. Both analyses point to strong evidence for the presence of higher multipoles in the signal.

5. TESTS OF GENERAL RELATIVITY

GW190814 is the gravitational-wave event with the most unequal mass ratio to date, and can therefore be used to test general relativity (GR) in a region of parameter space previously unexplored with strong-field tests of GR (Abbott et al. 2016g, 2019e,d). The asymmetric nature of a system excites the higher multipole moments of the gravitational signal, which allows us to test the multipolar structure of gravity (Kastha et al. 2018, 2019; Dhanpal et al. 2019; Islam et al. 2020). The addition of information from the higher harmonics of a signal also breaks certain degeneracies in the description of the source, and could potentially enable us to place stronger constraints on certain deviations from GR (Van Den Broeck & Sengupta 2007b,a). We perform several null tests of GR using GW190814. These tests assume GW190814 is a (quasi-circular) BBH merger as described in GR, and look for inconsistencies between the observed signal and predictions of the theory. An incon-

sistency might arise from an incomplete understanding of the underlying signal (or noise), and could indicate a non-BBH nature of the signal or a potential departure from GR.

First, as a consistency test of the signal reconstruction, we subtract from the data the maximum likelihood compact binary coalescence waveforms, Phenom (Khan et al. 2016), Phenom HM (Kalaghatgi et al. 2019), Phenom PHM (Khan et al. 2020), and EOBNR PHM (Ossokine et al. 2020) and analyze 4 s of the resulting residual data centered around the time of merger with the morphology-independent transient analysis BAYESWAVE (Cornish & Littenberg 2015; Littenberg & Cornish 2015a). We measure the 90% credible upper limit on the coherent SNR, ρ_{90} , and compare it to the SNR, ρ_{90}^N , recovered by analyzing 175 randomly selected data segments in surrounding time (off-source data) with the same configuration settings. If the residual data are consistent with the noise, we expect ρ_{90} to be consistent with ρ_{90}^N . We compute the p-value by comparing the distribution of ρ_{90}^N to ρ_{90} through $p = P(\rho_{90}^N < \rho_{90})$. We obtain p-values of 0.59, 0.82, 0.82, and 0.75 for Phenom, Phenom HM, Phenom PHM, and EOBNR PHM, respectively. Hence, we find no evidence for deviations in the behavior of the residual data stream.

We also look for deviations in the spin-induced quadrupole moments of the binary components. According to the no-hair conjecture (Carter 1971; Hansen 1974) the multipole moments of a Kerr BH are completely described by its mass and spin angular momentum. At leading order in spin, the spin-induced quadrupole moment scalar is (Hartle 1967; Pappas & Apostolatos 2012), $Q = -\kappa a^2 m^3$, where (m, a) are the mass and dimensionless spin of the compact object, and κ is a dimensionless deformation parameter characterizing deviations in the spin-induced quadrupole moment. Kerr BHs have $\kappa = 1$ (Thorne 1980), while $\kappa \sim 2\text{--}14$ for NSs (depending on the equation of state) and $\kappa \sim 10\text{--}150$ for spinning boson stars with large self-interaction (Ryan 1997). The deformation parameter can even be negative for (slowly-rotating, thin-shelled) gravastars (Uchikata et al. 2016). Hence, an accurate measurement of κ sheds light onto the nature of the compact object. For compact binaries, the spin-induced quadrupole moment terms appear at second post-Newtonian order (Poisson 1998). For Kerr BHs in GR, $\kappa_1 = \kappa_2 = 1$, where κ_1, κ_2 are the individual deformation parameters of the primary and secondary compact objects in the binary. Since κ_1 and κ_2 are strongly degenerate in the gravitational waveform, we instead measure a linear symmetric combination of these quantities, $\kappa_s = (\kappa_1 + \kappa_2)/2$, which

is 1 for a BBH in GR. The posteriors on κ_s are relatively uninformative, and nearly span the prior range of $[0, 500]$, with increased support at $\kappa_s = 0$ relative to the prior. The upper bound of the prior was chosen to accommodate all the objects listed above. The result shows that GW190814 is consistent with having a BBH source described by GR. However, the broad posterior means that we cannot exclude the possibility that one or both components of the source is not a BH. We can attempt to understand this result in terms of the spin measurements for the binary. The measurements of κ_s and a non-zero χ_{eff} are highly correlated (Krishnendu et al. 2019), and for a system with small χ_{eff} the bounds on the measured value of κ_s are weak.

Finally, we investigate the source dynamics of the binary through a parameterized test of gravitational waveform generation, where we allow for the coefficients describing the post-Newtonian inspiral of a BBH coalescence to deviate away from their predictions in GR (Arun et al. 2006a,b; Yunes & Pretorius 2009; Mishra et al. 2010; Cornish et al. 2011; Li et al. 2012; Meidam et al. 2018). We use an aligned-spin EOB waveform without higher modes (EOBNR), and find no deviations in the post-Newtonian coefficients from their nominal values in GR. In summary, none of our tests of GR indicate any departure from the predictions of the theory, and GW190814 is consistent with the description of a compact binary merger in GR.

6. ASTROPHYSICAL IMPLICATIONS

The highly unequal mass ratio of $0.112^{+0.008}_{-0.009}$ and unusual secondary mass of $2.59^{+0.08}_{-0.09} M_\odot$ make the source of GW190814 unlike any other compact binary coalescence observed so far. The average mass ratio for BBH coalescences detected by the LVC during O1 and O2 is $\simeq 0.9$ (Roulet & Zaldarriaga 2019), and an inference of the underlying population predicted that 99% of detectable BBHs have mass ratios $q \geq 0.5$ (Fishbach & Holz 2020). However, the paucity of events from O1 and O2 means that this picture is limited. Indeed, the discovery of GW190412 has already changed the picture substantially (Abbott et al. 2020d).

GW190814's secondary mass lies in the hypothesized lower mass gap of $2.5\text{--}5 M_\odot$ (Bailyn et al. 1998; Özel et al. 2010; Farr et al. 2011; Özel et al. 2012) between known NSs and BHs. It is heavier than the most massive pulsar in the Galaxy (Cromartie et al. 2019), and almost certainly exceeds the mass of the $1.61\text{--}2.52 M_\odot$ primary component of GW190425, which is itself an outlier relative to the Galactic population of BNSs (Abbott et al. 2020a). On the other hand, it is comparable in mass to two BH candidates: the $\simeq 2.7 M_\odot$ merger rem-

nant of GW170817 (Abbott et al. 2019b) and the 2.6–6.1 M_{\odot} compact object (95% confidence interval) discovered by Thompson et al. (2019).² It is also comparable to the millisecond pulsar PSR J1748–2021B (Freire et al. 2008), whose mass is claimed as $2.74^{+0.21}_{-0.21} M_{\odot}$ at 68% confidence. However, this estimate, obtained via measurement of the periastron advance, could be inaccurate if the system inclination is low or the pulsar’s companion is rapidly rotating (Freire et al. 2008). In sum, it is not clear if GW190814’s secondary is a BH or a NS.

GW190814 poses a challenge for our understanding of the population of merging compact binaries. In what follows, we estimate the merger rate density of the compact binary subpopulation represented by this source, investigate the nature of its secondary component and possible implications for the NS equation of state, discuss how the system may have formed, and study its implications for cosmology.

6.1. Merger Rate Density

Given the unprecedented combination of component masses found in GW190814, we take the system to represent a new class of compact binary mergers, and use our analysis of its source properties to estimate a merger rate density for GW190814-like events. Following a method described in Kim et al. (2003), we calculate a simple, single-event rate density estimate \mathcal{R} according to our sensitivity to a population of systems drawn from the parameter-estimation posteriors. As in Abbott et al. (2020a), we calculate our surveyed space-time volume $\langle VT \rangle$ semi-analytically, imposing single-detector and network SNR thresholds of 5 and 10, respectively (Tiwari 2018). The semi-analytic $\langle VT \rangle$ for GW190814 is then multiplied by a calibration factor to match results from the search pipelines assuming a once-per-century FAR threshold. The sensitivity of a search pipeline is estimated using a set of simulated signals. For computational efficiency, this was done using pre-existing search pipeline simulations and the mass properties were not highly optimized. However, given that we are estimating a rate based on a single source, the calibration errors are much smaller than the statistical errors associated with the estimate. The simulated sources were uniformly distributed in comoving volume, component masses, and component spins aligned with the orbital angular momentum. For O1 and O2, the simulated BH mass range was 5–100 M_{\odot} , but for the first part of O3 we are analyzing here, the injected range was 2.5–

² See van den Heuvel & Tauris (2020) and Thompson et al. (2020) for discussion about the interpretation of this observation.

40 M_{\odot} (following our updated knowledge of the BH mass distribution); the NS mass range was 1–3 M_{\odot} , and component spins are < 0.95 . As GW190814 occurred when LIGO Hanford was not in nominal observing mode, it is not included in the production PyCBC results, and we use GstLAL results to calculate the merger rate.

We assume a Poisson likelihood over the astrophysical rate with a single count and we apply a Jeffreys $\mathcal{R}^{-1/2}$ prior to obtain rate posteriors. The analysis was done using samples from the Phenom PHM posterior and separately from the EOBNR PHM posterior, producing the same result in both cases. We find the merger rate density of GW190814-like systems to be 7^{+16}_{-6} Gpc $^{-3}$ yr $^{-1}$.

As a consistency check, we used the PyCBC search results to calculate an upper limit. Repeating the rate calculation with a PyCBC-based $\langle VT \rangle$ calibration and zero event count, we obtain an upper limit consistent (to within 10%) with the upper limit of the merger rate estimated using GstLAL search results. We conclude that the uncertainty in our estimate of the rate density for the class of mergers represented by GW190814 is primarily dominated by Poisson statistics.

6.2. Nature of the Secondary Component

The primary mass measurement of $23.2^{+1.1}_{-1.0} M_{\odot}$ securely identifies the heavier component of GW190814 as a BH, but the secondary mass of $2.59^{+0.08}_{-0.09} M_{\odot}$ may be compatible with either a NS or a BH depending on the maximum mass supported by the unknown NS equation of state (EOS). The source’s asymmetric masses, the non-detection of an electromagnetic counterpart and the lack of a clear signature of tides or spin-induced quadrupole effects in the waveform do not allow us to distinguish between a BBH or a NSBH. Instead, we rely on comparisons between m_2 and different estimates of the maximum NS mass, M_{\max} , to indicate the source classification preferred by data: if $m_2 > M_{\max}$, then the NSBH scenario is untenable.

While some candidate EOSs from nuclear theory can support nonrotating NSs with masses of up to $\sim 3 M_{\odot}$ (e.g., Müller & Serot 1996), such large values of M_{\max} are disfavored by the relatively small tidal deformabilities measured in GW170817 (Abbott et al. 2017a, 2019b), which correlate with smaller internal pressure gradients as a function of density and hence a lower threshold for gravitational collapse. By adopting a phenomenological model for the EOS, conditioning it on GW170817, and extrapolating the constraints to the high densities relevant for the maximum mass, Lim & Holt (2019) and Essick et al. (2020) place $M_{\max} \lesssim 2.3 M_{\odot}$. Similarly, the EOS inference reported in Abbott et al. (2018), based on an analysis of GW170817 with

a spectral parameterization (Lindblom 2010; Lindblom & Indik 2012, 2014) for the EOS, implies a 90% credible upper bound of $M_{\max} \leq 2.43 M_{\odot}$, with tenuous but non-zero posterior support beyond $2.6 M_{\odot}$. We calculate the corresponding M_{\max} posterior distribution, shown in the right panel of Figure 3, from the GW170817-informed spectral EOS samples used in Abbott et al. (2018) by reconstructing each EOS from its parameters and computing its maximum mass. Comparison with the m_2 posterior suggests that the secondary component of GW190814 is probably more massive than this prediction for M_{\max} : the posterior probability of $m_2 \leq M_{\max}$, marginalized over the uncertainty in m_2 and M_{\max} , is only 3%. Nevertheless, the maximum mass predictions from these kinds of EOS inferences come with important caveats: their extrapolations are sensitive to the phenomenological model assumed for the EOS; they use hard M_{\max} thresholds on the EOS prior to account for the existence of the heaviest Galactic pulsars, which is known to bias the inferred maximum mass distribution towards the threshold (Miller et al. 2020); and they predate the NICER observatory’s recent simultaneous mass and radius measurement for J0030+0451, which may increase the M_{\max} estimates by a few percent (Landry et al. 2020) because it favors slightly stiffer EOSs than GW170817 (Raaijmakers et al. 2019; Riley et al. 2019; Miller et al. 2019; Jiang et al. 2020).

NS mass measurements also inform bounds on M_{\max} independently of EOS assumptions. Fitting the known population of NSs in binaries to a double-Gaussian mass distribution with a high-mass cutoff, Alsing et al. (2018) obtained an empirical constraint of $M_{\max} \leq 2.6 M_{\odot}$ (one-sided 90% confidence interval). Farr & Chatziioannou (2020) recently updated this analysis to include PSR J0740+6620 (Cromartie et al. 2019), which had not been discovered at the time of the original study. Based on samples from the Farr & Chatziioannou (2020) maximum-mass posterior distribution, which is plotted in the right panel of Figure 3, we find $M_{\max} = 2.25^{+0.81}_{-0.26} M_{\odot}$. In this case, the posterior probability of $m_2 \leq M_{\max}$ is 29%, again favoring the $m_2 > M_{\max}$ scenario, albeit less strongly because of the distribution’s long tail up to $\sim 3 M_{\odot}$. However, the empirical M_{\max} prediction is sensitive to selection effects that could potentially bias it (Alsing et al. 2018). In particular, masses are only measurable for binary pulsars, and the mass distribution of isolated NSs could be different. Additionally, the discovery of GW190425 (Abbott et al. 2020a) should also be taken into account in the population when predicting M_{\max} .

Finally, the NS maximum mass is constrained by studies of the merger remnant of GW170817. Although no

postmerger gravitational waves were observed (Abbott et al. 2017g, 2019f), modeling of the associated kilonova (Abbott et al. 2017b; Kasen et al. 2017; Villar et al. 2017; Cowperthwaite et al. 2017; Abbott et al. 2017d) suggests that the merger remnant collapsed to a BH after a brief supramassive or hypermassive NS phase during which it was stabilized by uniform or differential rotation. Assuming this ultimate fate for the merger remnant immediately implies that no NS can be stable above $\sim 2.7 M_{\odot}$, but it places a more stringent constraint on NSs that are not rotationally supported. The precise mapping from the collapse threshold mass of the remnant to M_{\max} depends on the EOS, but by developing approximate prescriptions based on sequences of rapidly rotating stars for a range of candidate EOSs, M_{\max} has been bounded below approximately 2.2 – $2.3 M_{\odot}$ (Margalit & Metzger 2017; Rezzolla et al. 2018; Ruiz et al. 2018; Shibata et al. 2019; Abbott et al. 2020c). Although the degree of EOS uncertainty in these results is difficult to quantify precisely, if we take the more conservative $2.3 M_{\odot}$ bound at face value, then m_2 is almost certainly not a NS: the m_2 posterior distribution has negligible support below $2.3 M_{\odot}$.

Overall, these considerations suggest that GW190814 is probably not the product of a NSBH coalescence, despite its preliminary classification as such. Nonetheless, the possibility that the secondary component is a NS cannot be completely discounted due to the current uncertainty in M_{\max} .

There are two further caveats to this assessment. First, because the secondary’s spin is unconstrained, it could conceivably be rotating rapidly enough for m_2 to exceed M_{\max} without triggering gravitational collapse: rapid uniform rotation can stabilize a star up to $\sim 20\%$ more massive than the nonrotating maximum mass (Cook et al. 1994), in which case only the absolute upper bound of $\sim 2.7 M_{\odot}$ is relevant. However, it is very unlikely that a NSBH system could merge before dissipating such extreme natal NS spin angular momentum.

Second, our discussion has thus far neglected the possibility that the secondary component is an exotic compact object, such as a boson star (Kaup 1968) or a gravastar (Mazur & Mottola 2004), instead of a NS or a BH. Depending on the model, some exotic compact objects can potentially support masses up to and beyond $2.6 M_{\odot}$ (Cardoso & Pani 2019). Our analysis does not exclude this hypothesis for the secondary.

Since the NSBH scenario cannot be definitively ruled out, we examine GW190814’s potential implications for the NS EOS, assuming that the secondary proves to be a NS. This would require M_{\max} to be no less than m_2 , a condition that severely constrains the distribution of

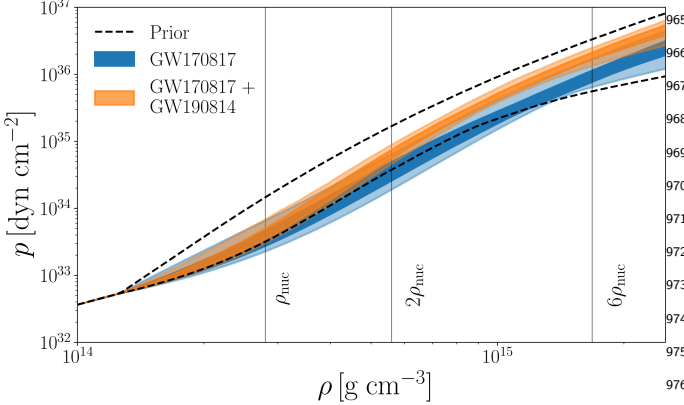


Figure 8. Constraints on the NS EOS assuming GW190814 was produced by a BBH (blue) or a NSBH (orange) coalescence. The 90% and 50% credible contours of the posterior in the pressure-density plane are shown. The constraints are calculated by assuming a spectral decomposition for the EOS, following Abbott et al. (2018). The BBH constraints are identical to those from the analysis of GW170817, while for the NSBH case the posterior is reweighted by the probability that each EOS’s maximum mass is at least m_2 . The dashed lines indicate the 90% credible region of the prior.

From a theoretical point of view, accurately calculating the masses of compact remnants at formation is challenging, because it depends on the complex physics of the supernova explosion and the details of stellar evolution, especially for the late evolutionary stages of massive stars (Janka 2012; Müller 2016; Burrows et al. 2018; Burrows et al. 2019). Whether the models favor the presence of a gap or a smooth transition between NSs and BHs is still unclear, and in fact some models have been developed with the purpose of reproducing this lower mass gap (Ugliano et al. 2012; Fryer et al. 2012; Kochanek 2014; Sukhbold & Woosley 2014; Ertl et al. 2016). Therefore, our robust discovery of an object with a well-constrained mass in this regime may provide crucial constraints on compact-object formation models. In fact, GW190814 demonstrates the need to adjust remnant mass prescriptions previously designed to produce a perceived mass gap. The combination of mass ratio and component masses challenges most results obtained from population synthesis simulations for isolated binaries (Dominik et al. 2012, 2015; Marchant et al. 2017; Giacobbo & Mapelli 2018; Mapelli & Giacobbo 2018; Kruckow et al. 2018; Neijssel et al. 2019; Mapelli et al. 2019; Spera et al. 2019; Olejak et al. 2020).

Population synthesis models distinguish between NSs and BHs using only a mass threshold, which is generally in the range $2\text{--}3 M_\odot$. Thus, depending on the adopted threshold and on the adopted supernova explosion model, a GW190814-like event may be labeled as either a NSBH merger or a BBH merger. Most BBH mergers have $q > 0.5$, while the distributions of merging NSBH binaries suggest that systems with $q \lesssim 0.1$ may be up to $\sim 10^3$ times less common than more symmetric ones ($q > 0.1$) and that the mass-ratio distribution peaks at $q \approx 0.2$. Furthermore, models tend to favor mergers of massive ($\gtrsim 1.3 M_\odot$) NSs with relatively small BHs ($\lesssim 15 M_\odot$) in environments with sub-solar metallicity ($Z \lesssim 0.5 Z_\odot$). The tendency to disfavor mergers with highly asymmetric masses in isolated binaries may be the consequence of mass transfer (e.g., Postnov & Yungelson 2014) and common envelope episodes (e.g., Ivanova et al. 2013) that cause systems with initially asymmetric masses to evolve towards more symmetric configurations. Overall, producing mergers with such unequal masses, with a secondary in the perceived mass gap, and at the rate implied by this discovery is a challenge for current models.

Nevertheless, particular choices of poorly constrained assumptions within rapid population synthesis models may increase the number of mergers with $q \lesssim 0.1$ so that the latter may be only a few times less common than (or even comparable to) systems with $q \simeq 0.2$ (e.g.,

EOSs compatible with existing astrophysical data. The combined constraints on the EOS from GW170817 and this hypothetical maximum mass information are shown in Figure 8. Specifically, we have taken the spectral EOS distribution conditioned on GW170817 from Abbott et al. (2018) and reweighted each EOS by the probability that its maximum mass is at least as large as m_2 . The updated posterior favors stiffer EOSs, which translates to larger radii for NSs of a given mass. The corresponding constraints on the radius and tidal deformability of a canonical $1.4 M_\odot$ NS are $R_{1.4} = 12.9^{+0.8}_{-0.7}$ km and $\Lambda_{1.4} = 616^{+273}_{-158}$.

6.3. Origins of GW190814-like Systems

The source of GW190814 represents a previously undetected class of coalescences that has the potential to shed light on the formation of merging compact-object binaries with highly asymmetric masses.

Electromagnetic observations of Galactic NSs and stellar-mass BHs suggest a dearth of compact objects in the $\sim 2.5 M_\odot$ to $5 M_\odot$ range (Bailyn et al. 1998; Özel et al. 2010; Farr et al. 2011; Özel et al. 2012). Observations of a few candidates with masses in this range seem to disfavor the existence of a gap (Freire et al. 2008; Neustroev et al. 2014; Giesers et al. 2018; Wyrzykowski & Mandel 2020; Thompson et al. 2019), but whether the mass gap is physical or caused by selection biases is still a matter of debate (e.g., Kreidberg et al. 2012).

1017 Eldridge & Stanway 2016; Eldridge et al. 2017; Giacobbo
 1018 & Mapelli 2018).

1019 Another possibility is that GW190814 is of dynamical
 1020 origin. Dynamical exchanges in dense stellar environments tend to pair up massive compact objects with
 1021 similar masses (e.g., Sigurdsson & Hernquist 1993). This
 1022 process is effective for globular clusters, where compact-
 1023 object binaries may undergo tens of exchanges before
 1024 they get ejected from the cluster (Portegies Zwart &
 1025 McMillan 2000; Rodriguez et al. 2016; Park et al. 2017;
 1026 Askar et al. 2017; Rodriguez et al. 2019). For such envi-
 1027 ronments, models predict that most merging BBHs have
 1028 $q \simeq 1$ (e.g., Rodriguez et al. 2016), and the formation
 1029 of NSBH binaries is highly suppressed because BHs dy-
 1030 namically dominate the cores over the complete lifetime
 1031 of the clusters, preventing the interactions between BHs
 1032 and NSs, with the consequence that the merger rate of
 1033 NSBH binaries in globular clusters in the local Universe
 1034 is $\sim 10^{-2} - 10^{-1} \text{ Gpc}^{-3} \text{ yr}^{-1}$ (Clausen et al. 2013; Ye et al.
 1035 2020; Arca Sedda 2020). The rate for GW190814-like
 1036 events, with a secondary in the perceived mass gap, is
 1037 likely even lower. In contrast, the NSBH merger rate
 1038 may be significantly higher in young star clusters (e.g.,
 1039 Ziosi et al. 2014) and the latter can effectively increase
 1040 the number of progenitors leading to merging compact-
 1041 object binaries with $q \lesssim 0.15$ (Di Carlo et al. 2019;
 1042 Rastello et al. 2020). Thus, young star clusters may
 1043 be promising hosts for GW190814-like events, but the
 1044 parameter space relevant for GW190814 is mostly unex-
 1045 plored in the context of star clusters.

1046 In dense stellar environments, GW190814-like sys-
 1047 tems may also form from a low-mass merger remnant
 1048 that acquires a BH companion via dynamical interac-
 1049 tions (Gupta et al. 2019). Gupta et al. (2019) pre-
 1050 dicts a population of second-generation BHs in the $2.2 -$
 1051 $3.8 M_{\odot}$ range, with a peak in the distribution at $2.6 M_{\odot}$,
 1052 assuming a double-Gaussian mass distribution for the
 1053 NSs. However, recent dynamical simulations of globular
 1054 clusters (e.g., Ye et al. 2020) find the subsequent merger
 1055 of such a second-generation BH with a larger stellar-
 1056 mass BH to be exceedingly rare. A high component spin
 1057 could be a distinguishing feature of a second-generation
 1058 compact object, but the uninformative spin posterior
 1059 for the lighter component of GW190814 provides no ev-
 1060 idence for or against this hypothesis.

1061 A GW190814-like merger may also have originated
 1062 from a hierarchical triple in the field (e.g., Silsbee &
 1063 Tremaine 2017; Fragione & Loeb 2019; Antonini et al.
 1064 2017), from a wide hierarchical quadruple system (Sa-
 1065 farzadeh et al. 2020), or from hierarchical triples in
 1066 galactic centers, where the tertiary body is a supermas-
 1067 sive BH (Antonini & Perets 2012; Stephan et al. 2019;

1068 Petrovich & Antonini 2017; Hoang et al. 2018; Fragione
 1069 et al. 2019). Specifically, Safarzadeh et al. (2020) ex-
 1070 plore the possibility that a second-generation remnant
 1071 with mass $3 M_{\odot}$ may merge with a $30 M_{\odot}$ BH, cata-
 1072 lyzed by a $50 M_{\odot}$ -BH perturber. The mass-ratio dis-
 1073 tributions of BBH and NSBH mergers from hierarchical
 1074 systems are similar to those of field binaries and it is
 1075 unclear whether hierarchies may enhance the formation
 1076 of merging compact-object binaries with highly asym-
 1077 metric masses (e.g., Silsbee & Tremaine 2017).

1078 Disks of gas around supermassive BHs in active galac-
 1079 tic nuclei may be promising environments for the forma-
 1080 tion of GW190814-like systems. For such environments,
 1081 theoretical models show that merging compact-object
 1082 binaries with asymmetric masses are likely, but cannot
 1083 necessarily accommodate masses as low as the secondary
 1084 mass of GW190814 (e.g., Yang et al. 2019). However,
 1085 McKernan et al. (2020) show that the median mass ratio
 1086 of NSBH mergers in active galactic nucleus disks may be
 1087 as low as ~ 0.07 .

1088 We conclude that the combination of masses, mass
 1089 ratio and inferred rate of GW190814 is challenging to
 1090 explain, but potentially consistent with multiple forma-
 1091 tion scenarios. However, it is not possible to assess the
 1092 validity of models that produce the right properties but
 1093 do not make quantitative predictions about formation
 1094 rates, even at some order-of-magnitude level.

1095 Young star clusters and active galactic nucleus disks
 1096 seem to be more promising hosts for GW190814-like
 1097 mergers, since both these environments may enhance
 1098 the formation of either progenitors of or directly merg-
 1099 ing compact-object binaries with more asymmetric
 1100 masses to relevant rates. In contrast, globular-cluster
 1101 models provide more robust predictions, showing that
 1102 GW190814-like mergers with such asymmetric masses
 1103 are outliers in the population predictions, even though a
 1104 revision of the remnant-mass prescription is still needed.
 1105 Isolated binaries binaries could prove possible progeni-
 1106 tors provided similar revisions are implemented. The
 1107 importance of field multiples remains to be fully ex-
 1108 plored. Future gravitational-wave observations will pro-
 1109 vide further insights into the dominance of different
 1110 channels.

1112 6.4. Cosmological Implications

1113 Luminosity distances inferred directly from observed
 1114 gravitational-wave events can be used with measure-
 1115 ments of source redshifts in the electromagnetic spec-
 1116 trum to constrain cosmological parameters (Schutz
 1117 1986). Redshifts can be either obtained directly from
 1118 counterparts to the gravitational-wave source (Holz &
 1119 Hughes 2005), as was the case for GW170817 (Ab-

bott et al. 2017a,b,e), by cross-correlation of the gravitational-wave localization posterior with catalogs of galaxy redshifts (Del Pozzo 2012; Nair et al. 2018; Chen et al. 2018; Fishbach et al. 2019; Gray et al. 2019; Soares-Santos et al. 2019; Abbott et al. 2019c), by exploiting information in the neutron star equation of state (Messenger & Read 2012), or by using the redshifted masses inferred from the gravitational wave observation and assumptions about the mass distribution of the sources (Chernoff & Finn 1993; Taylor et al. 2012; Taylor & Gair 2012; Farr et al. 2019). At current sensitivities, the cosmological parameter to which LIGO–Virgo observations are most sensitive is the Hubble constant, H_0 . The gravitational-wave observation of GW170817 provided a posterior on H_0 with mode and 68.3% highest posterior density interval of $H_0 = 69^{+22}_{-8} \text{ km s}^{-1} \text{ Mpc}^{-1}$ (Abbott et al. 2017e, 2019b,c), assuming a flat prior on H_0 .

GW190814 is the best localized dark siren, i.e., gravitational-wave source without an electromagnetic counterpart, observed to date, and so it is a good candidate for the statistical cross-correlation method. For a fixed reference cosmology (Ade et al. 2016), the GLADE galaxy catalog (Dálya et al. 2018) is approximately 40% complete at the distance of GW190814 and contains 472 galaxies within the 90% posterior credible volume of GW190814. To obtain a constrain on H_0 , we use the methodology described in Abbott et al. (2019c) and the GLADE catalog. We take a flat prior for $H_0 \in [20, 140] \text{ km s}^{-1} \text{ Mpc}^{-1}$ and assign a probability to each galaxy that it is the true host of the event that is proportional to its B-band luminosity. Using the posterior distribution on the distance obtained from the combined PHM samples, we obtain $H_0 = 75^{+59}_{-13} \text{ km s}^{-1} \text{ Mpc}^{-1}$ using GW190814 alone (mode and 68.3% highest posterior density interval; the median and 90% symmetric credible interval is $H_0 = 83^{+55}_{-53} \text{ km s}^{-1} \text{ Mpc}^{-1}$), which can be compared to $H_0 = 75^{+40}_{-32} \text{ km s}^{-1} \text{ Mpc}^{-1}$ (Soares-Santos et al. 2019) obtained using the dark siren GW170814 alone. The GW190814 result is the most precise measurement from a single dark siren observation to date, albeit comparable to the GW170814 result, which is expected given GW190814’s small localization volume ($\sim 39000 \text{ Mpc}^3$). The result is not very constraining, with the 68.3% highest posterior density interval comprising 60% of the prior range. Combining the result for GW190814 with the result obtained from GW170817, we see an improvement over the GW170817-only result, to $H_0 = 70^{+17}_{-8} \text{ km s}^{-1} \text{ Mpc}^{-1}$ (the median and 90% symmetric credible interval is $H_0 = 77^{+33}_{-23} \text{ km s}^{-1} \text{ Mpc}^{-1}$). This result is not yet sufficiently constraining to provide further insight into current tensions in low and high

redshift measurements of the Hubble constant (Verde et al. 2019), but these constraints will continue to improve as further gravitational-wave observations are included (e.g., projections in Chen et al. 2018; Vitale & Chen 2018; Gray et al. 2019; Feeney et al. 2019).

7. CONCLUSIONS

During their third observing run, on 2019 August 14, 21:10:39 UTC, the LIGO and Virgo detectors observed GW190814, a novel source unlike any other known compact binary coalescence. Thanks in part to the observation of significant power in subdominant multipoles of the gravitational radiation, and the conclusive measurement of little to no spin precession, we obtain precise measurements of its physical source properties that clearly set it apart from other compact binaries.

In particular, (a) its mass ratio of $q = 0.112^{+0.008}_{-0.009}$ is the most unequal ever observed with gravitational waves, (b) the bound $\chi_1 \leq 0.07$ on the spin of the $23.2^{+1.1}_{-1.0} M_\odot$ BH is the strongest constraint on a primary spin for any gravitational-wave source to date, and (c) the secondary mass measurement of $2.59^{+0.08}_{-0.09} M_\odot$ makes it the lightest BH or the heaviest NS discovered in a double compact-object system. We find no evidence of measurable tidal effects in the signal, and no electromagnetic counterpart to the gravitational waves has been identified.

Comparisons between the secondary mass and several current estimates of the maximum NS mass suggest that GW190814 is unlikely to originate in a NSBH coalescence. Nevertheless, the M_{\max} estimates are uncertain enough that improved knowledge of the NS EOS or further observations of the astrophysical population of compact objects could alter this assessment. For this reason, we cannot firmly exclude the possibility that the secondary is a NS, nor can we be certain that it is a BH. Regardless, this event sheds new light on the compact-object mass distribution at the interface between known NSs and BHs.

The unique combination of masses and inferred merger rate for this event is difficult to produce in population synthesis models of multi-component systems in galactic fields or dense stellar environments. The discovery of GW190814 may therefore reshape our understanding of the processes by which the lightest BHs or the most massive NSs form. Based on our rate density estimate, we may reasonably expect to detect more systems of this kind after a year at design sensitivity. This discovery may prove to be the first hint of a larger population that could change our perspective on the formation and mass spectrum of compact objects.

Segments of data containing the signal from all three interferometers, and samples from the posterior distributions for the source parameters, are available from the Gravitational Wave Open Science Center (<https://doi.org/10.7935/zzw5-ak90>). The software packages used in our analysis are open source.

The authors gratefully acknowledge the support of the United States National Science Foundation (NSF) for the construction and operation of the LIGO Laboratory and Advanced LIGO as well as the Science and Technology Facilities Council (STFC) of the United Kingdom, the Max-Planck-Society (MPS), and the State of Niedersachsen/Germany for support of the construction of Advanced LIGO and construction and operation of the GEO600 detector. Additional support for Advanced LIGO was provided by the Australian Research Council. The authors gratefully acknowledge the Italian Istituto Nazionale di Fisica Nucleare (INFN), the French Centre National de la Recherche Scientifique (CNRS) and the Netherlands Organization for Scientific Research, for the construction and operation of the Virgo detector and the creation and support of the EGO consortium.

The authors also gratefully acknowledge research support from these agencies as well as by the Council of Scientific and Industrial Research of India, the Department of Science and Technology, India, the Science & Engineering Research Board (SERB), India, the Ministry of Human Resource Development, India, the Spanish Agencia Estatal de Investigación, the Vicepresidència i Conselleria d'Innovació, Recerca i Turisme and the Conselleria d'Educació i Universitat del Govern de les Illes Balears, the Conselleria d'Innovació, Universitats, Ciència i Societat Digital de la Generalitat Valenciana and the CERCA Programme Generalitat de Catalunya, Spain, the National Science Centre of Poland, the Swiss National Science Foundation (SNSF), the Russian Foundation for Basic Research, the Russian Science Foundation, the European Commission, the European Regional Development Funds (ERDF), the Royal Society, the Scottish Funding Council, the Scottish Universities Physics Alliance, the Hungarian Scientific Research Fund (OTKA), the French Lyon Institute of Origins (LIO), the Belgian Fonds de la Recherche Scientifique (FRS-FNRS), Actions de Recherche Concertées (ARC) and Fonds Wetenschappelijk Onderzoek – Vlaanderen (FWO), Belgium, the Paris Île-de-France Region, the National Research, Development and Innovation Office

Hungary (NKFIH), the National Research Foundation of Korea, Industry Canada and the Province of Ontario through the Ministry of Economic Development and Innovation, the Natural Science and Engineering Research Council Canada, the Canadian Institute for Advanced Research, the Brazilian Ministry of Science, Technology, Innovations, and Communications, the International Center for Theoretical Physics South American Institute for Fundamental Research (ICTP-SAIFR), the Research Grants Council of Hong Kong, the National Natural Science Foundation of China (NSFC), the Leverhulme Trust, the Research Corporation, the Ministry of Science and Technology (MOST), Taiwan and the Kavli Foundation. The authors gratefully acknowledge the support of the NSF, STFC, INFN and CNRS for provision of computational resources. Some of the parameter estimation analyses presented in this paper were performed using the supercomputer cluster at the Swinburne University of Technology (OzSTAR and SSTAR).

We would like to thank all of the essential workers who put their health at risk during the COVID-19 pandemic, without whom we would not have been able to complete this work.

Software: The detection of the signal and subsequent significance evaluation were performed with the GSTLAL-based inspiral software pipeline (Cannon et al. 2012; Privitera et al. 2014; Messick et al. 2017; Sachdev et al. 2019; Hanna et al. 2020), built on the LALSUITE software library (LIGO Scientific Collaboration 2018), and with the PYCBC (Nitz et al. 2018, 2019; Usman et al. 2016) and MBTAONLINE (Adams et al. 2016) packages. Parameter estimation was performed with the LALINFERENCE (Veitch et al. 2015) and LALSIMULATION libraries within LALSUITE (LIGO Scientific Collaboration 2018), as well as the BILBY and PBILBY Libraries (Ashton et al. 2019; Smith & Ashton 2019) and the DYNESTY nested sampling package (Speagle 2020). Estimates of the noise spectra were obtained using BAYESWAVE (Cornish & Littenberg 2015; Littenberg & Cornish 2015b). Plots were prepared with Matplotlib (Hunter 2007). The sky map plot also used Astropy (<http://www.astropy.org>) a community-developed core Python package for Astronomy (Astropy Collaboration et al. 2013; Price-Whelan et al. 2018) and ligo.skymap (<https://lscsoft.docs.ligo.org/ligo.skymap>).

REFERENCES

- | | |
|--|--|
| <p>1316 Aasi, J., Abbott, B. P., Abbott, R., et al. 2015, CQGra, 32,
1317 074001, doi: 10.1088/0264-9381/32/7/074001</p> | <p>1318 Abbott, B. P., Abbott, R., Abbott, T. D., et al. 2016a,
1319 PhRvL, 116, 061102,
1320 doi: 10.1103/PhysRevLett.116.061102</p> |
|--|--|

- 1321 —. 2016b, PhRvX, 6, 041015,
 1322 doi: [10.1103/PhysRevX.6.041015](https://doi.org/10.1103/PhysRevX.6.041015)
- 1323 —. 2016c, CQGra, 33, 134001,
 1324 doi: [10.1088/0264-9381/33/13/134001](https://doi.org/10.1088/0264-9381/33/13/134001)
- 1325 —. 2016d, PhRvD, 93, 122003,
 1326 doi: [10.1103/PhysRevD.93.122003](https://doi.org/10.1103/PhysRevD.93.122003)
- 1327 —. 2016e, PhRvD, 93, 122004,
 1328 doi: [10.1103/PhysRevD.93.122004](https://doi.org/10.1103/PhysRevD.93.122004)
- 1329 —. 2016f, PhRvL, 116, 241102,
 1330 doi: [10.1103/PhysRevLett.116.241102](https://doi.org/10.1103/PhysRevLett.116.241102)
- 1331 —. 2016g, PhRvL, 116, 221101,
 1332 doi: [10.1103/PhysRevLett.116.221101](https://doi.org/10.1103/PhysRevLett.116.221101)
- 1333 —. 2017a, PhRvL, 119, 161101,
 1334 doi: [10.1103/PhysRevLett.119.161101](https://doi.org/10.1103/PhysRevLett.119.161101)
- 1335 —. 2017b, ApJL, 848, L12, doi: [10.3847/2041-8213/aa91c9](https://doi.org/10.3847/2041-8213/aa91c9)
- 1336 —. 2017c, ApJL, 848, L13, doi: [10.3847/2041-8213/aa920c](https://doi.org/10.3847/2041-8213/aa920c)
- 1337 —. 2017d, ApJL, 850, L39, doi: [10.3847/2041-8213/aa9478](https://doi.org/10.3847/2041-8213/aa9478)
- 1338 —. 2017e, Nat, 551, 85, doi: [10.1038/nature24471](https://doi.org/10.1038/nature24471)
- 1339 —. 2017f, ApJL, 851, L35, doi: [10.3847/2041-8213/aa9f0c](https://doi.org/10.3847/2041-8213/aa9f0c)
- 1340 —. 2017g, ApJL, 851, L16, doi: [10.3847/2041-8213/aa9a35](https://doi.org/10.3847/2041-8213/aa9a35)
- 1341 —. 2018, PhRvL, 121, 161101,
 1342 doi: [10.1103/PhysRevLett.121.161101](https://doi.org/10.1103/PhysRevLett.121.161101)
- 1343 —. 2019a, PhRvX, 9, 031040,
 1344 doi: [10.1103/PhysRevX.9.031040](https://doi.org/10.1103/PhysRevX.9.031040)
- 1345 —. 2019b, PhRvX, 9, 011001,
 1346 doi: [10.1103/PhysRevX.9.011001](https://doi.org/10.1103/PhysRevX.9.011001)
- 1347 —. 2019c, arXiv:1908.06060
- 1348 —. 2019d, PhRvL, 123, 011102,
 1349 doi: [10.1103/PhysRevLett.123.011102](https://doi.org/10.1103/PhysRevLett.123.011102)
- 1350 —. 2019e, PhRvD, 100, 104036,
 1351 doi: [10.1103/PhysRevD.100.104036](https://doi.org/10.1103/PhysRevD.100.104036)
- 1352 —. 2019f, ApJ, 875, 160, doi: [10.3847/1538-4357/ab0f3d](https://doi.org/10.3847/1538-4357/ab0f3d)
- 1353 —. 2020a, ApJL, 892, L3, doi: [10.3847/2041-8213/ab75f5](https://doi.org/10.3847/2041-8213/ab75f5)
- 1354 —. 2020b, arXiv:1304.0670v10
- 1355 —. 2020c, CQGra, 37, 045006,
 1356 doi: [10.1088/1361-6382/ab5f7c](https://doi.org/10.1088/1361-6382/ab5f7c)
- 1357 Abbott, R., Abbott, T. D., Abraham, S., et al. 2020d,
 1358 arXiv:2004.08342
- 1359 Accadia, T., Acernese, F., Antonucci, F., et al. 2010,
 1360 CQGra, 27, 194011,
 1361 doi: [10.1088/0264-9381/27/19/194011](https://doi.org/10.1088/0264-9381/27/19/194011)
- 1362 Acernese, F., Adams, T., Agatsuma, K., et al. 2018,
 1363 CQGra, 35, 205004, doi: [10.1088/1361-6382/aadf1a](https://doi.org/10.1088/1361-6382/aadf1a)
- 1364 Acernese, F., Agathos, M., Agatsuma, K., et al. 2015,
 1365 CQGra, 32, 024001, doi: [10.1088/0264-9381/32/2/024001](https://doi.org/10.1088/0264-9381/32/2/024001)
- 1366 Ackley, K., Amati, L., Barbieri, C., et al. 2020,
 1367 arXiv:2002.01950
- 1368 Adams, T., Buskulic, D., Germain, V., et al. 2016, CQGra,
 1369 33, 175012, doi: [10.1088/0264-9381/33/17/175012](https://doi.org/10.1088/0264-9381/33/17/175012)
- 1370 Ade, P. A. R., Aghanim, N., Arnaud, M., et al. 2016, A&A,
 1371 594, A13, doi: [10.1051/0004-6361/201525830](https://doi.org/10.1051/0004-6361/201525830)
- 1372 Ageron, M., Baret, B., Coleiro, A., et al. 2019, GCN,
 1373 25330. <https://gcn.gsfc.nasa.gov/gcn3/25330.gcn>
- 1374 Ajith, P., Fotopoulos, N., Privitera, S., Neunzert, A., &
 1375 Weinstein, A. J. 2014, PhRvD, 89, 084041,
 1376 doi: [10.1103/PhysRevD.89.084041](https://doi.org/10.1103/PhysRevD.89.084041)
- 1377 Ajith, P., Hannam, M., Husa, S., et al. 2011, PhRvL, 106,
 1378 241101, doi: [10.1103/PhysRevLett.106.241101](https://doi.org/10.1103/PhysRevLett.106.241101)
- 1379 Alsing, J., Silva, H. O., & Berti, E. 2018, MNRAS, 478,
 1380 1377, doi: [10.1093/mnras/sty1065](https://doi.org/10.1093/mnras/sty1065)
- 1381 Andreoni, I., Goldstein, D. A., Kasliwal, M. M., et al. 2020,
 1382 ApJ, 890, 131, doi: [10.3847/1538-4357/ab6a1b](https://doi.org/10.3847/1538-4357/ab6a1b)
- 1383 Antier, S., Agayeva, S., Aivazyan, V., et al. 2020, MNRAS,
 1384 492, 3904, doi: [10.1093/mnras/stz3142](https://doi.org/10.1093/mnras/stz3142)
- 1385 Antonini, F., & Perets, H. B. 2012, ApJ, 757, 27,
 1386 doi: [10.1088/0004-637X/757/1/27](https://doi.org/10.1088/0004-637X/757/1/27)
- 1387 Antonini, F., Toonen, S., & Hamers, A. S. 2017, ApJ, 841,
 1388 77, doi: [10.3847/1538-4357/aa6f5e](https://doi.org/10.3847/1538-4357/aa6f5e)
- 1389 Apostolatos, T. A., Cutler, C., Sussman, G. J., & Thorne,
 1390 K. S. 1994, PhRvD, 49, 6274,
 1391 doi: [10.1103/PhysRevD.49.6274](https://doi.org/10.1103/PhysRevD.49.6274)
- 1392 Arca Sedda, M. 2020, CmPhy, 3, 43,
 1393 doi: [10.1038/s42005-020-0310-x](https://doi.org/10.1038/s42005-020-0310-x)
- 1394 Arun, K. G., Buonanno, A., Faye, G., & Ochsner, E. 2009,
 1395 PhRvD, 79, 104023, doi: [10.1103/PhysRevD.79.104023](https://doi.org/10.1103/PhysRevD.79.104023)
- 1396 Arun, K. G., Iyer, B. R., Qusailah, M. S. S., &
 1397 Sathyaprakash, B. S. 2006a, PhRvD, 74, 024006,
 1398 doi: [10.1103/PhysRevD.74.024006](https://doi.org/10.1103/PhysRevD.74.024006)
- 1399 —. 2006b, CQGra, 23, L37–L43,
 1400 doi: [10.1088/0264-9381/23/9/101](https://doi.org/10.1088/0264-9381/23/9/101)
- 1401 Ashton, G., Hübner, M., Lasky, P. D., et al. 2019, ApJS,
 1402 241, 27, doi: [10.3847/1538-4365/ab06fc](https://doi.org/10.3847/1538-4365/ab06fc)
- 1403 Askar, A., Szkladarek, M., Gondek-Rosińska, D., Giersz,
 1404 M., & Bulik, T. 2017, MNRAS, 464, L36,
 1405 doi: [10.1093/mnrasl/slw177](https://doi.org/10.1093/mnrasl/slw177)
- 1406 Astropy Collaboration, Robitaille, T. P., Tollerud, E. J.,
 1407 et al. 2013, A&A, 558, A33,
 1408 doi: [10.1051/0004-6361/201322068](https://doi.org/10.1051/0004-6361/201322068)
- 1409 Babak, S., Taracchini, A., & Buonanno, A. 2017, PhRvD,
 1410 95, 024010, doi: [10.1103/PhysRevD.95.024010](https://doi.org/10.1103/PhysRevD.95.024010)
- 1411 Bailyn, C. D., Jain, R. K., Coppi, P., & Orosz, J. A. 1998,
 1412 ApJ, 499, 367, doi: [10.1086/305614](https://doi.org/10.1086/305614)
- 1413 Bailyn, C. D., Jain, R. K., Coppi, P., & Orosz, J. A. 1998,
 1414 ApJ, 499, 367, doi: [10.1086/305614](https://doi.org/10.1086/305614)
- 1415 Baird, E., Fairhurst, S., Hannam, M., & Murphy, P. 2013,
 1416 PhRvD, 87, 024035, doi: [10.1103/PhysRevD.87.024035](https://doi.org/10.1103/PhysRevD.87.024035)
- 1417 Blanchet, L. 2014, LRR, 17, 2, doi: [10.12942/lrr-2014-2](https://doi.org/10.12942/lrr-2014-2)

- 1418 Blanchet, L., Damour, T., Esposito-Farèse, G., & Iyer,
 1419 B. R. 2005, PhRvD, 71, 124004,
 1420 doi: [10.1103/PhysRevD.71.124004](https://doi.org/10.1103/PhysRevD.71.124004)
- 1421 Blanchet, L., Damour, T., Iyer, B. R., Will, C. M., &
 1422 Wiseman, A. G. 1995, PhRvL, 74, 3515,
 1423 doi: [10.1103/PhysRevLett.74.3515](https://doi.org/10.1103/PhysRevLett.74.3515)
- 1424 Blanchet, L., Faye, G., Iyer, B. R., & Sinha, S. 2008,
 1425 CQGra, 25, 165003, doi: [10.1088/0264-9381/25/16/165003](https://doi.org/10.1088/0264-9381/25/16/165003), [10.1088/0264-9381/29/23/239501](https://doi.org/10.1088/0264-9381/29/23/239501)
- 1426 Bohé, A., Shao, L., Taracchini, A., et al. 2017, PhRvD, 95,
 1427 044028, doi: [10.1103/PhysRevD.95.044028](https://doi.org/10.1103/PhysRevD.95.044028)
- 1428 Brown, D. A., Kumar, P., & Nitz, A. H. 2013, PhRvD, 87,
 1429 082004, doi: [10.1103/PhysRevD.87.082004](https://doi.org/10.1103/PhysRevD.87.082004)
- 1430 Buonanno, A., & Damour, T. 1999, PhRvD, 59, 084006,
 1431 doi: [10.1103/PhysRevD.59.084006](https://doi.org/10.1103/PhysRevD.59.084006)
- 1432 Buonanno, A., et al. 2003, PhRvD, 67, 104025, doi: [10.1103/PhysRevD.67.104025](https://doi.org/10.1103/PhysRevD.67.104025), [10.1103/PhysRevD.74.029904](https://doi.org/10.1103/PhysRevD.74.029904)
- 1433 Burrows, A., Radice, D., & Vartanyan, D. 2019, MNRAS,
 1434 485, 3153, doi: [10.1093/mnras/stz543](https://doi.org/10.1093/mnras/stz543)
- 1435 Burrows, A., Vartanyan, D., Dolence, J. C., Skinner, M. A.,
 1436 & Radice, D. 2018, SSRv, 214, 33,
 1437 doi: [10.1007/s11214-017-0450-9](https://doi.org/10.1007/s11214-017-0450-9)
- 1438 Cannon, K., Cariou, R., Chapman, A., et al. 2012, ApJ,
 1439 748, 136, doi: [10.1088/0004-637X/748/2/136](https://doi.org/10.1088/0004-637X/748/2/136)
- 1440 Capano, C., Dent, T., Hanna, C., et al. 2016a, PhRvD, 96,
 1441 082002, doi: [10.1103/PhysRevD.96.082002](https://doi.org/10.1103/PhysRevD.96.082002)
- 1442 Capano, C., Harry, I., Privitera, S., & Buonanno, A. 2016b,
 1443 PhRvD, 93, 124007, doi: [10.1103/PhysRevD.93.124007](https://doi.org/10.1103/PhysRevD.93.124007)
- 1444 Cardoso, V., & Pani, P. 2019, LRR, 22, 4,
 1445 doi: [10.1007/s41114-019-0020-4](https://doi.org/10.1007/s41114-019-0020-4)
- 1446 Carter, B. 1971, PhRvL, 26, 331,
 1447 doi: [10.1103/PhysRevLett.26.331](https://doi.org/10.1103/PhysRevLett.26.331)
- 1448 Chatterji, S., et al. 2004, CQGra, 21, S1809,
 1449 doi: [10.1088/0264-9381/21/20/024](https://doi.org/10.1088/0264-9381/21/20/024)
- 1450 Chen, H.-Y., Fishbach, M., & Holz, D. E. 2018, Nat, 562,
 1451 545, doi: [10.1038/s41586-018-0606-0](https://doi.org/10.1038/s41586-018-0606-0)
- 1452 Chernoff, D. F., & Finn, L. S. 1993, ApJL, 411, L5,
 1453 doi: [10.1086/186898](https://doi.org/10.1086/186898)
- 1454 Chornock, R., Berger, E., Kasen, D., et al. 2017, ApJL,
 1455 848, L19, doi: [10.3847/2041-8213/aa905c](https://doi.org/10.3847/2041-8213/aa905c)
- 1456 Clausen, D., Sigurdsson, S., & Chernoff, D. F. 2013,
 1457 MNRAS, 428, 3618, doi: [10.1093/mnras/sts295](https://doi.org/10.1093/mnras/sts295)
- 1458 Cokelaer, T. 2007, PhRvD, 76, 102004,
 1459 doi: [10.1103/PhysRevD.76.102004](https://doi.org/10.1103/PhysRevD.76.102004)
- 1460 Cook, G. B., Shapiro, S. L., & Teukolsky, S. A. 1994, ApJ,
 1461 424, 823, doi: [10.1086/173934](https://doi.org/10.1086/173934)
- 1462 Cornish, N., Sampson, L., Yunes, N., & Pretorius, F. 2011,
 1463 PhRvD, 84, 062003, doi: [10.1103/PhysRevD.84.062003](https://doi.org/10.1103/PhysRevD.84.062003)
- 1464 Cornish, N. J., & Littenberg, T. B. 2015, CQGra, 32,
 1465 135012, doi: [10.1088/0264-9381/32/13/135012](https://doi.org/10.1088/0264-9381/32/13/135012)
- 1466 Cotesta, R., Buonanno, A., Bohé, A., et al. 2018, PhRvD,
 1467 98, 084028, doi: [10.1103/PhysRevD.98.084028](https://doi.org/10.1103/PhysRevD.98.084028)
- 1468 Coughlin, M. W., Dietrich, T., Antier, S., et al. 2020,
 1469 MNRAS, 492, 863, doi: [10.1093/mnras/stz3457](https://doi.org/10.1093/mnras/stz3457)
- 1470 Cowperthwaite, P. S., Berger, E., Villar, V. A., et al. 2017,
 1471 ApJL, 848, L17, doi: [10.3847/2041-8213/aa8fc7](https://doi.org/10.3847/2041-8213/aa8fc7)
- 1472 Cromartie, H. T., Fonseca, E., Ransom, S. M., et al. 2019,
 1473 NatAs, 439, doi: [10.1038/s41550-019-0880-2](https://doi.org/10.1038/s41550-019-0880-2)
- 1474 Cutler, C., & Flanagan, E. E. 1994, PhRvD, 49, 2658,
 1475 doi: [10.1103/PhysRevD.49.2658](https://doi.org/10.1103/PhysRevD.49.2658)
- 1476 Dálya, G., Galgóczi, G., Dobos, L., et al. 2018, MNRAS,
 1477 479, 2374, doi: [10.1093/mnras/sty1703](https://doi.org/10.1093/mnras/sty1703)
- 1478 Damour, T. 2001, Phys. Rev., D64, 124013,
 1479 doi: [10.1103/PhysRevD.64.124013](https://doi.org/10.1103/PhysRevD.64.124013)
- 1480 Damour, T., Jaradowski, P., & Schäfer, G. 2001, PhLB,
 1481 513, 147, doi: [10.1016/S0370-2693\(01\)00642-6](https://doi.org/10.1016/S0370-2693(01)00642-6)
- 1482 Davies, G. S., Dent, T., Tápai, M., et al. 2020,
 1483 arXiv:[2002.08291](https://arxiv.org/abs/2002.08291)
- 1484 Del Pozzo, W. 2012, PhRvD, 86, 043011,
 1485 doi: [10.1103/PhysRevD.86.043011](https://doi.org/10.1103/PhysRevD.86.043011)
- 1486 Dhanpal, S., Ghosh, A., Mehta, A. K., Ajith, P., &
 1487 Sathyaprakash, B. 2019, PhRvD, 99,
 1488 doi: [10.1103/physrevd.99.104056](https://doi.org/10.1103/physrevd.99.104056)
- 1489 Di Carlo, U. N., Giacobbo, N., Mapelli, M., et al. 2019,
 1490 MNRAS, 487, 2947, doi: [10.1093/mnras/stz1453](https://doi.org/10.1093/mnras/stz1453)
- 1491 Dobie, D., Stewart, A., Murphy, T., et al. 2019, ApJL, 887,
 1492 L13, doi: [10.3847/2041-8213/ab59db](https://doi.org/10.3847/2041-8213/ab59db)
- 1493 Dominik, M., Belczynski, K., Fryer, C., et al. 2012, ApJ,
 1494 759, 52, doi: [10.1088/0004-637X/759/1/52](https://doi.org/10.1088/0004-637X/759/1/52)
- 1495 Dominik, M., Berti, E., O'Shaughnessy, R., et al. 2015,
 1496 ApJ, 806, 263, doi: [10.1088/0004-637X/806/2/263](https://doi.org/10.1088/0004-637X/806/2/263)
- 1497 Effler, A., Schofield, R. M. S., Frolov, V. V., et al. 2015,
 1498 CQGra, 32, 035017, doi: [10.1088/0264-9381/32/3/035017](https://doi.org/10.1088/0264-9381/32/3/035017)
- 1499 Eldridge, J. J., & Stanway, E. R. 2016, MNRAS, 462, 3302,
 1500 doi: [10.1093/mnras/stw1772](https://doi.org/10.1093/mnras/stw1772)
- 1501 Eldridge, J. J., Stanway, E. R., Xiao, L., et al. 2017, PASA,
 1502 34, e058, doi: [10.1017/pasa.2017.51](https://doi.org/10.1017/pasa.2017.51)
- 1503 Ertl, T., Janka, H. T., Woosley, S. E., Sukhbold, T., &
 1504 Ugliano, M. 2016, ApJ, 818, 124,
 1505 doi: [10.3847/0004-637X/818/2/124](https://doi.org/10.3847/0004-637X/818/2/124)
- 1506 Essick, R., Landry, P., & Holz, D. E. 2020, PhRvD, 101,
 1507 063007, doi: [10.1103/PhysRevD.101.063007](https://doi.org/10.1103/PhysRevD.101.063007)
- 1508 Fairhurst, S., et al. 2019a, arXiv:[1908.00555](https://arxiv.org/abs/1908.00555)
- 1509 —. 2019b, arXiv:[1908.05707](https://arxiv.org/abs/1908.05707)
- 1510 Farr, B., Berry, C. P. L., Farr, W. M., et al. 2016, ApJ,
 1511 825, 116, doi: [10.3847/0004-637X/825/2/116](https://doi.org/10.3847/0004-637X/825/2/116)
- 1512 Farr, W. M., & Chatzioannou, K. 2020, Research Notes of
 1513 the American Astronomical Society, 4, 65,
 1514 doi: [10.3847/2515-5172/ab9088](https://doi.org/10.3847/2515-5172/ab9088)

- 1517 Farr, W. M., Fishbach, M., Ye, J., & Holz, D. E. 2019,
 1518 ApJL, 883, L42, doi: [10.3847/2041-8213/ab4284](https://doi.org/10.3847/2041-8213/ab4284)
- 1519 Farr, W. M., Sravan, N., Cantrell, A., et al. 2011, ApJ, 741,
 1520 103, doi: [10.1088/0004-637X/741/2/103](https://doi.org/10.1088/0004-637X/741/2/103)
- 1521 Feeney, S. M., Peiris, H. V., Williamson, A. R., et al. 2019,
 1522 PhRvL, 122, 061105,
 1523 doi: [10.1103/PhysRevLett.122.061105](https://doi.org/10.1103/PhysRevLett.122.061105)
- 1524 Fishbach, M., Gray, R., Magaña Hernandez, I., Qi, H., &
 1525 Sur, A. 2019, ApJ, 871, L13,
 1526 doi: [10.3847/2041-8213/aaf96e](https://doi.org/10.3847/2041-8213/aaf96e)
- 1527 Fishbach, M., & Holz, D. E. 2020, ApJL, 891, L27,
 1528 doi: [10.3847/2041-8213/ab7247](https://doi.org/10.3847/2041-8213/ab7247)
- 1529 Flanagan, E. E., & Hinderer, T. 2008, PhRvD, 77, 021502,
 1530 doi: [10.1103/PhysRevD.77.021502](https://doi.org/10.1103/PhysRevD.77.021502)
- 1531 Foucart, F., Buchman, L., Duez, M. D., et al. 2013,
 1532 PhRvD, 88, 064017, doi: [10.1103/PhysRevD.88.064017](https://doi.org/10.1103/PhysRevD.88.064017)
- 1533 Fragione, G., Grishin, E., Leigh, N. W. C., Perets, H. B., &
 1534 Perna, R. 2019, MNRAS, 488, 47,
 1535 doi: [10.1093/mnras/stz1651](https://doi.org/10.1093/mnras/stz1651)
- 1536 Fragione, G., & Loeb, A. 2019, MNRAS, 486, 4443,
 1537 doi: [10.1093/mnras/stz1131](https://doi.org/10.1093/mnras/stz1131)
- 1538 Freire, P. C. C., Ransom, S. M., Bégin, S., et al. 2008, ApJ,
 1539 675, 670, doi: [10.1088/0004-637X/675/1/670](https://doi.org/10.1088/0004-637X/675/1/670)
- 1540 Fryer, C. L., Belczynski, K., Wiktorowicz, G., et al. 2012,
 1541 ApJ, 749, 91, doi: [10.1088/0004-637X/749/1/91](https://doi.org/10.1088/0004-637X/749/1/91)
- 1542 Giacobbo, N., & Mapelli, M. 2018, MNRAS, 480, 2011,
 1543 doi: [10.1093/mnras/sty1999](https://doi.org/10.1093/mnras/sty1999)
- 1544 Giesers, B., Dreizler, S., Husser, T.-O., et al. 2018,
 1545 MNRAS, 475, L15, doi: [10.1093/mnrasl/slx203](https://doi.org/10.1093/mnrasl/slx203)
- 1546 Gomez, S., Hosseinzadeh, G., Cowperthwaite, P. S., et al.
 1547 2019, ApJL, 884, L55, doi: [10.3847/2041-8213/ab4ad5](https://doi.org/10.3847/2041-8213/ab4ad5)
- 1548 Gray, R., Magaña Hernandez, I., Qi, H., et al. 2019,
 1549 arXiv:1908.06050
- 1550 Gupta, A., Gerosa, D., Arun, K. G., Berti, E., &
 1551 Sathyaprakash, B. S. 2019, arXiv:1909.05804
- 1552 Hanna, C., Caudill, S., Messick, C., et al. 2020, PhRvD,
 1553 101, 022003, doi: [10.1103/PhysRevD.101.022003](https://doi.org/10.1103/PhysRevD.101.022003)
- 1554 Hansen, R. O. 1974, JMP, 15, 46, doi: [10.1063/1.1666501](https://doi.org/10.1063/1.1666501)
- 1555 Harry, I., et al. 2014, PhRvD, 89, 024010,
 1556 doi: [10.1103/PhysRevD.89.024010](https://doi.org/10.1103/PhysRevD.89.024010)
- 1557 Harry, I. W., Allen, B., & Sathyaprakash, B. S. 2009,
 1558 PhRvD, 80, 104014, doi: [10.1103/PhysRevD.80.104014](https://doi.org/10.1103/PhysRevD.80.104014)
- 1559 Hartle, J. B. 1967, ApJ, 150, 1005, doi: [10.1086/149400](https://doi.org/10.1086/149400)
- 1560 Healy, J., & Lousto, C. O. 2017, PhRvD, 95, 024037,
 1561 doi: [10.1103/PhysRevD.95.024037](https://doi.org/10.1103/PhysRevD.95.024037)
- 1562 Hoang, B.-M., Naoz, S., Kocsis, B., Rasio, F. A., &
 1563 Dosopoulou, F. 2018, ApJ, 856, 140,
 1564 doi: [10.3847/1538-4357/aaafce](https://doi.org/10.3847/1538-4357/aaafce)
- 1565 Hofmann, F., Barausse, E., & Rezzolla, L. 2016, ApJL, 825,
 1566 L19, doi: [10.3847/2041-8205/825/2/L19](https://doi.org/10.3847/2041-8205/825/2/L19)
- 1567 Holz, D. E., & Hughes, S. A. 2005, ApJ, 629, 15,
 1568 doi: [10.1086/431341](https://doi.org/10.1086/431341)
- 1569 Hunter, J. D. 2007, CSE, 9, 90, doi: [10.1109/MCSE.2007.55](https://doi.org/10.1109/MCSE.2007.55)
- 1570 Husa, S., Khan, S., Hannam, M., et al. 2016, PhRvD, 93,
 1571 044006, doi: [10.1103/PhysRevD.93.044006](https://doi.org/10.1103/PhysRevD.93.044006)
- 1572 Indik, N., Fehrmann, H., Harke, F., Krishnan, B., &
 1573 Nielsen, A. B. 2018, PhRvD, 97, 124008,
 1574 doi: [10.1103/PhysRevD.97.124008](https://doi.org/10.1103/PhysRevD.97.124008)
- 1575 Islam, T., Mehta, A. K., Ghosh, A., et al. 2020, PhRvD,
 1576 101, doi: [10.1103/physrevd.101.024032](https://doi.org/10.1103/physrevd.101.024032)
- 1577 Ivanova, N., Justham, S., Chen, X., et al. 2013, A&A Rv,
 1578 21, 59, doi: [10.1007/s00159-013-0059-2](https://doi.org/10.1007/s00159-013-0059-2)
- 1579 Janka, H.-T. 2012, ARNPS, 62, 407,
 1580 doi: [10.1146/annurev-nucl-102711-094901](https://doi.org/10.1146/annurev-nucl-102711-094901)
- 1581 Jiang, J.-L., Tang, S.-P., Wang, Y.-Z., Fan, Y.-Z., & Wei,
 1582 D.-M. 2020, ApJ, 892, 55, doi: [10.3847/1538-4357/abf247](https://doi.org/10.3847/1538-4357/abf247)
- 1583 Jiménez-Forteza, X., Keitel, D., Husa, S., et al. 2017,
 1584 PhRvD, 95, 064024, doi: [10.1103/PhysRevD.95.064024](https://doi.org/10.1103/PhysRevD.95.064024)
- 1585 Johnson-McDaniel, N. K., et al. 2016, Determining the final
 1586 spin of a binary black hole system including in-plane
 1587 spins: Method and checks of accuracy, Tech. Rep.
 1588 LIGO-T1600168, LIGO Project.
 1589 <https://dcc.ligo.org/T1600168/public>
- 1590 Kalaghatgi, C., Hannam, M., & Raymond, V. 2019,
 1591 arXiv:1909.10010
- 1592 Kapadia, S. J., et al. 2020, CQGra, 37, 045007,
 1593 doi: [10.1088/1361-6382/ab5f2d](https://doi.org/10.1088/1361-6382/ab5f2d)
- 1594 Karki, S., Tuyenbayev, D., Kandhasamy, S., et al. 2016,
 1595 RSci, 87, 114503, doi: [10.1063/1.4967303](https://doi.org/10.1063/1.4967303)
- 1596 Kasen, D., Metzger, B., Barnes, J., Quataert, E., &
 1597 Ramirez-Ruiz, E. 2017, Nat, 551, 80,
 1598 doi: [10.1038/nature24453](https://doi.org/10.1038/nature24453)
- 1599 Kasliwal, M. M., Kasen, D., Lau, R. M., et al. 2019,
 1600 MNRAS, L14, doi: [10.1093/mnrasl/slz007](https://doi.org/10.1093/mnrasl/slz007)
- 1601 Kasprzack, M., & Yu, H. 2017, Beam Position from Angle
 1602 to Length minimization, Tech. Rep. LIGO-T1600397,
 1603 LIGO Project. <https://dcc.ligo.org/T1600397/public>
- 1604 Kastha, S., Gupta, A., Arun, K., Sathyaprakash, B., & Van
 1605 Den Broeck, C. 2018, PhRvD, 98,
 1606 doi: [10.1103/physrevd.98.124033](https://doi.org/10.1103/physrevd.98.124033)
- 1607 Kastha, S., Gupta, A., Arun, K. G., Sathyaprakash, B. S.,
 1608 & Van Den Broeck, C. 2019, PhRvD, 100, 044007,
 1609 doi: [10.1103/PhysRevD.100.044007](https://doi.org/10.1103/PhysRevD.100.044007)
- 1610 Kaup, D. J. 1968, PhRv, 172, 1331,
 1611 doi: [10.1103/PhysRev.172.1331](https://doi.org/10.1103/PhysRev.172.1331)
- 1612 Kawaguchi, K., Shibata, M., & Tanaka, M. 2020,
 1613 arXiv:2002.01662
- 1614 Khan, S., Chatzioannou, K., Hannam, M., & Ohme, F.
 1615 2019, PhRvD, 100, 024059,
 1616 doi: [10.1103/PhysRevD.100.024059](https://doi.org/10.1103/PhysRevD.100.024059)

- 1617 Khan, S., Husa, S., Hannam, M., et al. 2016, PhRvD, 93,
 1618 044007, doi: [10.1103/PhysRevD.93.044007](https://doi.org/10.1103/PhysRevD.93.044007)
- 1619 Khan, S., Ohme, F., Chatzioannou, K., & Hannam, M.
 1620 2020, PhRvD, 101, 024056,
 1621 doi: [10.1103/PhysRevD.101.024056](https://doi.org/10.1103/PhysRevD.101.024056)
- 1622 Kidder, L. E. 2008, PhRvD, 77, 044016,
 1623 doi: [10.1103/PhysRevD.77.044016](https://doi.org/10.1103/PhysRevD.77.044016)
- 1624 Kim, C., Kalogera, V., & Lorimer, D. R. 2003, ApJ, 584,
 1625 985, doi: [10.1086/345740](https://doi.org/10.1086/345740)
- 1626 Klimenko, S., et al. 2008, CQGra, 25, 114029
 1627 —. 2016, PhRvD, 93, 042004,
 1628 doi: [10.1103/PhysRevD.93.042004](https://doi.org/10.1103/PhysRevD.93.042004)
- 1629 Kochanek, C. S. 2014, ApJ, 785, 28,
 1630 doi: [10.1088/0004-637X/785/1/28](https://doi.org/10.1088/0004-637X/785/1/28)
- 1631 Kreidberg, L., Bailyn, C. D., Farr, W. M., & Kalogera, V.
 1632 2012, ApJ, 757, 36, doi: [10.1088/0004-637X/757/1/36](https://doi.org/10.1088/0004-637X/757/1/36)
- 1633 Krishnendu, N. V., Saleem, M., Samajdar, A., et al. 2019,
 1634 PhRvD, 100, 104019, doi: [10.1103/PhysRevD.100.104019](https://doi.org/10.1103/PhysRevD.100.104019)
- 1635 Kruckow, M. U., Tauris, T. M., Langer, N., Kramer, M., &
 1636 Izzard, R. G. 2018, MNRAS, 481, 1908,
 1637 doi: [10.1093/mnras/sty2190](https://doi.org/10.1093/mnras/sty2190)
- 1638 Kumar, P., Pürrer, M., & Pfeiffer, H. P. 2017, PhRvD, 95,
 1639 044039, doi: [10.1103/PhysRevD.95.044039](https://doi.org/10.1103/PhysRevD.95.044039)
- 1640 Kumar, P., Blackman, J., Field, S. E., et al. 2019, PhRvD,
 1641 99, 124005, doi: [10.1103/PhysRevD.99.124005](https://doi.org/10.1103/PhysRevD.99.124005)
- 1642 Landry, P., Essick, R., & Chatzioannou, K. 2020,
 1643 arXiv:2003.04880
- 1644 Li, T. G. F., Del Pozzo, W., Vitale, S., et al. 2012, PhRvD,
 1645 85, 082003, doi: [10.1103/PhysRevD.85.082003](https://doi.org/10.1103/PhysRevD.85.082003)
- 1646 LIGO Scientific Collaboration. 2018, LIGO Algorithm
 1647 Library, doi: [10.7935/GT1W-FZ16](https://doi.org/10.7935/GT1W-FZ16)
- 1648 LIGO Scientific Collaboration, Virgo Collaboration. 2019a,
 1649 GCN. https://gcn.gsfc.nasa.gov/notices_1/S190814bv.lvc
- 1650 —. 2019b, Public Alerts User Guide.
<https://emfollow.docs.ligo.org/userguide/content.html>
- 1651 —. 2019c, GraceDB, S190814bv.
<https://gracedb.ligo.org/superevents/S190814bv/>
- 1652 —. 2019d, GCN, 25324.
<https://gcn.gsfc.nasa.gov/other/GW190814bv.gcn3>
- 1653 —. 2019e, GCN, 25333.
<https://gcn.gsfc.nasa.gov/gcn3/25333.gcn3>
- 1654 Lim, Y., & Holt, J. W. 2019, EPJA, 55, 209,
 1655 doi: [10.1140/epja/i2019-12917-9](https://doi.org/10.1140/epja/i2019-12917-9)
- 1656 Lindblom, L. 2010, PhRvD, 82, 103011,
 1657 doi: [10.1103/PhysRevD.82.103011](https://doi.org/10.1103/PhysRevD.82.103011)
- 1658 Lindblom, L., & Indik, N. M. 2012, PhRvD, 86, 084003,
 1659 doi: [10.1103/PhysRevD.86.084003](https://doi.org/10.1103/PhysRevD.86.084003)
- 1660 —. 2014, PhRvD, 89, 064003,
 1661 doi: [10.1103/PhysRevD.89.064003](https://doi.org/10.1103/PhysRevD.89.064003)
- 1662 Lipunov, V., Gorbovskoy, E., Kornilov, V., et al. 2019,
 1663 GCN, 25354.
<https://gcn.gsfc.nasa.gov/gcn3/25354.gcn3>
- 1664 Littenberg, T. B., & Cornish, N. J. 2015a, PhRvD, 91,
 1665 084034, doi: [10.1103/PhysRevD.91.084034](https://doi.org/10.1103/PhysRevD.91.084034)
- 1666 —. 2015b, PhRvD, 91, 084034,
 1667 doi: [10.1103/PhysRevD.91.084034](https://doi.org/10.1103/PhysRevD.91.084034)
- 1668 London, L., Khan, S., Fauchon-Jones, E., et al. 2018,
 1669 PhRvL., 120, 161102,
 1670 doi: [10.1103/PhysRevLett.120.161102](https://doi.org/10.1103/PhysRevLett.120.161102)
- 1671 Mapelli, M., & Giacobbo, N. 2018, MNRAS, 479, 4391,
 1672 doi: [10.1093/mnras/sty1613](https://doi.org/10.1093/mnras/sty1613)
- 1673 Mapelli, M., Giacobbo, N., Santoliquido, F., & Artale,
 1674 M. C. 2019, MNRAS, doi: [10.1093/mnras/stz1150](https://doi.org/10.1093/mnras/stz1150)
- 1675 Marchant, P., Langer, N., Podsiadlowski, P., et al. 2017,
 1676 A&A, 604, A55, doi: [10.1051/0004-6361/201630188](https://doi.org/10.1051/0004-6361/201630188)
- 1677 Margalit, B., & Metzger, B. D. 2017, ApJL, 850, L19,
 1678 doi: [10.3847/2041-8213/aa991c](https://doi.org/10.3847/2041-8213/aa991c)
- 1679 Matas, A., et al. 2020, arXiv:2004.10001
- 1680 Mazur, P. O., & Mottola, E. 2004, PNAS, 101, 9545,
 1681 doi: [10.1073/pnas.0402717101](https://doi.org/10.1073/pnas.0402717101)
- 1682 McKernan, B., Ford, K. E. S., & O’Shaughnessy, R. 2020,
 1683 arXiv:2002.00046
- 1684 Meidam, J., Tsang, K. W., Goldstein, J., et al. 2018,
 1685 PhRvD, 97, 044033, doi: [10.1103/PhysRevD.97.044033](https://doi.org/10.1103/PhysRevD.97.044033)
- 1686 Messenger, C., & Read, J. 2012, PhRvL, 108, 091101,
 1687 doi: [10.1103/PhysRevLett.108.091101](https://doi.org/10.1103/PhysRevLett.108.091101)
- 1688 Messick, C., Blackburn, K., Brady, P., et al. 2017, PhRvD,
 1689 95, 042001, doi: [10.1103/PhysRevD.95.042001](https://doi.org/10.1103/PhysRevD.95.042001)
- 1690 Miller, M. C., Chirenti, C., & Lamb, F. K. 2020, ApJ, 888,
 1691 12, doi: [10.3847/1538-4357/ab4ef9](https://doi.org/10.3847/1538-4357/ab4ef9)
- 1692 Miller, M. C., Lamb, F. K., Dittmann, A. J., et al. 2019,
 1693 ApJL, 887, L24, doi: [10.3847/2041-8213/ab50c5](https://doi.org/10.3847/2041-8213/ab50c5)
- 1694 Mills, J. C., & Fairhurst, S. 2020, Measuring
 1695 gravitational-wave subdominant multipoles, Tech. Rep.
 1696 <https://dcc.ligo.org/P2000136/public>
- 1697 Mishra, C. K., Arun, K. G., Iyer, B. R., & Sathyaprakash,
 1698 B. S. 2010, PhRvD, 82, 064010,
 1699 doi: [10.1103/PhysRevD.82.064010](https://doi.org/10.1103/PhysRevD.82.064010)
- 1700 Mishra, C. K., Kela, A., Arun, K. G., & Faye, G. 2016,
 1701 PhRvD, 93, 084054, doi: [10.1103/PhysRevD.93.084054](https://doi.org/10.1103/PhysRevD.93.084054)
- 1702 Müller, B. 2016, PASA, 33, e048, doi: [10.1017/pasa.2016.40](https://doi.org/10.1017/pasa.2016.40)
- 1703 Müller, H., & Serot, B. D. 1996, NuPhA, 606, 508,
 1704 doi: [10.1016/0375-9474\(96\)00187-X](https://doi.org/10.1016/0375-9474(96)00187-X)
- 1705 Nair, R., Bose, S., & Saini, T. D. 2018, PhRvD, 98, 023502,
 1706 doi: [10.1103/PhysRevD.98.023502](https://doi.org/10.1103/PhysRevD.98.023502)
- 1707 Neijssel, C. J., Vigna-Gómez, A., Stevenson, S., et al. 2019,
 1708 MNRAS, 490, 3740, doi: [10.1093/mnras/stz2840](https://doi.org/10.1093/mnras/stz2840)

- 1715 Neustroev, V. V., Veledina, A., Poutanen, J., et al. 2014,
 1716 MNRAS, 445, 2424, doi: [10.1093/mnras/stu1924](https://doi.org/10.1093/mnras/stu1924)
- 1717 Ng, K. K. Y., Vitale, S., Zimmerman, A., et al. 2018,
 1718 PhRvD, 98, 083007, doi: [10.1103/PhysRevD.98.083007](https://doi.org/10.1103/PhysRevD.98.083007)
- 1719 Nitz, A., Harry, I., Brown, D., et al. 2019, gwastro/pycbc:
 1720 PyCBC Release v1.15.2, doi: [10.5281/zenodo.3596447](https://doi.org/10.5281/zenodo.3596447)
- 1721 Nitz, A. H., Dal Canton, T., Davis, D., & Reyes, S. 2018,
 1722 PhRvD, 98, 024050, doi: [10.1103/PhysRevD.98.024050](https://doi.org/10.1103/PhysRevD.98.024050)
- 1723 Nitz, A. H., Dent, T., Dal Canton, T., Fairhurst, S., &
 1724 Brown, D. A. 2017, arXiv:[1705.01513](https://arxiv.org/abs/1705.01513)
- 1725 Nitz, A. H., Dent, T., Davies, G. S., et al. 2020, ApJ, 891,
 1726 123, doi: [10.3847/1538-4357/ab733f](https://doi.org/10.3847/1538-4357/ab733f)
- 1727 Nuttall, L. K. 2018, RSPTA, 376, 20170286,
 1728 doi: [10.1098/rsta.2017.0286](https://doi.org/10.1098/rsta.2017.0286)
- 1729 Olejak, A., Belczynski, K., Holz, D. E., et al. 2020,
 1730 arXiv:[2004.11866](https://arxiv.org/abs/2004.11866)
- 1731 Ossokine, S., et al. 2020, arXiv:[2004.09442](https://arxiv.org/abs/2004.09442)
- 1732 Owen, B. J. 1996, PhRvD, 53, 6749,
 1733 doi: [10.1103/PhysRevD.53.6749](https://doi.org/10.1103/PhysRevD.53.6749)
- 1734 Owen, B. J., & Sathyaprakash, B. S. 1999, PhRvD, 60,
 1735 022002, doi: [10.1103/PhysRevD.60.022002](https://doi.org/10.1103/PhysRevD.60.022002)
- 1736 Özel, F., Psaltis, D., Narayan, R., & McClintock, J. E.
 1737 2010, ApJ, 725, 1918,
 1738 doi: [10.1088/0004-637X/725/2/1918](https://doi.org/10.1088/0004-637X/725/2/1918)
- 1739 Özel, F., Psaltis, D., Narayan, R., & Villarreal, A. S. 2012,
 1740 ApJ, 757, 55, doi: [10.1088/0004-637X/757/1/55](https://doi.org/10.1088/0004-637X/757/1/55)
- 1741 Pappas, G., & Apostolatos, T. A. 2012, PhRvL, 108,
 1742 231104, doi: [10.1103/PhysRevLett.108.231104](https://doi.org/10.1103/PhysRevLett.108.231104)
- 1743 Park, D., Kim, C., Lee, H. M., Bae, Y.-B., & Belczynski, K.
 1744 2017, MNRAS, 469, 4665, doi: [10.1093/mnras/stx1015](https://doi.org/10.1093/mnras/stx1015)
- 1745 Payne, E., Talbot, C., & Thrane, E. 2019, PhRvD, 100,
 1746 123017, doi: [10.1103/PhysRevD.100.123017](https://doi.org/10.1103/PhysRevD.100.123017)
- 1747 Petrovich, C., & Antonini, F. 2017, ApJ, 846, 146,
 1748 doi: [10.3847/1538-4357/aa8628](https://doi.org/10.3847/1538-4357/aa8628)
- 1749 Poisson, E. 1998, PhRvD, 57, 5287,
 1750 doi: [10.1103/PhysRevD.57.5287](https://doi.org/10.1103/PhysRevD.57.5287)
- 1751 Poisson, E., & Will, C. M. 1995, PhRvD, 52, 848,
 1752 doi: [10.1103/PhysRevD.52.848](https://doi.org/10.1103/PhysRevD.52.848)
- 1753 Portegies Zwart, S. F., & McMillan, S. L. W. 2000, ApJL,
 1754 528, L17, doi: [10.1086/312422](https://doi.org/10.1086/312422)
- 1755 Postnov, K. A., & Yungelson, L. R. 2014, LRR, 17, 3,
 1756 doi: [10.12942/lrr-2014-3](https://doi.org/10.12942/lrr-2014-3)
- 1757 Price-Whelan, A. M., Sipőcz, B. M., Günther, H. M., et al.
 1758 2018, AJ, 156, 123, doi: [10.3847/1538-3881/aabc4f](https://doi.org/10.3847/1538-3881/aabc4f)
- 1759 Privitera, S., Mohapatra, S. R. P., Ajith, P., et al. 2014,
 1760 PhRvD, 89, 024003, doi: [10.1103/PhysRevD.89.024003](https://doi.org/10.1103/PhysRevD.89.024003)
- 1761 Prodi, G., Vedovato, G., Drago, M., et al. 2020, Technical
 1762 note on the measurement of inspiral higher order modes
 1763 by coherent WaveBurst in GW190814, Tech. Rep.
 1764 LIGO-T2000124, LIGO Project.
<https://dcc.ligo.org/T2000124/public>
- 1765 Pürrer, M. 2016, PhRvD, 93, 064041,
 1766 doi: [10.1103/PhysRevD.93.064041](https://doi.org/10.1103/PhysRevD.93.064041)
- 1767 Raaijmakers, G., Riley, T. E., Watts, A. L., et al. 2019,
 1768 ApJL, 887, L22, doi: [10.3847/2041-8213/ab451a](https://doi.org/10.3847/2041-8213/ab451a)
- 1769 Racine, E. 2008, PhRvD, 78, 044021,
 1770 doi: [10.1103/PhysRevD.78.044021](https://doi.org/10.1103/PhysRevD.78.044021)
- 1771 Rastello, S., Mapelli, M., Di Carlo, U. N., et al. 2020,
 1772 arXiv:[2003.02277](https://arxiv.org/abs/2003.02277)
- 1773 Rezzolla, L., Most, E. R., & Weih, L. R. 2018, ApJL, 852,
 1774 L25, doi: [10.3847/2041-8213/aaa401](https://doi.org/10.3847/2041-8213/aaa401)
- 1775 Riley, T. E., Watts, A. L., Bogdanov, S., et al. 2019, ApJL,
 1776 887, L21, doi: [10.3847/2041-8213/ab481c](https://doi.org/10.3847/2041-8213/ab481c)
- 1777 Rodriguez, C. L., Chatterjee, S., & Rasio, F. A. 2016,
 1778 PhRvD, 93, 084029, doi: [10.1103/PhysRevD.93.084029](https://doi.org/10.1103/PhysRevD.93.084029)
- 1779 Rodriguez, C. L., Zevin, M., Amaro-Seoane, P., et al. 2019,
 1780 PhRvD, 100, 043027, doi: [10.1103/PhysRevD.100.043027](https://doi.org/10.1103/PhysRevD.100.043027)
- 1781 Rosswog, S., Sollerman, J., Feindt, U., et al. 2018, A&A,
 1782 615, A132, doi: [10.1051/0004-6361/201732117](https://doi.org/10.1051/0004-6361/201732117)
- 1783 Roulet, J., & Zaldarriaga, M. 2019, MNRAS, 484, 4216,
 1784 doi: [10.1093/mnras/stz226](https://doi.org/10.1093/mnras/stz226)
- 1785 Roy, S., Sengupta, A. S., & Ajith, P. 2019, PhRvD, 99,
 1786 024048, doi: [10.1103/PhysRevD.99.024048](https://doi.org/10.1103/PhysRevD.99.024048)
- 1787 Roy, S., Sengupta, A. S., & Arun, K. G. 2019,
 1788 arXiv:[1910.04565](https://arxiv.org/abs/1910.04565)
- 1789 Roy, S., Sengupta, A. S., & Thakor, N. 2017, PhRvD, 95,
 1790 104045, doi: [10.1103/PhysRevD.95.104045](https://doi.org/10.1103/PhysRevD.95.104045)
- 1791 Ruiz, M., Shapiro, S. L., & Tsokaros, A. 2018, PhRvD, 97,
 1792 021501, doi: [10.1103/PhysRevD.97.021501](https://doi.org/10.1103/PhysRevD.97.021501)
- 1793 Ryan, F. D. 1997, PhRvD, 55, 6081,
 1794 doi: [10.1103/PhysRevD.55.6081](https://doi.org/10.1103/PhysRevD.55.6081)
- 1795 Sachdev, S., Caudill, S., Fong, H., et al. 2019,
 1796 arXiv:[1901.08580](https://arxiv.org/abs/1901.08580)
- 1797 Safarzadeh, M., Hamers, A. S., Loeb, A., & Berger, E.
 1798 2020, ApJL, 888, L3, doi: [10.3847/2041-8213/ab5dc8](https://doi.org/10.3847/2041-8213/ab5dc8)
- 1799 Santamaría, L., Ohme, F., Ajith, P., et al. 2010, PhRvD,
 1800 82, 064016, doi: [10.1103/PhysRevD.82.064016](https://doi.org/10.1103/PhysRevD.82.064016)
- 1801 Sathyaprakash, B., & Dhurandhar, S. 1991, PhRvD, 44,
 1802 3819, doi: [10.1103/PhysRevD.44.3819](https://doi.org/10.1103/PhysRevD.44.3819)
- 1803 Schmidt, P., Ohme, F., & Hannam, M. 2015, PhRvD, 91,
 1804 024043, doi: [10.1103/PhysRevD.91.024043](https://doi.org/10.1103/PhysRevD.91.024043)
- 1805 Schutz, B. F. 1986, Nat, 323, 310, doi: [10.1038/323310a0](https://doi.org/10.1038/323310a0)
- 1806 Shibata, M., Zhou, E., Kiuchi, K., & Fujibayashi, S. 2019,
 1807 PhRvD, 100, 023015, doi: [10.1103/PhysRevD.100.023015](https://doi.org/10.1103/PhysRevD.100.023015)
- 1808 Sigurdsson, S., & Hernquist, L. 1993, Nat, 364, 423,
 1809 doi: [10.1038/364423a0](https://doi.org/10.1038/364423a0)
- 1810

- 1811 Silsbee, K., & Tremaine, S. 2017, ApJ, 836, 39,
 1812 doi: [10.3847/1538-4357/aa5729](https://doi.org/10.3847/1538-4357/aa5729)
- 1813 Singer, L. P., & Price, L. 2016, PhRvD, 93, 024013,
 1814 doi: [10.1103/PhysRevD.93.024013](https://doi.org/10.1103/PhysRevD.93.024013)
- 1815 Smith, R., & Ashton, G. 2019, arXiv:[1909.11873](https://arxiv.org/abs/1909.11873)
- 1816 Soares-Santos, M., Palmese, A., Hartley, W., et al. 2019,
 1817 ApJL, 876, L7, doi: [10.3847/2041-8213/ab14f1](https://doi.org/10.3847/2041-8213/ab14f1)
- 1818 Speagle, J. S. 2020, MNRAS, 493, 3132–3158,
 1819 doi: [10.1093/mnras/staa278](https://doi.org/10.1093/mnras/staa278)
- 1820 Spera, M., Mapelli, M., Giacobbo, N., et al. 2019, MNRAS,
 1821 485, 889, doi: [10.1093/mnras/stz359](https://doi.org/10.1093/mnras/stz359)
- 1822 Stephan, A. P., Naoz, S., Ghez, A. M., et al. 2019, ApJ,
 1823 878, 58, doi: [10.3847/1538-4357/ab1e4d](https://doi.org/10.3847/1538-4357/ab1e4d)
- 1824 Sukhbold, T., & Woosley, S. E. 2014, ApJ, 783, 10,
 1825 doi: [10.1088/0004-637X/783/1/10](https://doi.org/10.1088/0004-637X/783/1/10)
- 1826 Tanvir, N. R., Levan, A. J., González-Fernández, C., et al.
 1827 2017, ApJL, 848, L27, doi: [10.3847/2041-8213/aa90b6](https://doi.org/10.3847/2041-8213/aa90b6)
- 1828 Taylor, S. R., & Gair, J. R. 2012, PhRvD, 86, 023502,
 1829 doi: [10.1103/PhysRevD.86.023502](https://doi.org/10.1103/PhysRevD.86.023502)
- 1830 Taylor, S. R., Gair, J. R., & Mandel, I. 2012, PhRvD, 85,
 1831 023535, doi: [10.1103/PhysRevD.85.023535](https://doi.org/10.1103/PhysRevD.85.023535)
- 1832 The IceCube Collaboration. 2019, GCN, 25557.
<https://gcn.gsfc.nasa.gov/gcn3/25557.gcn3>
- 1833 Thompson, J. E., Fauchon-Jones, E., Khan, S., et al. 2020,
 1834 arXiv:[2002.08383](https://arxiv.org/abs/2002.08383)
- 1835 Thompson, T. A., Kochanek, C. S., Stanek, K. Z., et al.
 1836 2019, Sci, 366, 637, doi: [10.1126/science.aau4005](https://doi.org/10.1126/science.aau4005)
- 1837 Thompson, T. A., Kochanek, C. S., Stanek, K. Z., et al.
 1838 2020, Sci, 368, eaba4356, doi: [10.1126/science.aba4356](https://doi.org/10.1126/science.aba4356)
- 1839 Thorne, K. S. 1980, RvMP, 52, 299,
 1840 doi: [10.1103/RevModPhys.52.299](https://doi.org/10.1103/RevModPhys.52.299)
- 1841 Tiwari, V. 2018, CQGra, 35, 145009,
 1842 doi: [10.1088/1361-6382/aac89d](https://doi.org/10.1088/1361-6382/aac89d)
- 1843 Uchikata, N., Yoshida, S., & Pani, P. 2016, PhRvD, 94,
 1844 064015, doi: [10.1103/PhysRevD.94.064015](https://doi.org/10.1103/PhysRevD.94.064015)
- 1845 Ugliano, M., Janka, H.-T., Marek, A., & Arcones, A. 2012,
 1846 ApJ, 757, 69, doi: [10.1088/0004-637X/757/1/69](https://doi.org/10.1088/0004-637X/757/1/69)
- 1847 Usman, S. A., Mills, J. C., & Fairhurst, S. 2019, ApJ, 877,
 1848 82, doi: [10.3847/1538-4357/ab0b3e](https://doi.org/10.3847/1538-4357/ab0b3e)
- 1849 Usman, S. A., Nitz, A. H., Harry, I. W., et al. 2016, CQGra,
 1850 33, 215004, doi: [10.1088/0264-9381/33/21/215004](https://doi.org/10.1088/0264-9381/33/21/215004)
- 1851 Van Den Broeck, C., & Sengupta, A. S. 2007a, CQGra, 24,
 1852 155, doi: [10.1088/0264-9381/24/1/009](https://doi.org/10.1088/0264-9381/24/1/009)
- 1853 —. 2007b, CQGra, 24, 1089,
 1854 doi: [10.1088/0264-9381/24/5/005](https://doi.org/10.1088/0264-9381/24/5/005)
- 1855 van den Heuvel, E. P. J., & Tauris, T. M. 2020, Sci, 368,
 1856 eaba3282, doi: [10.1126/science.aba3282](https://doi.org/10.1126/science.aba3282)
- 1857 Veitch, J., Raymond, V., Farr, B., et al. 2015, PhRvD, 91,
 1858 042003, doi: [10.1103/PhysRevD.91.042003](https://doi.org/10.1103/PhysRevD.91.042003)
- 1859 Veitch, J., et al. 2015, PhRvD, 91, 042003,
 1860 doi: [10.1103/PhysRevD.91.042003](https://doi.org/10.1103/PhysRevD.91.042003)
- 1861 Venumadhav, T., Zackay, B., Roulet, J., Dai, L., &
 1862 Zaldarriaga, M. 2019, arXiv:[1904.07214](https://arxiv.org/abs/1904.07214)
- 1863 Verde, L., Treu, T., & Riess, A. G. 2019, NatAs, 3, 891,
 1864 doi: [10.1038/s41550-019-0902-0](https://doi.org/10.1038/s41550-019-0902-0)
- 1865 Vieira, N., Ruan, J. J., Haggard, D., et al. 2020,
 1866 arXiv:[2003.09437](https://arxiv.org/abs/2003.09437)
- 1867 Viets, A. D. Wade, M., Urban, A. L., et al. 2018, CQGra,
 1868 35, 095015, doi: [10.1088/1361-6382/aab658](https://doi.org/10.1088/1361-6382/aab658)
- 1869 Villar, V. A., Guillochon, J., Berger, E., et al. 2017, ApJL,
 1870 851, L21, doi: [10.3847/2041-8213/aa9c84](https://doi.org/10.3847/2041-8213/aa9c84)
- 1871 Vitale, S., & Chen, H.-Y. 2018, PhRvL, 121, 021303,
 1872 doi: [10.1103/PhysRevLett.121.021303](https://doi.org/10.1103/PhysRevLett.121.021303)
- 1873 Vitale, S., Lynch, R., Raymond, V., et al. 2017, PhRvD, 95,
 1874 064053, doi: [10.1103/PhysRevD.95.064053](https://doi.org/10.1103/PhysRevD.95.064053)
- 1875 Vitale, S., Lynch, R., Veitch, J., Raymond, V., & Sturani,
 1876 R. 2014, PhRvL, 112, 251101,
 1877 doi: [10.1103/PhysRevLett.112.251101](https://doi.org/10.1103/PhysRevLett.112.251101)
- 1878 Watson, A. M., Butler, N. R., Lee, W. H., et al. 2020,
 1879 MNRAS, 159, doi: [10.1093/mnras/staa161](https://doi.org/10.1093/mnras/staa161)
- 1880 Watson, D., Hansen, C. J., Selsing, J., et al. 2019, Nat, 574,
 1881 497, doi: [10.1038/s41586-019-1676-3](https://doi.org/10.1038/s41586-019-1676-3)
- 1882 Wyrzykowski, L., & Mandel, I. 2020, A&A, 636, A20,
 1883 doi: [10.1051/0004-6361/201935842](https://doi.org/10.1051/0004-6361/201935842)
- 1884 Yang, Y., Bartos, I., Haiman, Z., et al. 2019, ApJ, 876, 122,
 1885 doi: [10.3847/1538-4357/ab16e3](https://doi.org/10.3847/1538-4357/ab16e3)
- 1886 Ye, C. S., Fong, W.-F., Kremer, K., et al. 2020, ApJL, 888,
 1887 L10, doi: [10.3847/2041-8213/ab5dc5](https://doi.org/10.3847/2041-8213/ab5dc5)
- 1888 Yunes, N., & Pretorius, F. 2009, PhRvD, 80, 122003,
 1889 doi: [10.1103/PhysRevD.80.122003](https://doi.org/10.1103/PhysRevD.80.122003)
- 1890 Zackay, B., Dai, L., Venumadhav, T., Roulet, J., &
 1891 Zaldarriaga, M. 2019a, arXiv:[1910.09528](https://arxiv.org/abs/1910.09528)
- 1892 Zackay, B., Venumadhav, T., Dai, L., Roulet, J., &
 1893 Zaldarriaga, M. 2019b, PhRvD, 100, 023007,
 1894 doi: [10.1103/PhysRevD.100.023007](https://doi.org/10.1103/PhysRevD.100.023007)
- 1895 Ziosi, B. M., Mapelli, M., Branchesi, M., & Tormen, G.
 1896 2014, MNRAS, 441, 3703, doi: [10.1093/mnras/stu824](https://doi.org/10.1093/mnras/stu824)
- 1897

All Authors and Affiliations

- 1898 R. ABBOTT,¹ T. D. ABBOTT,² S. ABRAHAM,³ F. ACERNESE,^{4,5} K. ACKLEY,⁶ C. ADAMS,⁷ R. X. ADHIKARI,¹
 1899 V. B. ADYA,⁸ C. AFFELDT,^{9,10} M. AGATHOS,^{11,12} K. AGATSUMA,¹³ N. AGGARWAL,¹⁴ O. D. AGUIAR,¹⁵ A. AICH,¹⁶
 1900 L. AIELLO,^{17,18} A. AIN,³ P. AJITH,¹⁹ S. AKCAY,^{20,11} G. ALLEN,²¹ A. ALLOCCHA,²² P. A. ALTIN,⁸ A. AMATO,²³
 1901 S. ANAND,¹ A. ANANYEVA,¹ S. B. ANDERSON,¹ W. G. ANDERSON,²⁴ S. V. ANGELOVA,²⁵ S. ANSOLDI,^{26,27}
 1902 S. ANTIER,²⁸ S. APPERT,¹ K. ARAI,¹ M. C. ARAYA,¹ J. S. AREEDA,²⁹ M. ARÈNE,²⁸ N. ARNAUD,^{30,31}
 1903 S. M. ARONSON,³² K. G. ARUN,³³ Y. ASALI,³⁴ S. ASCENZI,^{17,35} G. ASHTON,⁶ S. M. ASTON,⁷ P. ASTONE,³⁶
 1904 F. AUBIN,³⁷ P. AUFMUTH,¹⁰ K. AULTONEAL,³⁸ C. AUSTIN,² V. AVENDANO,³⁹ S. BABAK,²⁸ P. BACON,²⁸
 1905 F. BADARACCO,^{17,18} M. K. M. BADER,⁴⁰ S. BAE,⁴¹ A. M. BAER,⁴² J. BAIRD,²⁸ F. BALDACCINI,^{43,44}
 1906 G. BALLARDIN,³¹ S. W. BALLMER,⁴⁵ A. BALS,³⁸ A. BALSAMO,⁴² G. BALTUS,⁴⁶ S. BANAGIRI,⁴⁷ D. BANKAR,³
 1907 R. S. BANKAR,³ J. C. BARAYOGA,¹ C. BARBIERI,^{48,49} B. C. BARISH,¹ D. BARKER,⁵⁰ K. BARKETT,⁵¹
 1908 P. BARNEO,⁵² F. BARONE,^{53,5} B. BARR,⁵⁴ L. BARSOTTI,⁵⁵ M. BARSUGLIA,²⁸ D. BARTA,⁵⁶ J. BARTLETT,⁵⁰
 1909 I. BARTOS,³² R. BASSIRI,⁵⁷ A. BASTI,^{58,22} M. BAWAJ,^{59,44} J. C. BAYLEY,⁵⁴ M. BAZZAN,^{60,61} B. BÉCSY,⁶²
 1910 M. BEJGER,⁶³ I. BELAHcene,³⁰ A. S. BELL,⁵⁴ D. BENIWAL,⁶⁴ M. G. BENJAMIN,³⁸ R. BENKEL,⁶⁵
 1911 J. D. BENTLEY,¹³ F. BERGAMIN,⁹ B. K. BERGER,⁵⁷ G. BERGMANN,^{9,10} S. BERNUZZI,¹¹ C. P. L. BERRY,¹⁴
 1912 D. BERSANETTI,⁶⁶ A. BERTOLINI,⁴⁰ J. BETZWIESER,⁷ R. BHANDARE,⁶⁷ A. V. BHANDARI,³ J. BIDLER,²⁹
 1913 E. BIGGS,²⁴ I. A. BILENKO,⁶⁸ G. BILLINGSLEY,¹ R. BIRNEY,⁶⁹ O. BIRNHOLTZ,^{70,71} S. BISCANS,^{1,55} M. BISCHI,^{72,73}
 1914 S. BISCOVEANU,⁵⁵ A. BISHT,¹⁰ G. BISSENBAYEVA,¹⁶ M. BITOSSI,^{31,22} M. A. BIZOUARD,⁷⁴ J. K. BLACKBURN,¹
 1915 J. BLACKMAN,⁵¹ C. D. BLAIR,⁷ D. G. BLAIR,⁷⁵ R. M. BLAIR,⁵⁰ F. BOBBA,^{76,77} N. BODE,^{9,10} M. BOER,⁷⁴
 1916 Y. BOETZEL,⁷⁸ G. BOGAERT,⁷⁴ F. BONDU,⁷⁹ E. BONILLA,⁵⁷ R. BONNAND,³⁷ P. BOOKER,^{9,10} B. A. BOOM,⁴⁰
 1917 R. BORK,¹ V. BOSCHI,²² S. BOSE,³ V. BOSSILKOV,⁷⁵ J. BOSVELD,⁷⁵ Y. BOUFFANAI,^{60,61} A. BOZZI,³¹
 1918 C. BRADASCHIA,²² P. R. BRADY,²⁴ A. BRAMLEY,⁷ M. BRANCHESI,^{17,18} J. E. BRAU,⁸⁰ M. BRESCHI,¹¹
 1919 T. BRIANT,⁸¹ J. H. BRIGGS,⁵⁴ F. BRIGHENTI,^{72,73} A. BRILLET,⁷⁴ M. BRINKMANN,^{9,10} R. BRITO,^{82,36,65}
 1920 P. BROCKILL,²⁴ A. F. BROOKS,¹ J. BROOKS,³¹ D. D. BROWN,⁶⁴ S. BRUNETT,¹ G. BRUNO,⁸³ R. BRUNTZ,⁴²
 1921 A. BUIKEMA,⁵⁵ T. BULIK,⁸⁴ H. J. BULLEN,^{85,40} A. BUONANNO,^{65,86} D. BUSKULIC,³⁷ R. L. BYER,⁵⁷
 1922 M. CABERO,^{9,10} L. CADONATI,⁸⁷ G. CAGNOLI,⁸⁸ C. CAHILLANE,¹ J. CALDERÓN BUSTILLO,⁶ J. D. CALLAGHAN,⁵⁴
 1923 T. A. CALLISTER,¹ E. CALLONI,^{89,5} J. B. CAMP,⁹⁰ M. CANEPA,^{91,66} K. C. CANNON,⁹² H. CAO,⁶⁴ J. CAO,⁹³
 1924 G. CARAPELLA,^{76,77} F. CARBOGNANI,³¹ S. CARIDE,⁹⁴ M. F. CARNEY,¹⁴ G. CARULLO,^{58,22} J. CASANUEVA DIAZ,²²
 1925 C. CASENTINI,^{95,35} J. CASTAÑEDA,⁵² S. CAUDILL,⁴⁰ M. CAVAGLIA,⁹⁶ F. CAVALIER,³⁰ R. CAVALIERI,³¹ G. CELLA,²²
 1926 P. CERDÁ-DURÁN,⁹⁷ E. CESARINI,^{98,35} O. CHAIBI,⁷⁴ K. CHAKRAVARTI,³ C. CHAN,⁹² M. CHAN,⁵⁴ S. CHAO,⁹⁹
 1927 P. CHARLTON,¹⁰⁰ E. A. CHASE,¹⁴ E. CHASSANDE-MOTTIN,²⁸ D. CHATTERJEE,²⁴ M. CHATURVEDI,⁶⁷
 1928 K. CHATZIOANNOU,^{101,102} H. Y. CHEN,¹⁰³ X. CHEN,⁷⁵ Y. CHEN,⁵¹ H.-P. CHENG,³² C. K. CHEONG,¹⁰⁴
 1929 H. Y. CHIA,³² F. CHIADINI,^{105,77} R. CHIERICI,¹⁰⁶ A. CHINCARINI,⁶⁶ A. CHIUMMO,³¹ G. CHO,¹⁰⁷ H. S. CHO,¹⁰⁸
 1930 M. CHO,⁸⁶ N. CHRISTENSEN,⁷⁴ Q. CHU,⁷⁵ S. CHUA,⁸¹ K. W. CHUNG,¹⁰⁴ S. CHUNG,⁷⁵ G. CIANI,^{60,61}
 1931 P. CIECIELAG,⁶³ M. CIEŚLAR,⁶³ A. A. CIOBANU,⁶⁴ R. CIOLFI,^{109,61} F. CIPRIANO,⁷⁴ A. CIRONE,^{91,66} F. CLARA,⁵⁰
 1932 J. A. CLARK,⁸⁷ P. CLEARWATER,¹¹⁰ S. CLESSE,⁸³ F. CLEVA,⁷⁴ E. COCCIA,^{17,18} P.-F. COHADON,⁸¹ D. COHEN,³⁰
 1933 M. COLLEONI,¹¹¹ C. G. COLLETTE,¹¹² C. COLLINS,¹³ M. COLPI,^{48,49} M. CONSTANCIO JR.,¹⁵ L. CONTI,⁶¹
 1934 S. J. COOPER,¹³ P. CORBAN,⁷ T. R. CORBITT,² I. CORDERO-CARRIÓN,¹¹³ S. COREZZI,^{43,44} K. R. CORLEY,³⁴
 1935 N. CORNISH,⁶² D. CORRE,³⁰ A. CORSI,⁹⁴ S. CORTESE,³¹ C. A. COSTA,¹⁵ R. COTESTA,⁶⁵ M. W. COUGHLIN,¹
 1936 S. B. COUGHLIN,^{114,14} J.-P. COULON,⁷⁴ S. T. COUNTRYMAN,³⁴ P. COUVARES,¹ P. B. COVAS,¹¹¹ D. M. COWARD,⁷⁵
 1937 M. J. COWART,⁷ D. C. COYNE,¹ R. COYNE,¹¹⁵ J. D. E. CREIGHTON,²⁴ T. D. CREIGHTON,¹⁶ J. CRIPE,²
 1938 M. CROQUETTE,⁸¹ S. G. CROWDER,¹¹⁶ J.-R. CUDELL,⁴⁶ T. J. CULLEN,² A. CUMMING,⁵⁴ R. CUMMINGS,⁵⁴
 1939 L. CUNNINGHAM,⁵⁴ E. CUOCO,³¹ M. CURYLO,⁸⁴ T. DAL CANTON,⁶⁵ G. DÁLYA,¹¹⁷ A. DANA,⁵⁷
 1940 L. M. DANESHGARAN-BAJASTANI,¹¹⁸ B. D'ANGELO,^{91,66} S. L. DANILISHIN,^{9,10} S. D'ANTONIO,³⁵ K. DANZMANN,^{10,9}
 1941 C. DARSOW-FROMM,¹¹⁹ A. DASGUPTA,¹²⁰ L. E. H. DATRIER,⁵⁴ V. DATTILO,³¹ I. DAVE,⁶⁷ M. DAVIER,³⁰
 1942 G. S. DAVIES,¹²¹ D. DAVIS,⁴⁵ E. J. DAW,¹²² D. DEBRA,⁵⁷ M. DEENADAYALAN,³ J. DEGALLAIX,²³
 1943 M. DE LAURENTIS,^{89,5} S. DELÉGLISE,⁸¹ M. DELFAVERO,⁷⁰ N. DE LILLO,⁵⁴ W. DEL POZZO,^{58,22} L. M. DEMARCHI,¹⁴
 1944 V. D'EMILIO,¹¹⁴ N. DEMOS,⁵⁵ T. DENT,¹²¹ R. DE PIETRI,^{123,124} R. DE ROSA,^{89,5} C. DE ROSSI,³¹ R. DESALVO,¹²⁵
 1945 O. DE VARONA,^{9,10} S. DHURANDHAR,³ M. C. DÍAZ,¹⁶ M. DIAZ-ORTIZ JR.,³² T. DIETRICH,⁴⁰ L. DI FIORE,⁵
 1946 C. DI FRONZO,¹³ C. DI GIORGIO,^{76,77} F. DI GIOVANNI,⁹⁷ M. DI GIOVANNI,^{126,127} T. DI GIROLAMO,^{89,5}
 1947 A. DI LIETO,^{58,22} B. DING,¹¹² S. DI PACE,^{82,36} I. DI PALMA,^{82,36} F. DI RENZO,^{58,22} A. K. DIVAKARLA,³²
 1948 A. DMITRIEV,¹³ Z. DOCTOR,¹⁰³ F. DONOVAN,⁵⁵ K. L. DOOLEY,¹¹⁴ S. DORAVARI,³ I. DORRINGTON,¹¹⁴
 1949 T. P. DOWNES,²⁴ M. DRAGO,^{17,18} J. C. DRIGGERS,⁵⁰ Z. DU,⁹³ J.-G. DUCOIN,³⁰ P. DUPEJ,⁵⁴ O. DURANTE,^{76,77}
 1950 D. D'URSO,^{128,129} S. E. DWYER,⁵⁰ P. J. EASTER,⁶ G. EDDOLLS,⁵⁴ B. EDELMAN,⁸⁰ T. B. EDO,¹²² O. EDY,¹³⁰
 1951 A. EFFLER,⁷ P. EHRENS,¹ J. EICHHOLZ,⁸ S. S. EIKENBERRY,³² M. EISENMANN,³⁷ R. A. EISENSTEIN,⁵⁵
 1952 A. EJLLI,¹¹⁴ L. ERRICO,^{89,5} R. C. ESSICK,¹⁰³ H. ESTELLES,¹¹¹ D. ESTEVEZ,³⁷ Z. B. ETIENNE,¹³¹ T. ETZEL,¹
 1953 M. EVANS,⁵⁵ T. M. EVANS,⁷ B. E. EWING,¹³² V. FAFONE,^{95,35,17} S. FAIRHURST,¹¹⁴ X. FAN,⁹³ S. FARINON,⁶⁶
 1954 B. FARR,⁸⁰ W. M. FARR,^{101,102} E. J. FAUCHON-JONES,¹¹⁴ M. FAVATA,³⁹ M. FAYS,¹²² M. FAZIO,¹³³ J. FEICHT,¹
 1955 M. M. FEJER,⁵⁷ F. FENG,²⁸ E. FENYVESI,^{56,134} D. L. FERGUSON,⁸⁷ A. FERNANDEZ-GALIANA,⁵⁵ I. FERRANTE,^{58,22}
 1956 E. C. FERREIRA,¹⁵ T. A. FERREIRA,¹⁵ F. FIDECARO,^{58,22} I. FIORI,³¹ D. FIORUCCI,^{17,18} M. FISHBACH,¹⁰³
 1957 R. P. FISHER,⁴² R. FITTIPALDI,^{135,77} M. FITZ-AXEN,⁴⁷ V. FIUMARA,^{136,77} R. FLAMINIO,^{37,137} E. FLODEN,⁴⁷

- 1958 E. FLYNN,²⁹ H. FONG,⁹² J. A. FONT,^{97,138} P. W. F. FORSYTH,⁸ J.-D. FOURNIER,⁷⁴ S. FRASCA,^{82,36}
 1959 F. FRASCONI,²² Z. FREI,¹¹⁷ A. FREISE,¹³ R. FREY,⁸⁰ V. FREY,³⁰ P. FRITSCHEL,⁵⁵ V. V. FROLOV,⁷
 1960 G. FRONZÉ,¹³⁹ P. FULDA,³² M. FYFFE,⁷ H. A. GABBARD,⁵⁴ B. U. GADRE,⁶⁵ S. M. GAEBEL,¹³ J. R. GAIR,⁶⁵
 1961 S. GALAUDAGE,⁶ D. GANAPATHY,⁵⁵ A. GANGULY,¹⁹ S. G. GAONKAR,³ C. GARCÍA-QUIRÓS,¹¹¹ F. GARUFI,^{89,5}
 1962 B. GATELEY,⁵⁰ S. GAUDIO,³⁸ V. GAYATHRI,¹⁴⁰ G. GEMME,⁶⁶ E. GENIN,³¹ A. GENNAI,²² D. GEORGE,²¹
 1963 J. GEORGE,⁶⁷ L. GERGELY,¹⁴¹ S. GHONGE,⁸⁷ ABHIRUP GHOSH,⁶⁵ ARCHISMAN GHOSH,^{142,143,144,40} S. GHOSH,²⁴
 1964 B. GIACOMAZZO,^{126,127} J. A. GIAIME,^{2,7} K. D. GIARDINA,⁷ D. R. GIBSON,⁶⁹ C. GIER,²⁵ K. GILL,³⁴ J. GLANZER,²
 1965 J. GNIESMER,¹¹⁹ P. GODWIN,¹³² E. GOETZ,^{2,96} R. GOETZ,³² N. GOHLKE,^{9,10} B. GONCHAROV,⁶ G. GONZÁLEZ,²
 1966 A. GOPAKUMAR,¹⁴⁵ S. E. GOSSAN,¹ M. GOSELIN,^{31,58,22} R. GOUATY,³⁷ B. GRACE,⁸ A. GRADO,^{146,5}
 1967 M. GRANATA,²³ A. GRANT,⁵⁴ S. GRAS,⁵⁵ P. GRASSIA,¹ C. GRAY,⁵⁰ R. GRAY,⁵⁴ G. GRECO,^{72,73} A. C. GREEN,³²
 1968 R. GREEN,¹¹⁴ E. M. GRETARSSON,³⁸ H. L. GRIGGS,⁸⁷ G. GRIGNANI,^{43,44} A. GRIMALDI,^{126,127} S. J. GRIMM,^{17,18}
 1969 H. GROTE,¹¹⁴ S. GRUNEWALD,⁶⁵ P. GRUNING,³⁰ G. M. GUIDI,^{72,73} A. R. GUIMARAES,² G. GUIXÉ,⁵²
 1970 H. K. GULATI,¹²⁰ Y. GUO,⁴⁰ A. GUPTA,¹³² ANCHAL GUPTA,¹ P. GUPTA,⁴⁰ E. K. GUSTAFSON,¹ R. GUSTAFSON,¹⁴⁷
 1971 L. HAEGEL,¹¹¹ O. HALIM,^{18,17} E. D. HALL,⁵⁵ E. Z. HAMILTON,¹¹⁴ G. HAMMOND,⁵⁴ M. HANEY,⁷⁸
 1972 M. M. HANKE,^{9,10} J. HANKS,⁵⁰ C. HANNA,¹³² M. D. HANNAM,¹¹⁴ O. A. HANNUKSELA,¹⁰⁴ T. J. HANSEN,³⁸
 1973 J. HANSON,⁷ T. HARDER,⁷⁴ T. HARDWICK,² K. HARIS,¹⁹ J. HARMS,^{17,18} G. M. HARRY,¹⁴⁸ I. W. HARRY,¹³⁰
 1974 R. K. HASSKEW,⁷ C.-J. HASTER,⁵⁵ K. HAUGHIAN,⁵⁴ F. J. HAYES,⁵⁴ J. HEALY,⁷⁰ A. HEIDMANN,⁸¹
 1975 M. C. HEINTZE,⁷ J. HEINZE,^{9,10} H. HEITMANN,⁷⁴ F. HELLMAN,¹⁴⁹ P. HELLO,³⁰ G. HEMMING,³¹ M. HENDRY,⁵⁴
 1976 I. S. HENG,⁵⁴ E. HENNES,⁴⁰ J. HENNIG,^{9,10} M. HEURS,^{9,10} S. HILD,^{150,54} T. HINDERER,^{144,40,142}
 1977 S. Y. HOBACK,^{29,148} S. HOCHHEIM,^{9,10} E. HOFGARD,⁵⁷ D. HOFMAN,²³ A. M. HOLGADO,²¹ N. A. HOLLAND,⁸
 1978 K. HOLT,⁷ D. E. HOLZ,¹⁰³ P. HOPKINS,¹¹⁴ C. HORST,²⁴ J. HOUGH,⁵⁴ E. J. HOWELL,⁷⁵ C. G. HOY,¹¹⁴
 1979 Y. HUANG,⁵⁵ M. T. HÜBNER,⁶ E. A. HUERTA,²¹ D. HUET,³⁰ B. HUGHEY,³⁸ V. HUI,³⁷ S. HUSA,¹¹¹
 1980 S. H. HUTTNER,⁵⁴ R. HUXFORD,¹³² T. HUYNH-DINH,⁷ B. IDZKOWSKI,⁸⁴ A. IESS,^{95,35} H. INCHAUSPE,³²
 1981 C. INGRAM,⁶⁴ G. INTINI,^{82,36} J.-M. ISAC,⁸¹ M. ISI,⁵⁵ B. R. IYER,¹⁹ T. JACQMIN,⁸¹ S. J. JADHAV,¹⁵¹
 1982 S. P. JADHAV,³ A. L. JAMES,¹¹⁴ K. JANI,⁸⁷ N. N. JANTHALUR,¹⁵¹ P. JARANOWSKI,¹⁵² D. JARIWALA,³²
 1983 R. JAUME,¹¹¹ A. C. JENKINS,¹⁵³ J. JIANG,³² G. R. JOHNS,⁴² N. K. JOHNSON-MCDANIEL,¹² A. W. JONES,¹³
 1984 D. I. JONES,¹⁵⁴ J. D. JONES,⁵⁰ P. JONES,¹³ R. JONES,⁵⁴ R. J. G. JONKER,⁴⁰ L. JU,⁷⁵ J. JUNKER,^{9,10}
 1985 C. V. KALAGHATGI,¹¹⁴ V. KALOGERA,¹⁴ B. KAMAI,¹ S. KANDHASAMY,³ G. KANG,⁴¹ J. B. KANNER,¹
 1986 S. J. KAPADIA,¹⁹ S. KARKI,⁸⁰ R. KASHYAP,¹⁹ M. KASPRZACK,¹ W. KASTAUN,^{9,10} S. KATSANEVAS,³¹
 1987 E. KATSAVOUNIDIS,⁵⁵ W. KATZMAN,⁷ S. KAUFER,¹⁰ K. KAWABE,⁵⁰ F. KÉFÉLIAN,⁷⁴ D. KEITEL,¹³⁰ A. KEIVANI,³⁴
 1988 R. KENNEDY,¹²² J. S. KEY,¹⁵⁵ S. KHADKA,⁵⁷ F. Y. KHALILI,⁶⁸ I. KHAN,^{17,35} S. KHAN,^{9,10} Z. A. KHAN,⁹³
 1989 E. A. KHAZANOV,¹⁵⁶ N. KHETAN,^{17,18} M. KHURSHEED,⁶⁷ N. KIJBUNCHOO,⁸ CHUNGLEE KIM,¹⁵⁷ G. J. KIM,⁸⁷
 1990 J. C. KIM,¹⁵⁸ K. KIM,¹⁰⁴ W. KIM,⁶⁴ W. S. KIM,¹⁵⁹ Y.-M. KIM,¹⁶⁰ C. KIMBALL,¹⁴ P. J. KING,⁵⁰
 1991 M. KINLEY-HANLON,⁵⁴ R. KIRCHHOFF,^{9,10} J. S. KISSEL,⁵⁰ L. KLEYBOLTE,¹¹⁹ S. KLIMENKO,³² T. D. KNOWLES,¹³¹
 1992 E. KNYAZEV,⁵⁵ P. KOCH,^{9,10} S. M. KOEHLENBECK,^{9,10} G. KOEKOEK,^{40,150} S. KOLEY,⁴⁰ V. KONDRAшOV,¹
 1993 A. KONTOS,¹⁶¹ N. KOPER,^{9,10} M. KOROBKO,¹¹⁹ W. Z. KORTH,¹ M. KOVALAM,⁷⁵ D. B. KOZAK,¹ V. KRINGEL,^{9,10}
 1994 N. V. KRISHNENDU,³³ A. KRÓLAK,^{162,163} N. KRUPINSKI,²⁴ G. KUEHN,^{9,10} A. KUMAR,¹⁵¹ P. KUMAR,¹⁶⁴
 1995 RAHUL KUMAR,⁵⁰ RAKESH KUMAR,¹²⁰ S. KUMAR,¹⁹ L. KUO,⁹⁹ A. KUTYNIA,¹⁶² B. D. LACKEY,⁶⁵ D. LAGHI,^{58,22}
 1996 E. LALANDE,¹⁶⁵ T. L. LAM,¹⁰⁴ A. LAMBERTS,^{74,166} M. LANDRY,⁵⁰ P. LANDRY,²⁹ B. B. LANE,⁵⁵ R. N. LANG,¹⁶⁷
 1997 J. LANGE,⁷⁰ B. LANTZ,⁵⁷ R. K. LANZA,⁵⁵ I. LA ROSA,³⁷ A. LARTAUX-VOLLARD,³⁰ P. D. LASKY,⁶ M. LAXEN,⁷
 1998 A. LAZZARINI,¹ C. LAZZARO,⁶¹ P. LEACI,^{82,36} S. LEAVEY,^{9,10} Y. K. LECOEUCHE,⁵⁰ C. H. LEE,¹⁰⁸ H. M. LEE,¹⁶⁸
 1999 H. W. LEE,¹⁵⁸ J. LEE,¹⁰⁷ K. LEE,⁵⁷ J. LEHMANN,^{9,10} N. LEROY,³⁰ N. LETENDRE,³⁷ Y. LEVIN,⁶ A. K. Y. LI,¹⁰⁴
 2000 J. Li,⁹³ K. Li,¹⁰⁴ T. G. F. Li,¹⁰⁴ X. Li,⁵¹ F. LINDE,^{169,40} S. D. LINKER,¹¹⁸ J. N. LINLEY,⁵⁴
 2001 T. B. LITTENBERG,¹⁷⁰ J. LIU,^{9,10} X. LIU,²⁴ M. LLORENСS-MONTEAGUDO,⁹⁷ R. K. L. LO,¹ A. LOCKWOOD,¹⁷¹
 2002 L. T. LONDON,⁵⁵ A. LONGO,^{172,173} M. LORENZINI,^{17,18} V. LORIETTE,¹⁷⁴ M. LORMAND,⁷ G. LOSURDO,²²
 2003 J. D. LOUGH,^{9,10} C. O. LOUSTO,⁷⁰ G. LOVELACE,²⁹ H. LÜCK,^{10,9} D. LUMACA,^{95,35} A. P. LUNDGREN,¹³⁰ Y. MA,⁵¹
 2004 R. MACAS,¹¹⁴ S. MACFOY,²⁵ M. MACINNIS,⁵⁵ D. M. MACLEOD,¹¹⁴ I. A. O. MACMILLAN,¹⁴⁸ A. MACQUET,⁷⁴
 2005 I. MAGAÑA HERNANDEZ,²⁴ F. MAGAÑA-SANDOVAL,³² R. M. MAGEE,¹³² E. MAJORANA,³⁶ I. MAKSMOVIC,¹⁷⁴
 2006 A. MALIK,⁶⁷ N. MAN,⁷⁴ V. MANDIC,⁴⁷ V. MANGANO,^{54,82,36} G. L. MANSSELL,^{50,55} M. MANSKE,²⁴
 2007 M. MANTOVANI,³¹ M. MAPELLI,^{60,61} F. MARCHESONI,^{59,44,175} F. MARION,³⁷ S. MÁRKA,³⁴ Z. MÁRKA,³⁴
 2008 C. MARKAKIS,¹² A. S. MARKOSYAN,⁵⁷ A. MARKOWITZ,¹ E. MAROS,¹ A. MARQUINA,¹¹³ S. MARSAT,²⁸
 2009 F. MARTELLI,^{72,73} I. W. MARTIN,⁵⁴ R. M. MARTIN,³⁹ V. MARTINEZ,⁸⁸ D. V. MARTYNOV,¹³ H. MASALEHDAN,¹¹⁹
 2010 K. MASON,⁵⁵ E. MASSERA,¹²² A. MASSEROT,³⁷ T. J. MASSINGER,⁵⁵ M. MASSO-REID,⁵⁴ S. MASTROGIOVANNI,²⁸
 2011 A. MATAS,⁶⁵ F. MATICHARD,^{1,55} N. MAVALVALA,⁵⁵ E. MAYNARD,² J. J. MCCANN,⁷⁵ R. McCARTHY,⁵⁰
 2012 D. E. MCCLELLAND,⁸ S. MCCORMICK,⁷ L. McCULLER,⁵⁵ S. C. McGuire,¹⁷⁶ C. MCISAAC,¹³⁰ J. McIVER,¹
 2013 D. J. McMANUS,⁸ T. MCRAE,⁸ S. T. McWILLIAMS,¹³¹ D. MEACHER,²⁴ G. D. MEADORS,⁶ M. MEHMET,^{9,10}
 2014 A. K. MEHTA,¹⁹ E. MEJUTO VILLA,^{125,77} A. MELATOS,¹¹⁰ G. MENDELL,⁵⁰ R. A. MERCER,²⁴ L. MERENI,²³
 2015 K. MERFELD,⁸⁰ E. L. MERILH,⁵⁰ J. D. MERRITT,⁸⁰ M. MERZOUGUI,⁷⁴ S. MESHKOV,¹ C. MESSENGER,⁵⁴
 2016 C. MESSICK,¹⁷⁷ R. METZDORFF,⁸¹ P. M. MEYERS,¹¹⁰ F. MEYLAHN,^{9,10} A. MIANI,^{126,127} H. MIAO,¹³
 2017 I. MICHALOLIAKOS,³² C. MICHEL,²³ H. MIDDLETON,¹¹⁰ L. MILANO,^{89,5} A. L. MILLER,^{32,82,36} M. MILLHOUSE,¹¹⁰
 2018 J. C. MILLS,¹¹⁴ E. MILOTTI,^{178,27} M. C. MILOVICH-GOFF,¹¹⁸ O. MINAZZOLI,^{74,179} Y. MINENKOV,³⁵ A. MISHKIN,³²
 2019 C. MISHRA,¹⁸⁰ T. MISTRY,¹²² S. MITRA,³ V. P. MITROFANOV,⁶⁸ G. MITSELMAKHER,³² R. MITTELMAN,⁵⁵

- 2020 G. MO,⁵⁵ K. MOGUSHI,⁹⁶ S. R. P. MOHAPATRA,⁵⁵ S. R. MOHITE,²⁴ M. MOLINA-RUIZ,¹⁴⁹ M. MONDIN,¹¹⁸
 2021 M. MONTANI,^{72,73} C. J. MOORE,¹³ D. MORARU,⁵⁰ F. MORAWSKI,⁶³ G. MORENO,⁵⁰ S. MORISAKI,⁹² B. MOURS,¹⁸¹
 2022 C. M. MOW-LOWRY,¹³ S. MOZZON,¹³⁰ F. MUCIACCIA,^{82,36} ARUNAVA MUKHERJEE,⁵⁴ D. MUKHERJEE,¹³²
 2023 S. MUKHERJEE,¹⁶ SUBROTO MUKHERJEE,¹²⁰ N. MUKUND,^{9,10} A. MULLAVEY,⁷ J. MUNCH,⁶⁴ E. A. MUÑIZ,⁴⁵
 2024 P. G. MURRAY,⁵⁴ A. NAGAR,^{98,139,182} I. NARDECCHIA,^{95,35} L. NATICCHIONI,^{82,36} R. K. NAYAK,¹⁸³ B. F. NEIL,⁷⁵
 2025 J. NEILSON,^{125,77} G. NELEMANS,^{184,40} T. J. N. NELSON,⁷ M. NERY,^{9,10} A. NEUNZERT,¹⁴⁷ K. Y. NG,⁵⁵ S. NG,⁶⁴
 2026 C. NGUYEN,²⁸ P. NGUYEN,⁸⁰ D. NICHOLS,^{144,40} S. A. NICHOLS,² S. NISSANKE,^{144,40} F. NOCERA,³¹ M. NOH,⁵⁵
 2027 C. NORTH,¹¹⁴ D. NOTHARD,¹⁸⁵ L. K. NUTTALL,¹³⁰ J. OBERLING,⁵⁰ B. D. O'BRIEN,³² G. OGANESYAN,^{17,18}
 2028 G. H. OGIN,¹⁸⁶ J. J. OH,¹⁵⁹ S. H. OH,¹⁵⁹ F. OHME,^{9,10} H. OHTA,⁹² M. A. OKADA,¹⁵ M. OLIVER,¹¹¹
 2029 C. OLIVETTO,³¹ P. OPPERMANN,^{9,10} RICHARD J. ORAM,⁷ B. O'REILLY,⁷ R. G. ORMISTON,⁴⁷ L. F. ORTEGA,³²
 2030 R. O'SHAUGHNESSY,⁷⁰ S. OSSOKINE,⁶⁵ C. OSTHELDER,¹ D. J. OTTAWAY,⁶⁴ H. OVERMIER,⁷ B. J. OWEN,⁹⁴
 2031 A. E. PACE,¹³² G. PAGANO,^{58,22} M. A. PAGE,⁷⁵ G. PAGLIAROLI,^{17,18} A. PAI,¹⁴⁰ S. A. PAI,⁶⁷ J. R. PALAMOS,⁸⁰
 2032 O. PALASHOV,¹⁵⁶ C. PALOMBA,³⁶ H. PAN,⁹⁹ P. K. PANDA,¹⁵¹ P. T. H. PANG,⁴⁰ C. PANKOW,¹⁴
 2033 F. PANNARALE,^{82,36} B. C. PANT,⁶⁷ F. PAOLETTI,²² A. PAOLI,³¹ A. PARIDA,³ W. PARKER,^{7,176} D. PASCUCCI,^{54,40}
 2034 A. PASQUALETTI,³¹ R. PASSAQUIETI,^{58,22} D. PASSUELLO,²² B. PATRICELLI,^{58,22} E. PAYNE,⁶ B. L. PEARLSTONE,⁵⁴
 2035 T. C. PECHSIRI,³² A. J. PEDERSEN,⁴⁵ M. PEDRAZA,¹ A. PELE,⁷ S. PENN,¹⁸⁷ A. PEREGO,^{126,127} C. J. PEREZ,⁵⁰
 2036 C. PÉRIGOIS,³⁷ A. PERRECA,^{126,127} S. PERRIÈS,¹⁰⁶ J. PETERMANN,¹¹⁹ H. P. PFEIFFER,⁶⁵ M. PHELPS,^{9,10}
 2037 K. S. PHUKON,^{3,169,40} O. J. PICCINNI,^{82,36} M. PICHOT,⁷⁴ M. PIENDIBENE,^{58,22} F. PIERGIOVANNI,^{72,73}
 2038 V. PIERRO,^{125,77} G. PILLANT,³¹ L. PINARD,²³ I. M. PINTO,^{125,77,98} K. PIOTRKOWSKI,⁸³ M. PIRELLO,⁵⁰
 2039 M. PITKIN,¹⁸⁸ W. PLASTINO,^{172,173} R. POGGIANI,^{58,22} D. Y. T. PONG,¹⁰⁴ S. PONRATHNAM,³ P. POPOLIZIO,³¹
 2040 E. K. PORTER,²⁸ J. POWELL,¹⁸⁹ A. K. PRAJAPATI,¹²⁰ K. PRASAI,⁵⁷ R. PRASANNA,¹⁵¹ G. PRATTEN,¹³
 2041 T. PRESTEGARD,²⁴ M. PRINCIPE,^{125,98,77} G. A. PRODI,^{126,127} L. PROKHOROV,¹³ M. PUNTURO,⁴⁴ P. PUPPO,³⁶
 2042 M. PÜRRER,⁶⁵ H. QI,¹¹⁴ V. QUETSCHKE,¹⁶ P. J. QUINONEZ,³⁸ F. J. RAAB,⁵⁰ G. RAAIJMAKERS,^{144,40}
 2043 H. RADKINS,⁵⁰ N. RADULESCO,⁷⁴ P. RAFFAI,¹¹⁷ H. RAFFERTY,¹⁹⁰ S. RAJA,⁶⁷ C. RAJAN,⁶⁷ B. RAJBHANDARI,⁹⁴
 2044 M. RAKHMANOV,¹⁶ K. E. RAMIREZ,¹⁶ A. RAMOS-BUADES,¹¹¹ JAVED RANA,³ K. RAO,¹⁴ P. RAPAGNANI,^{82,36}
 2045 V. RAYMOND,¹¹⁴ M. RAZZANO,^{58,22} J. READ,²⁹ T. REGIMBAU,³⁷ L. REI,⁶⁶ S. REID,²⁵ D. H. REITZE,^{1,32}
 2046 P. RETTEGNO,^{139,191} F. RICCI,^{82,36} C. J. RICHARDSON,³⁸ J. W. RICHARDSON,¹ P. M. RICKER,²¹
 2047 G. RIEMENSCHNEIDER,^{191,139} K. RILES,¹⁴⁷ M. RIZZO,¹⁴ N. A. ROBERTSON,^{1,54} F. ROBINET,³⁰ A. ROCCHI,³⁵
 2048 R. D. RODRIGUEZ-SOTO,³⁸ L. ROLLAND,³⁷ J. G. ROLLINS,¹ V. J. ROMA,⁸⁰ M. ROMANELLI,⁷⁹ R. ROMANO,^{4,5}
 2049 C. L. ROMEL,⁵⁰ I. M. ROMERO-SHAW,⁶ J. H. ROMIE,⁷ C. A. ROSE,²⁴ D. ROSE,²⁹ K. ROSE,¹⁸⁵ D. ROSÍNSKA,⁸⁴
 2050 S. G. ROSOFSKY,²¹ M. P. ROSS,¹⁷¹ S. ROWAN,⁵⁴ S. J. ROWLINSON,¹³ P. K. ROY,¹⁶ SANTOSH ROY,³
 2051 SOUMEN ROY,¹⁹² P. RUGGI,³¹ G. RUTINS,⁶⁹ K. RYAN,⁵⁰ S. SACHDEV,¹³² T. SADECKI,⁵⁰ M. SAKELLARIADOU,¹⁵³
 2052 O. S. SALAFIA,^{193,48,49} L. SALCONI,³¹ M. SALEEM,³³ F. SALEMI,¹²⁶ A. SAMAJDAR,⁴⁰ E. J. SANCHEZ,¹
 2053 L. E. SANCHEZ,¹ N. SANCHIS-GUAL,¹⁹⁴ J. R. SANDERS,¹⁹⁵ K. A. SANTIAGO,³⁹ E. SANTOS,⁷⁴ N. SARIN,⁶
 2054 B. SASSOLAS,²³ B. S. SATHYAPRAKASH,^{132,114} O. SAUTER,³⁷ R. L. SAVAGE,⁵⁰ V. SAVANT,³ D. SAWANT,¹⁴⁰
 2055 S. SAYAH,²³ D. SCHÄTZL,¹ P. SCHALE,⁸⁰ M. SCHEEL,⁵¹ J. SCHEUER,¹⁴ P. SCHMIDT,¹³ R. SCHNABEL,¹¹⁹
 2056 R. M. S. SCHOFIELD,⁸⁰ A. SCHÖNBECK,¹¹⁹ E. SCHREIBER,^{9,10} B. W. SCHULTE,^{9,10} B. F. SCHUTZ,¹¹⁴
 2057 O. SCHWARM,¹⁸⁶ E. SCHWARTZ,⁷ J. SCOTT,⁵⁴ S. M. SCOTT,⁸ E. SEIDEL,²¹ D. SELLERS,⁷ A. S. SENGUPTA,¹⁹²
 2058 N. SENNETT,⁶⁵ D. SENTENAC,³¹ V. SEQUINO,⁶⁶ A. SERGEEV,¹⁵⁶ Y. SETYAWATI,^{9,10} D. A. SHADDOCK,⁸
 2059 T. SHAFFER,⁵⁰ M. S. SHAHIARI,¹⁴ A. SHARMA,^{17,18} P. SHARMA,⁶⁷ P. SHAWHAN,⁸⁶ H. SHEN,²¹ M. SHIKAUCHI,⁹²
 2060 R. SHINK,¹⁶⁵ D. H. SHOEMAKER,⁵⁵ D. M. SHOEMAKER,⁸⁷ K. SHUKLA,¹⁴⁹ S. SHYAMSUNDAR,⁶⁷ K. SIELLEZ,⁸⁷
 2061 M. SIENIAWSKA,⁶³ D. SIGG,⁵⁰ L. P. SINGER,⁹⁰ D. SINGH,¹⁹⁶ N. SINGH,⁸⁴ A. SINGHA,⁵⁴ A. SINGHAL,^{17,36}
 2062 A. M. SINTES,¹¹¹ V. SIPALA,^{128,129} V. SKLIRIS,¹¹⁴ B. J. J. SLAGMOLEN,⁸ T. J. SLAVEN-BLAIR,⁷⁵ J. SMETANA,¹³
 2063 J. R. SMITH,²⁹ R. J. E. SMITH,⁶ S. SOMALA,¹⁹⁶ E. J. SON,¹⁵⁹ S. SONI,² B. SORAZU,⁵⁴ V. SORDINI,¹⁰⁶
 2064 F. SORRENTINO,⁶⁶ T. SOURADEEP,³ E. SOWELL,⁹⁴ A. P. SPENCER,⁵⁴ M. SPERA,^{60,61,14} A. K. SRIVASTAVA,¹²⁰
 2065 V. SRIVASTAVA,⁴⁵ K. STAATS,¹⁴ C. STACHIE,⁷⁴ M. STANDKE,^{9,10} D. A. STEER,²⁸ J. STEINHOFF,⁶⁵ M. STEINKE,^{9,10}
 2066 J. STEINLECHNER,^{119,54} S. STEINLECHNER,¹¹⁹ D. STEINMEYER,^{9,10} S. STEVENSON,¹⁸⁹ D. STOCKS,⁵⁷ D. J. STOPS,¹³
 2067 M. STOVER,¹⁸⁵ K. A. STRAIN,⁵⁴ G. STRATTA,^{197,73} A. STRUNK,⁵⁰ R. STURANI,¹⁹⁸ A. L. STUVER,¹⁹⁹
 2068 S. SUDHAGAR,³ V. SUDHIR,⁵⁵ T. Z. SUMMERSCALES,²⁰⁰ L. SUN,¹ S. SUNIL,¹²⁰ A. SUR,⁶³ J. SURESH,⁹²
 2069 P. J. SUTTON,¹¹⁴ B. L. SWINKELS,⁴⁰ M. J. SZCZEPANČZYK,³² M. TACCA,⁴⁰ S. C. TAIT,⁵⁴ C. TALBOT,⁶
 2070 A. J. TANASIJCUK,⁸³ D. B. TANNER,³² D. TAO,¹ A. TAPIA,¹⁴¹ A. TAPIA,²⁹ E. N. TAPIA SAN MARTIN,⁴⁰
 2071 J. D. TASSON,²⁰¹ R. TAYLOR,¹ R. TENORIO,¹¹¹ L. TERKOWSKI,¹¹⁹ M. P. THIRUGNANASAMBANDAM,³ M. THOMAS,⁷
 2072 P. THOMAS,⁵⁰ J. E. THOMPSON,¹¹⁴ S. R. THONDAPU,⁶⁷ K. A. THORNE,⁷ E. THRANE,⁶ C. L. TINSMAN,⁶
 2073 T. R. SARAVANAN,³ SHUBHANSU TIWARI,^{78,126,127} S. TIWARI,¹⁴⁵ V. TIWARI,¹¹⁴ K. TOLAND,⁵⁴ M. TONELLI,^{58,22}
 2074 Z. TORNASI,⁵⁴ A. TORRES-FORNÉ,⁶⁵ C. I. TORRIE,¹ I. TOSTA E MELO,^{128,129} D. TÖYRÄ,⁸ E. A. TRAIL,²
 2075 F. TRAVASSO,^{59,44} G. TRAYLOR,⁷ M. C. TRINGALI,⁸⁴ A. TRIPATHEE,¹⁴⁷ A. TROVATO,²⁸ R. J. TRUEAU,¹
 2076 K. W. TSANG,⁴⁰ M. TSE,⁵⁵ R. TSO,⁵¹ L. TSUKADA,⁹² D. TSUNA,⁹² T. TSUTSUI,⁹² M. TURCONI,⁷⁴ A. S. UBHI,¹³
 2077 K. UENO,⁹² D. UGOLINI,¹⁹⁰ C. S. UNNIKRISHNAN,¹⁴⁵ A. L. URBAN,² S. A. USMAN,¹⁰³ A. C. UTINA,⁵⁴
 2078 H. VAHLBRUCH,¹⁰ G. VAJENTE,¹ G. VALDES,² M. VALENTINI,^{126,127} N. VAN BAKEL,⁴⁰ M. VAN BEUZEKOM,⁴⁰
 2079 J. F. J. VAN DEN BRAND,^{85,150,40} C. VAN DEN BROECK,^{40,202} D. C. VANDER-HYDE,⁴⁵ L. VAN DER SCHAAF,⁴⁰
 2080 J. V. VAN HEIJNINGEN,⁷⁵ A. A. VAN VEGGEL,⁵⁴ M. VARDARO,^{169,40} V. VARMA,⁵¹ S. VASS,¹ M. VASÚTH,⁵⁶
 2081 A. VECCHIO,¹³ G. VEDOVATO,⁶¹ J. VEITCH,⁵⁴ P. J. VEITCH,⁶⁴ K. VENKATESWARA,¹⁷¹ G. VENUGOPALAN,¹

2082 D. VERKINDT,³⁷ D. VESKE,³⁴ F. VETRANO,^{72,73} A. VICERÉ,^{72,73} A. D. VIETS,²⁰³ S. VINCIGUERRA,¹³
 2083 D. J. VINE,⁶⁹ J.-Y. VINET,⁷⁴ S. VITALE,⁵⁵ FRANCISCO HERNANDEZ VIVANCO,⁶ T. VO,⁴⁵ H. VOCCA,^{43,44}
 2084 C. VORVICK,⁵⁰ S. P. VYATCHANIN,⁶⁸ A. R. WADE,⁸ L. E. WADE,¹⁸⁵ M. WADE,¹⁸⁵ R. WALET,⁴⁰ M. WALKER,²⁹
 2085 G. S. WALLACE,²⁵ L. WALLACE,¹ S. WALSH,²⁴ J. Z. WANG,¹⁴⁷ S. WANG,²¹ W. H. WANG,¹⁶ R. L. WARD,⁸
 2086 Z. A. WARDEN,³⁸ J. WARNER,⁵⁰ M. WAS,³⁷ J. WATCHI,¹¹² B. WEAVER,⁵⁰ L.-W. WEI,^{9,10} M. WEINERT,^{9,10}
 2087 A. J. WEINSTEIN,¹ R. WEISS,⁵⁵ F. WELLMANN,^{9,10} L. WEN,⁷⁵ P. WESSELS,^{9,10} J. W. WESTHOUSE,³⁸
 2088 K. WETTE,⁸ J. T. WHELAN,⁷⁰ B. F. WHITING,³² C. WHITTLE,⁵⁵ D. M. WILKEN,^{9,10} D. WILLIAMS,⁵⁴
 2089 J. L. WILLIS,¹ B. WILLKE,^{10,9} W. WINKLER,^{9,10} C. C. WIPF,¹ H. WITTEL,^{9,10} G. WOAN,⁵⁴ J. WOEHLER,^{9,10}
 2090 J. K. WOFFORD,⁷⁰ C. WONG,¹⁰⁴ J. L. WRIGHT,⁵⁴ D. S. WU,^{9,10} D. M. WYSOCKI,⁷⁰ L. XIAO,¹ H. YAMAMOTO,¹
 2091 L. YANG,¹³³ Y. YANG,³² Z. YANG,⁴⁷ M. J. YAP,⁸ M. YAZBACK,³² D. W. YEELES,¹¹⁴ HANG YU,⁵⁵
 2092 HAOCUN YU,⁵⁵ S. H. R. YUEN,¹⁰⁴ A. K. ZADROŻNY,¹⁶ A. ZADROŻNY,¹⁶² M. ZANOLIN,³⁸ T. ZELENOVA,³¹
 2093 J.-P. ZENDRI,⁶¹ M. ZEVIN,¹⁴ J. ZHANG,⁷⁵ L. ZHANG,¹ T. ZHANG,⁵⁴ C. ZHAO,⁷⁵ G. ZHAO,¹¹² M. ZHOU,¹⁴
 2094 Z. ZHOU,¹⁴ X. J. ZHU,⁶ A. B. ZIMMERMAN,¹⁷⁷ M. E. ZUCKER^{55,1} AND J. ZWEIZIG¹

LIGO SCIENTIFIC COLLABORATION AND VIRGO COLLABORATION

¹LIGO, California Institute of Technology, Pasadena, CA 91125, USA²Louisiana State University, Baton Rouge, LA 70803, USA³Inter-University Centre for Astronomy and Astrophysics, Pune 411007, India⁴Dipartimento di Farmacia, Università di Salerno, I-84084 Fisciano, Salerno, Italy⁵INFN, Sezione di Napoli, Complesso Universitario di Monte S.Angelo, I-80126 Napoli, Italy⁶OzGrav, School of Physics & Astronomy, Monash University, Clayton 3800, Victoria, Australia⁷LIGO Livingston Observatory, Livingston, LA 70754, USA⁸OzGrav, Australian National University, Canberra, Australian Capital Territory 0200, Australia⁹Max Planck Institute for Gravitational Physics (Albert Einstein Institute), D-30167 Hannover, Germany¹⁰Leibniz Universität Hannover, D-30167 Hannover, Germany¹¹Theoretisch-Physikalisches Institut, Friedrich-Schiller-Universität Jena, D-07743 Jena, Germany¹²University of Cambridge, Cambridge CB2 1TN, UK¹³University of Birmingham, Birmingham B15 2TT, UK¹⁴Center for Interdisciplinary Exploration & Research in Astrophysics (CIERA), Northwestern University, Evanston, IL 60208, USA¹⁵Instituto Nacional de Pesquisas Espaciais, 12227-010 São José dos Campos, São Paulo, Brazil¹⁶The University of Texas Rio Grande Valley, Brownsville, TX 78520, USA¹⁷Gran Sasso Science Institute (GSSI), I-67100 L'Aquila, Italy¹⁸INFN, Laboratori Nazionali del Gran Sasso, I-67100 Assergi, Italy¹⁹International Centre for Theoretical Sciences, Tata Institute of Fundamental Research, Bengaluru 560089, India²⁰University College Dublin, Dublin 4, Ireland²¹NCSA, University of Illinois at Urbana-Champaign, Urbana, IL 61801, USA²²INFN, Sezione di Pisa, I-56127 Pisa, Italy²³Laboratoire des Matériaux Avancés (LMA), IP2I - UMR 5822, CNRS, Université de Lyon, F-69622 Villeurbanne, France²⁴University of Wisconsin-Milwaukee, Milwaukee, WI 53201, USA²⁵SUPA, University of Strathclyde, Glasgow G1 1XQ, UK²⁶Dipartimento di Matematica e Informatica, Università di Udine, I-33100 Udine, Italy²⁷INFN, Sezione di Trieste, I-34127 Trieste, Italy²⁸APC, AstroParticule et Cosmologie, Université Paris Diderot, CNRS/IN2P3, CEA/Irfu, Observatoire de Paris, Sorbonne Paris Cité, F-75205 Paris Cedex 13, France²⁹California State University Fullerton, Fullerton, CA 92831, USA³⁰LAL, Univ. Paris-Sud, CNRS/IN2P3, Université Paris-Saclay, F-91898 Orsay, France³¹European Gravitational Observatory (EGO), I-56021 Cascina, Pisa, Italy³²University of Florida, Gainesville, FL 32611, USA³³Chennai Mathematical Institute, Chennai 603103, India³⁴Columbia University, New York, NY 10027, USA³⁵INFN, Sezione di Roma Tor Vergata, I-00133 Roma, Italy³⁶INFN, Sezione di Roma, I-00185 Roma, Italy³⁷Laboratoire d'Annecy de Physique des Particules (LAPP), Univ. Grenoble Alpes, Université Savoie Mont Blanc, CNRS/IN2P3, F-74941 Annecy, France³⁸Embry-Riddle Aeronautical University, Prescott, AZ 86301, USA³⁹Montclair State University, Montclair, NJ 07043, USA⁴⁰Nikhef, Science Park 105, 1098 XG Amsterdam, The Netherlands

- 2139 ⁴¹*Korea Institute of Science and Technology Information, Daejeon 34141, South Korea*
 2140 ⁴²*Christopher Newport University, Newport News, VA 23606, USA*
 2141 ⁴³*Università di Perugia, I-06123 Perugia, Italy*
 2142 ⁴⁴*INFN, Sezione di Perugia, I-06123 Perugia, Italy*
 2143 ⁴⁵*Syracuse University, Syracuse, NY 13244, USA*
 2144 ⁴⁶*Université de Liège, B-4000 Liège, Belgium*
 2145 ⁴⁷*University of Minnesota, Minneapolis, MN 55455, USA*
 2146 ⁴⁸*Università degli Studi di Milano-Bicocca, I-20126 Milano, Italy*
 2147 ⁴⁹*INFN, Sezione di Milano-Bicocca, I-20126 Milano, Italy*
 2148 ⁵⁰*LIGO Hanford Observatory, Richland, WA 99352, USA*
 2149 ⁵¹*Caltech CaRT, Pasadena, CA 91125, USA*
- 2150 ⁵²*Departament de Física Quàntica i Astrofísica, Institut de Ciències del Cosmos (ICCUB), Universitat de Barcelona (IEEC-UB), E-08028 Barcelona, Spain*
- 2151 ⁵³*Dipartimento di Medicina, Chirurgia e Odontoiatria "Scuola Medica Salernitana," Università di Salerno, I-84081 Baronissi, Salerno, Italy*
- 2152 ⁵⁴*SUPA, University of Glasgow, Glasgow G12 8QQ, UK*
- 2153 ⁵⁵*LIGO, Massachusetts Institute of Technology, Cambridge, MA 02139, USA*
- 2154 ⁵⁶*Wigner RCP, RMKI, H-1121 Budapest, Konkoly Thege Miklós út 29-33, Hungary*
- 2155 ⁵⁷*Stanford University, Stanford, CA 94305, USA*
- 2156 ⁵⁸*Università di Pisa, I-56127 Pisa, Italy*
- 2157 ⁵⁹*Università di Camerino, Dipartimento di Fisica, I-62032 Camerino, Italy*
- 2158 ⁶⁰*Università di Padova, Dipartimento di Fisica e Astronomia, I-35131 Padova, Italy*
- 2159 ⁶¹*INFN, Sezione di Padova, I-35131 Padova, Italy*
- 2160 ⁶²*Montana State University, Bozeman, MT 59717, USA*
- 2161 ⁶³*Nicolaus Copernicus Astronomical Center, Polish Academy of Sciences, 00-716, Warsaw, Poland*
- 2162 ⁶⁴*OzGrav, University of Adelaide, Adelaide, South Australia 5005, Australia*
- 2163 ⁶⁵*Max Planck Institute for Gravitational Physics (Albert Einstein Institute), D-14476 Potsdam-Golm, Germany*
- 2164 ⁶⁶*INFN, Sezione di Genova, I-16146 Genova, Italy*
- 2165 ⁶⁷*RRCAT, Indore, Madhya Pradesh 452013, India*
- 2166 ⁶⁸*Faculty of Physics, Lomonosov Moscow State University, Moscow 119991, Russia*
- 2167 ⁶⁹*SUPA, University of the West of Scotland, Paisley PA1 2BE, UK*
- 2168 ⁷⁰*Rochester Institute of Technology, Rochester, NY 14623, USA*
- 2169 ⁷¹*Bar-Ilan University, Ramat Gan 5290002, Israel*
- 2170 ⁷²*Università degli Studi di Urbino "Carlo Bo," I-61029 Urbino, Italy*
- 2171 ⁷³*INFN, Sezione di Firenze, I-50019 Sesto Fiorentino, Firenze, Italy*
- 2172 ⁷⁴*Artemis, Université Côte d'Azur, Observatoire Côte d'Azur, CNRS, CS 34229, F-06304 Nice Cedex 4, France*
- 2173 ⁷⁵*OzGrav, University of Western Australia, Crawley, Western Australia 6009, Australia*
- 2174 ⁷⁶*Dipartimento di Fisica "E.R. Caianiello," Università di Salerno, I-84084 Fisciano, Salerno, Italy*
- 2175 ⁷⁷*INFN, Sezione di Napoli, Gruppo Collegato di Salerno, Complesso Universitario di Monte S. Angelo, I-80126 Napoli, Italy*
- 2176 ⁷⁸*Physik-Institut, University of Zurich, Winterthurerstrasse 190, 8057 Zurich, Switzerland*
- 2177 ⁷⁹*Univ Rennes, CNRS, Institut FOTON - UMR6082, F-3500 Rennes, France*
- 2178 ⁸⁰*University of Oregon, Eugene, OR 97403, USA*
- 2179 ⁸¹*Laboratoire Kastler Brossel, Sorbonne Université, CNRS, ENS-Université PSL, Collège de France, F-75005 Paris, France*
- 2180 ⁸²*Università di Roma "La Sapienza," I-00185 Roma, Italy*
- 2181 ⁸³*Université catholique de Louvain, B-1348 Louvain-la-Neuve, Belgium*
- 2182 ⁸⁴*Astronomical Observatory Warsaw University, 00-478 Warsaw, Poland*
- 2183 ⁸⁵*VU University Amsterdam, 1081 HV Amsterdam, The Netherlands*
- 2184 ⁸⁶*University of Maryland, College Park, MD 20742, USA*
- 2185 ⁸⁷*School of Physics, Georgia Institute of Technology, Atlanta, GA 30332, USA*
- 2186 ⁸⁸*Université de Lyon, Université Claude Bernard Lyon 1, CNRS, Institut Lumière Matière, F-69622 Villeurbanne, France*
- 2187 ⁸⁹*Università di Napoli "Federico II," Complesso Universitario di Monte S. Angelo, I-80126 Napoli, Italy*
- 2188 ⁹⁰*NASA Goddard Space Flight Center, Greenbelt, MD 20771, USA*
- 2189 ⁹¹*Dipartimento di Fisica, Università degli Studi di Genova, I-16146 Genova, Italy*
- 2190 ⁹²*RESCEU, University of Tokyo, Tokyo, 113-0033, Japan.*
- 2191 ⁹³*Tsinghua University, Beijing 100084, China*
- 2192 ⁹⁴*Texas Tech University, Lubbock, TX 79409, USA*
- 2193 ⁹⁵*Università di Roma Tor Vergata, I-00133 Roma, Italy*

- 2196 ⁹⁶*Missouri University of Science and Technology, Rolla, MO 65409, USA*
- 2197 ⁹⁷*Departamento de Astronomía y Astrofísica, Universitat de València, E-46100 Burjassot, València, Spain*
- 2198 ⁹⁸*Museo Storico della Fisica e Centro Studi e Ricerche “Enrico Fermi,” I-00184 Roma, Italy*
- 2199 ⁹⁹*National Tsing Hua University, Hsinchu City, 30013 Taiwan, Republic of China*
- 2200 ¹⁰⁰*Charles Sturt University, Wagga Wagga, New South Wales 2678, Australia*
- 2201 ¹⁰¹*Physics and Astronomy Department, Stony Brook University, Stony Brook, NY 11794, USA*
- 2202 ¹⁰²*Center for Computational Astrophysics, Flatiron Institute, 162 5th Ave, New York, NY 10010, USA*
- 2203 ¹⁰³*University of Chicago, Chicago, IL 60637, USA*
- 2204 ¹⁰⁴*The Chinese University of Hong Kong, Shatin, NT, Hong Kong*
- 2205 ¹⁰⁵*Dipartimento di Ingegneria Industriale (DIIN), Università di Salerno, I-84084 Fisciano, Salerno, Italy*
- 2206 ¹⁰⁶*Institut de Physique des 2 Infinis de Lyon (IP2I) - UMR 5822, Université de Lyon, Université Claude Bernard, CNRS, F-69622 Villeurbanne, France*
- 2207 ¹⁰⁷*Seoul National University, Seoul 08826, South Korea*
- 2208 ¹⁰⁸*Pusan National University, Busan 46241, South Korea*
- 2209 ¹⁰⁹*INAF, Osservatorio Astronomico di Padova, I-35122 Padova, Italy*
- 2210 ¹¹⁰*OzGrav, University of Melbourne, Parkville, Victoria 3010, Australia*
- 2211 ¹¹¹*Universitat de les Illes Balears, IAC3—IEEC, E-07122 Palma de Mallorca, Spain*
- 2212 ¹¹²*Université Libre de Bruxelles, Brussels 1050, Belgium*
- 2213 ¹¹³*Departamento de Matemáticas, Universitat de València, E-46100 Burjassot, València, Spain*
- 2214 ¹¹⁴*Cardiff University, Cardiff CF24 3AA, UK*
- 2215 ¹¹⁵*University of Rhode Island, Kingston, RI 02881, USA*
- 2216 ¹¹⁶*Bellevue College, Bellevue, WA 98007, USA*
- 2217 ¹¹⁷*MTA-ELTE Astrophysics Research Group, Institute of Physics, Eötvös University, Budapest 1117, Hungary*
- 2218 ¹¹⁸*California State University, Los Angeles, 5151 State University Dr, Los Angeles, CA 90032, USA*
- 2219 ¹¹⁹*Universität Hamburg, D-22761 Hamburg, Germany*
- 2220 ¹²⁰*Institute for Plasma Research, Bhat, Gandhinagar 382428, India*
- 2221 ¹²¹*IGFAE, Campus Sur, Universidade de Santiago de Compostela, 15782 Spain*
- 2222 ¹²²*The University of Sheffield, Sheffield S10 2TN, UK*
- 2223 ¹²³*Dipartimento di Scienze Matematiche, Fisiche e Informatiche, Università di Parma, I-43124 Parma, Italy*
- 2224 ¹²⁴*INFN, Sezione di Milano Bicocca, Gruppo Collegato di Parma, I-43124 Parma, Italy*
- 2225 ¹²⁵*Dipartimento di Ingegneria, Università del Sannio, I-82100 Benevento, Italy*
- 2226 ¹²⁶*Università di Trento, Dipartimento di Fisica, I-38123 Povo, Trento, Italy*
- 2227 ¹²⁷*INFN, Trento Institute for Fundamental Physics and Applications, I-38123 Povo, Trento, Italy*
- 2228 ¹²⁸*Università degli Studi di Sassari, I-07100 Sassari, Italy*
- 2229 ¹²⁹*INFN, Laboratori Nazionali del Sud, I-95125 Catania, Italy*
- 2230 ¹³⁰*University of Portsmouth, Portsmouth, PO1 3FX, UK*
- 2231 ¹³¹*West Virginia University, Morgantown, WV 26506, USA*
- 2232 ¹³²*The Pennsylvania State University, University Park, PA 16802, USA*
- 2233 ¹³³*Colorado State University, Fort Collins, CO 80523, USA*
- 2234 ¹³⁴*Institute for Nuclear Research (Atomki), Hungarian Academy of Sciences, Bem tér 18/c, H-4026 Debrecen, Hungary*
- 2235 ¹³⁵*CNR-SPIN, c/o Università di Salerno, I-84084 Fisciano, Salerno, Italy*
- 2236 ¹³⁶*Scuola di Ingegneria, Università della Basilicata, I-85100 Potenza, Italy*
- 2237 ¹³⁷*National Astronomical Observatory of Japan, 2-21-1 Osawa, Mitaka, Tokyo 181-8588, Japan*
- 2238 ¹³⁸*Observatori Astronòmic, Universitat de València, E-46980 Paterna, València, Spain*
- 2239 ¹³⁹*INFN Sezione di Torino, I-10125 Torino, Italy*
- 2240 ¹⁴⁰*Indian Institute of Technology Bombay, Powai, Mumbai 400 076, India*
- 2241 ¹⁴¹*University of Szeged, Dóm tér 9, Szeged 6720, Hungary*
- 2242 ¹⁴²*Delta Institute for Theoretical Physics, Science Park 904, 1090 GL Amsterdam, The Netherlands*
- 2243 ¹⁴³*Lorentz Institute, Leiden University, PO Box 9506, Leiden 2300 RA, The Netherlands*
- 2244 ¹⁴⁴*GRAPPA, Anton Pannekoek Institute for Astronomy and Institute for High-Energy Physics, University of Amsterdam, Science Park 904, 1098 XH Amsterdam, The Netherlands*
- 2245 ¹⁴⁵*Tata Institute of Fundamental Research, Mumbai 400005, India*
- 2246 ¹⁴⁶*INAF, Osservatorio Astronomico di Capodimonte, I-80131 Napoli, Italy*
- 2247 ¹⁴⁷*University of Michigan, Ann Arbor, MI 48109, USA*
- 2248 ¹⁴⁸*American University, Washington, D.C. 20016, USA*
- 2249 ¹⁴⁹*University of California, Berkeley, CA 94720, USA*
- 2250 ¹⁵⁰*Maastricht University, P.O. Box 616, 6200 MD Maastricht, The Netherlands*

- 2253 ¹⁵¹*Directorate of Construction, Services & Estate Management, Mumbai 400094 India*
 2254 ¹⁵²*University of Białystok, 15-424 Białystok, Poland*
 2255 ¹⁵³*King's College London, University of London, London WC2R 2LS, UK*
 2256 ¹⁵⁴*University of Southampton, Southampton SO17 1BJ, UK*
 2257 ¹⁵⁵*University of Washington Bothell, Bothell, WA 98011, USA*
 2258 ¹⁵⁶*Institute of Applied Physics, Nizhny Novgorod, 603950, Russia*
 2259 ¹⁵⁷*Ewha Womans University, Seoul 03760, South Korea*
 2260 ¹⁵⁸*Inje University Gimhae, South Gyeongsang 50834, South Korea*
 2261 ¹⁵⁹*National Institute for Mathematical Sciences, Daejeon 34047, South Korea*
 2262 ¹⁶⁰*Ulsan National Institute of Science and Technology, Ulsan 44919, South Korea*
 2263 ¹⁶¹*Bard College, 30 Campus Rd, Annandale-On-Hudson, NY 12504, USA*
 2264 ¹⁶²*NCBJ, 05-400 Świerk-Otwock, Poland*
 2265 ¹⁶³*Institute of Mathematics, Polish Academy of Sciences, 00656 Warsaw, Poland*
 2266 ¹⁶⁴*Cornell University, Ithaca, NY 14850, USA*
 2267 ¹⁶⁵*Université de Montréal/Polytechnique, Montreal, Quebec H3T 1J4, Canada*
 2268 ¹⁶⁶*Lagrange, Université Côte d'Azur, Observatoire Côte d'Azur, CNRS, CS 34229, F-06304 Nice Cedex 4, France*
 2269 ¹⁶⁷*Hillsdale College, Hillsdale, MI 49242, USA*
 2270 ¹⁶⁸*Korea Astronomy and Space Science Institute, Daejeon 34055, South Korea*
 2271 ¹⁶⁹*Institute for High-Energy Physics, University of Amsterdam, Science Park 904, 1098 XH Amsterdam, The Netherlands*
 2272 ¹⁷⁰*NASA Marshall Space Flight Center, Huntsville, AL 35811, USA*
 2273 ¹⁷¹*University of Washington, Seattle, WA 98195, USA*
 2274 ¹⁷²*Dipartimento di Matematica e Fisica, Università degli Studi Roma Tre, I-00146 Roma, Italy*
 2275 ¹⁷³*INFN, Sezione di Roma Tre, I-00146 Roma, Italy*
 2276 ¹⁷⁴*ESPCI, CNRS, F-75005 Paris, France*
 2277 ¹⁷⁵*Center for Phononics and Thermal Energy Science, School of Physics Science and Engineering, Tongji University, 200092 Shanghai, People's Republic of China*
 2278 ¹⁷⁶*Southern University and A&M College, Baton Rouge, LA 70813, USA*
 2279 ¹⁷⁷*Department of Physics, University of Texas, Austin, TX 78712, USA*
 2280 ¹⁷⁸*Dipartimento di Fisica, Università di Trieste, I-34127 Trieste, Italy*
 2281 ¹⁷⁹*Centre Scientifique de Monaco, 8 quai Antoine Ier, MC-98000, Monaco*
 2282 ¹⁸⁰*Indian Institute of Technology Madras, Chennai 600036, India*
 2283 ¹⁸¹*Université de Strasbourg, CNRS, IPHC UMR 7178, F-67000 Strasbourg, France*
 2284 ¹⁸²*Institut des Hautes Etudes Scientifiques, F-91440 Bures-sur-Yvette, France*
 2285 ¹⁸³*IISER-Kolkata, Mohanpur, West Bengal 741252, India*
 2286 ¹⁸⁴*Department of Astrophysics/IMAPP, Radboud University Nijmegen, P.O. Box 9010, 6500 GL Nijmegen, The Netherlands*
 2287 ¹⁸⁵*Kenyon College, Gambier, OH 43022, USA*
 2288 ¹⁸⁶*Whitman College, 345 Boyer Avenue, Walla Walla, WA 99362 USA*
 2289 ¹⁸⁷*Hobart and William Smith Colleges, Geneva, NY 14456, USA*
 2290 ¹⁸⁸*Department of Physics, Lancaster University, Lancaster, LA1 4YB, UK*
 2291 ¹⁸⁹*OzGrav, Swinburne University of Technology, Hawthorn VIC 3122, Australia*
 2292 ¹⁹⁰*Trinity University, San Antonio, TX 78212, USA*
 2293 ¹⁹¹*Dipartimento di Fisica, Università degli Studi di Torino, I-10125 Torino, Italy*
 2294 ¹⁹²*Indian Institute of Technology, Gandhinagar Ahmedabad Gujarat 382424, India*
 2295 ¹⁹³*INAF, Osservatorio Astronomico di Brera sede di Merate, I-23807 Merate, Lecco, Italy*
 2296 ¹⁹⁴*Centro de Astrofísica e Gravitação (CENTRA), Departamento de Física, Instituto Superior Técnico, Universidade de Lisboa, 1049-001 Lisboa, Portugal*
 2297 ¹⁹⁵*Marquette University, 11420 W. Clybourn St., Milwaukee, WI 53233, USA*
 2298 ¹⁹⁶*Indian Institute of Technology Hyderabad, Sangareddy, Khamdi, Telangana 502285, India*
 2299 ¹⁹⁷*INAF, Osservatorio di Astrofisica e Scienza dello Spazio, I-40129 Bologna, Italy*
 2300 ¹⁹⁸*International Institute of Physics, Universidade Federal do Rio Grande do Norte, Natal RN 59078-970, Brazil*
 2301 ¹⁹⁹*Villanova University, 800 Lancaster Ave, Villanova, PA 19085, USA*
 2302 ²⁰⁰*Andrews University, Berrien Springs, MI 49104, USA*
 2303 ²⁰¹*Carleton College, Northfield, MN 55057, USA*
 2304 ²⁰²*Department of Physics, Utrecht University, 3584CC Utrecht, The Netherlands*
 2305 ²⁰³*Concordia University Wisconsin, 2800 N Lake Shore Dr, Mequon, WI 53097, USA*